uOttawa

L'Université canadienne
Canada's university

FACULTÉ DES ÉTUDES SUPÉRIEURES ET POSTOCTORALES

uOttawa

L'Université canadienne
Canada's university

FACULTY OF GRADUATE AND POSDOCTORAL STUDIES

Lisa Walrond
AUTEUR DE LA THÈSE / AUTHOR OF THESIS

M.Sc. (Chemistry)
GRADE / DEGREE

Department of Chemistry
FACULTÉ, ÉCOLE, DÉPARTEMENT / FACULTY, SCHOOL, DEPARTMENT

Stability and Chemistry of Boron Containing Cations, Anions, and Neutrals

TITRE DE LA THÈSE / TITLE OF THESIS

Dr. P. Mayer (absent)
DIRECTEUR (DIRECTRICE) DE LA THÈSE / THESIS SUPERVISOR

Dr. J. Holmes (replacing Dr. P. Mayer)
CO-DIRECTEUR (CO-DIRECTRICE) DE LA THÈSE / THESIS CO-SUPERVISOR

EXAMINATEURS (EXAMINATRICES) DE LA THÈSE / THESIS EXAMINERS

Dr. J. Giorgi

Dr. A. St-Amant

Gary W. Slater
Le Doyen de la Faculté des études supérieures et postdoctorales / Dean of the Faculty of Graduate and Postdoctoral Studies

# Stability and Chemistry of Boron Containing Cations, Anions, and Neutrals

**Lisa Walrond**

**Thesis submitted to the**

**Faculty of Graduate and Postdoctoral Studies**

**University of Ottawa**

**in partial fulfillment of the requirements for the**

**M. Sc. Degree in Chemistry**

**Ottawa-Carleton Chemistry Institute**

*Your file Votre référence*
*ISBN: 978-0-494-32486-8*
*Our file Notre référence*
*ISBN: 978-0-494-32486-8*

*Abstract*

The structure, thermochemistry, isomerization and dissociation of the $CH_2BH_2$ and $CH_3BH$ radicals, cations and anions have been explored with a wide range of ab initio levels of computational theory and their formation has been probed by tandem mass spectrometry and RRKM kinetic theory. Calculations predict that $CH_2BH_2^{+}$ is not an equilibrium structure on the potential energy surface. The $CH_3BH^{+}$ was characterized by its collision-induced dissociation mass spectrum and neutralization–reionization (NR) mass spectrometry was used to generate the $CH_3BH^{\bullet}$ radical. While both $CH_2BH_2^{\bullet}$ and $CH_3BH^{\bullet}$ are stable with respect to isomerization and dissociation, a relatively low barrier to the 1,2-hydrogen shift means that pure $CH_3BH^{\bullet}$ can only be made cold, and so the above NR experiment likely produces a mixture of neutrals, of which only $CH_3BH^{\bullet}$ can be reionized. Vertical electron attachment to $CH_3BH^{\bullet}$ is endothermic which means the $CH_3BH^{-}$ anion is unlikely to be made from the cation or radical. In addition, the anion lies in a shallow well of only 48 kJ $mol^{-1}$ and will undergo fast isomerization to $CH_2BH_2^{-}$ below the dissociation limit.

The $B(N(CH_3)_2)_3$ radical cation and dication structures and dissociation products have been investigated by high level ab initio calculations and experimentally characterized by tandem mass spectrometry. The KER was measured for the metastable dissociation products of the $B(N(CH_3)_2)_3$ dication. There were four observed dissociation channels, two involving neutral losses and two involving charge separations. The neutral loss channels successfully compete with the charge separations, the dominant process actually

being neutral loss of $H_2$. The KER for the four metastable dissociations were determined to be $T_{0.5\ (141++)} = 368 \pm 18$ meV, $T_{0.5\ (127++)} = 144 \pm 12$ meV, $T_{h\ (99+)} = 2365 \pm 156$ meV, $T_{h(44+)} = 2046 \pm 279$ meV, and $T_{h\ (128+)} = 1942 \pm 332$ meV.

# Table of contents

**List of Tables**

**List of Figures**

## Abbreviations

| | |
|---|---|
| B | magnetic sector |
| *B* | magnetic field strength |
| BN | boron nitride |
| BNCT | Boron Neutron Capture Therapy |
| CC | coupled cluster |
| CID | collision induced dissociation |
| CIDI | collisionally induced dissociative ionization |
| DFT | density functional theory |
| E | electric sector |
| EI | electron impact |
| ESA | electrostatic analyzer |
| HF | Hartree-Fock |
| ICR | ion cyclotron resonance |
| IRC | intrinsic reaction coordinate |
| G2 | Gaussian-2 |
| G3 | Gaussian-3 |
| KE | kinetic energy |
| KER | kinetic energy release |
| *m* | mass |
| MI | metastable ions |

| | |
|---|---|
| MIKES | mass analyzed kinetic energy spectrum |
| MO | molecular orbital |
| MP | Møller-Plesset perturbation theory |
| *m/z* | mass to charge |
| NRMS | neutralization reionization mass spectrometry |
| SD | singles and doubles excitation |
| SD(T) | singles doubles and triples excitation |
| TOF | time of flight |
| q | quadrupole ion trap |
| *q* | fundamental charge |
| QCI | quadratic configuration interaction |
| *z* | charge |

Acknowledgements

I would like to take this opportunity to thank Dr. Paul Mayer for his guidance and support over the course of this degree. It was his influence during my undergraduate degree that first got me interested in the field of mass spectrometry, for which I am extremely grateful. I was very fortunate to have had the opportunity to study part-time during the course of this Master's degree. During this time I have started a family (which is very soon about to get a little bigger) and been pursuing a career in the field of analytical mass spectrometry, first at the National Research Council of Canada and presently at Health Canada.

I would also like to thank the whole mass spectrometry group. In particular Dr. John Holmes for his helpful discussions, advice and insight and Dr. Sander Mommers for all the instrumentation help he has provided me. I would like to thank Anne-Marie, Clement, Emma, Julie, and Xian for the technical support they gave me when I was learning to use 'the ZAB'. I wish all the past and present group members success and happiness in the future.

Finally I would like to thank my whole family for their love and support. In particular, my husband and son picking up the slack at home while I was busy with work and school, for their love and patience and the joy they've brought to my life.

This thesis is lovingly dedicated to Xavier.

## Chapter 1: Introduction

One fundamental goal of gas-phase ion chemistry has been the identification and characterization of novel ion structures that participate in ion fragmentation mechanisms in mass spectrometry [1]. Theoretical *ab initio* molecular orbital (MO) calculations and experimental techniques like mass spectrometry can be used to reveal ion structures and fragmentation mechanisms. Understanding of the chemical behaviour and reaction mechanism of electron-deficient boron compounds is still inadequate [2]. To date relatively little attention has been paid to organoboron complexes; studies have primarily focused on oxygen and nitrogen substituted hydrocarbons.

There is little doubt that boron is one of the most fascinating elements in the periodic table [3]. Boron has two isotopes, $^{11}B$ and $^{10}B$, which account for approximately 80% and 20% of its relative abundance. It is the only nonmetal in Group 13 (IIIA) and shares some characteristics with both carbon and silicon, which are adjacent and diagonal to boron in the periodic chart, respectively. Like carbon and silicon, boron also exists in different allotropic forms from amorphous to crystalline. Boron is similar in size and slightly more positive than carbon having three valence electrons and four valence orbitals, whereas carbon has four valence electrons and four valence orbitals. Boron is able to form 3 $sp^2$ hybrid orbitals and still has an empty pure 2 p orbital, which gives it the ability to accept a lone pair of electrons; thus B is able to form three coordinate (planar) neutral complexes or four coordinate (tetrahedral) negatively charged complexes. Boron forms compounds that are isoelectronic with carbon compounds. For example, $R_3B$ and $R_3C^+$, $R_4B^-$ and $R_4C$, boron nitride and carbon (BN is equivalent to CC), HBO

and $HCO^+$ or HCN etc.). The diamond-like allotrope of BN in called cubic BN (c-BN) and the graphite-like allotrope of BN is called hexagonal BN (h-BN). Next to diamond, boron nitride and boron carbide are two of the hardest materials known.

Single bonds to B increase in strength along the periodic table and the same is true for C-containing single bonds. Considering bonds between $BH_2$ and $BH_2$, $CH_3$, $NH_2$, OH, and F the bond strength order is B—B (255 kJ $mol^{-1}$) < B—C (310 kJ $mol^{-1}$) < B—N (435 kJ $mol^{-1}$) < B—O (519 kJ $mol^{-1}$) < B—F (649 $kJmol^{-1}$) [4]. The same trend is seen for the bonds between $CH_3$ and $CH_3$, $NH_2$, OH, and F; C-C (368 kJ $mol^{-1}$) ~ C—N (364 kJ $mol^{-1}$) < C—O (381 kJ $mol^{-1}$) < C—F (456 kJ $mol^{-1}$) [4]. It is interesting to note from the above information that B—N, B—O, and B—F bonds are all stronger than the C—N, C—O and C—F bonds. The same is not true of B—B and B—C bonds, which are both weaker than C—C bonds. B—H bonds are also weaker than C—H bonds (eg. in $BH_3$ the B—H bond strength is 372 kJ $mol^{-1}$ vs. $CH_4$ where the C—H bond strength of 435 kJ $mol^{-1}$). Another difference in bonding in B and C systems is that formal B=N and B=C double bonds are only slightly stronger than B—N and B—C single bonds and B=B are actually weaker than B—B bonds [4], whereas the opposite is seen for carbon double bonds which increase dramatically in bond strength over the respective single bonds.

Boron has uses in many different disciplines of chemistry including medicinal, organic, materials chemistry, inorganic, and catalysis. In medicine, certain antibiotics are B containing and B is also used in a type of cancer therapy called Boron Neutron Capture Therapy (BNCT). There are numerous materials incorporating B including, borosilicate

glass (Pyrex®), enamels, ceramics, semiconductors, pyrotechnics, and borax, etc. Specifically, amorphous boron nitride (a-BN) is used in semiconductors, while h-BN can be included in ceramics, alloys, resins, plastics, and rubbers to give self-lubricating properties [5]. B also plays a very important role in organic chemistry, particularly stereodirected synthesis. Examples of organic reactions involving boron are hydroboration/oxidation (Anti-Markovnikov addition), Suzuki reaction, and stereodirected aldol condensation involving enolates, etc. University of Rochester chemist Guillermo Bazan (who is a graduate of the University of Ottawa and Massachusetts Institute of Technology) announced a breakthrough with metallocene catalysts by incorporating boron atoms into the standard metallocene structures [6]. The new catalysts show extreme promise in the production of alpha-olefins and produce 100% pure products at much milder reaction conditions than those currently in use [6].

## 1.1 Literature Review

The system of radicals, cations and anions of composition $CH_4B$ are isoelectronic with derivatives of ethene. Isomers $CH_2BH_2^{\bullet}$ and $CH_3BH^{\bullet}$ are isoelectronic with $CH_2CH_2^{+\bullet}$ and $CH_3CH^{+\bullet}$. As will be seen, while $CH_3BH^{\bullet}$ is a stable species, $CH_3CH^{+\bullet}$ has been shown not to occupy a minimum on the ionized ethene potential energy surface [7].

The formation of $CH_2BH_2^{\bullet}$ and $CH_3BH^{\bullet}$ by the reaction of boron atoms with methane has been observed by IR spectroscopy and investigated using theoretical calculations [8-11]. Reaction products $CH_3BH^{\bullet}$, $CH_2BH_2^{\bullet}$, $H_2C{=}BH$, $HC{=}BH^{\bullet}$ and $HB{=}C{=}BH$ were identified by isotopic substitution and comparisons from *ab initio* calculations. The major reaction product of B insertion into methane is $CH_3BH^{\bullet}$, which can rearrange to $CH_2BH_2^{\bullet}$ or lose a hydrogen atom to form $CH_2BH + H^{\bullet}$, both processes are energetically favourable. UV-vis and IR were used to follow the reaction of boron atoms and clusters with methane, methyl bromide and water under matrix isolation conditions [12, 13].

The analogous cations $CH_2BH_2^{+}$ and $CH_3BH^{+}$ are isoelectronic with the doubly charged $CH_2CH_2^{2+}$ and $CH_3CH^{2+}$ ions. Pople et al. [14] investigated the $CH_4B^{+}$ ions at the MP4SDTQ/6-31G*//HF/3-21G level of theory. It was found that $CH_2BH_2^{+}$ is 127 kJ $mol^{-1}$ higher in energy than $CH_3BH^{+}$ and that the transition state for their interconversion is only 32 kJ $mol^{-1}$ above $CH_2BH_2^{+}$. They determined that $CH_2BH_2^{+}$ rearranges to the more stable $CH_3BH^{+}$ with little or no activation energy. The transition state for the

interconversion was found to be a bridged structure having $C_S$ symmetry, while $CH_2BH_2^+$ and $CH_3BH^+$ have $C_{2V}$ and $C_{3V}$ symmetry, respectively. There have been no attempts to make either of these ions in the laboratory. Similarly, the anionic isomers $CH_2BH_2^-$ and $CH_3BH^-$, which are isoelectronic with $CH_2CH_2$ and $CH_3CH$, have not been experimentally investigated.

Dill, Schleyer, and Pople used molecular orbital theory to predict the geometries, and energies of 17 neutral molecules containing boron and C, N, O, or F calculated at the STO-3G and 6-31G* levels of theory [4]. They found that geometries of these neutral boron containing species corresponded to those calculated previously for isoelectronic carbocations, but that B is a stronger $\sigma$ donor and a weaker $\pi$ acceptor that $C^+$ [4]. Boron is stabilized by direct attachment to lone pair $\pi$ donors ($NH_2$, OH, F), which stabilizes $BH_2X$ relative to $BH_3$ by 222 - 243 kJ $mol^{-1}$ [4]. B is also stabilized by strong $\sigma$-acceptors, hyperconjugation, multicenter bonding, and complexation with certain $\sigma$-donor molecules [4].

Poon and Mayer calculated G3 heats of formation and bond strengths for several closed- and open-shell boron-containing neutral species [15]. Methyl substitution increases the B—C bond length and decreases its bond strength in both the open- and closed-shell species [15]. They found that the $\Delta_fH°_{298}$ decreases by 72 - 74 kJ $mol^{-1}$ with successive methyl substitution on $BH_2CH_3$ and a similar 62 - 66 kJ $mol^{-1}$ decrease is observed for $CH_2BH_2^{\bullet}$. The decrease in heat of formation of the B species is significantly larger than what is observed for methyl substitution on C.

Poon and Mayer also calculated G3 heats of formation and bond strengths (both homolytic and heterolytic) for $BH_2NH_2$, $BH_2NH^{\bullet}$, $(CH_3)HBNH_2$, $(CH_3)HBNH^{\bullet}$, $(CH_3)_2BNH_2$, and $(CH_3)_2BNH^{\bullet}$ [15]. The formation of the closed shell species is exothermic while the formation of the open shell species is endothermic. Both groups of molecules become more exothermic by ~ 60kJ $mol^{-1}$ with each addition of a methyl group. The bond lengths for the closed shell species lengthen by 0.01 Å with the addition of methyl groups while the bond lengths of the open shell species are lengthened by 0.053 Å. Both the homolytic and heterolytic bond strengths decrease with the addition of methyl groups to boron. The boron nitrogen bond of $BH_2NH^{\bullet}$ shows quite a bit of double bond character.

The reaction of laser ablated boron atoms with several small molecules including $CH_3NH_2$ [16], $CH_3OH$ [17], $CH_4$ [8-11], HCCH [18], $NH_3$ [19, 20], $CO_2$ [21], CO [22], and the halogens (X = F, Cl, Br, I) [23], have been the subject of several FTIR and theoretical studies. Lanzisera and Andrews studied the reactions of laser ablated boron atoms with methylamine ($CH_3NH_2$) using IR spectra and MP2 frequency calculations [16]. The reaction products observed were from insertion into the C—N and N—H bonds, rather than into the C—H bond [16]. These reactions and their decomposition pathways were the subject of a Gaussian-3 (G3) molecular orbital (MO) study by So [24]. The G3 relative energies of the four reaction products generated by the insertion of B into the C—N and N—H C—H bonds of $CH_3NH_2$ as well as complexation with $CH_3NH_2$

were $CH_3BNH_2^{\bullet}$ $\Delta E = 0$ kJ mol$^{-1}$, $CH_3N(BH)H^{\bullet}$ $\Delta E = 75$ kJ mol$^{-1}$, $CH_2(BH)NH_2^{\bullet}$, $\Delta E =$ 227 kJ mol$^{-1}$ and $CH_3NH_2{\cdot\cdot}B$ $\Delta E = 396$ kJ mol$^{-1}$ [24]. These results are in agreement with the IR study where the C—H insertion product was not observed. The C—H insertion product is 227 kJ mol$^{-1}$ and 152 kJ mol$^{-1}$ less stable than the C—N and N—H insertion products, respectively.

Lanzisera and Andrews also studied the reaction of laser ablated boron atoms with methanol ($CH_3OH$), using FTIR, isotopic substitution studies and MO calculations of the vibrational frequencies of the potential reaction products at the MP2 level of theory [17]. The major products they observed were $CH_3BO$, $CH_2BO^{\bullet}$, and HBO. They concluded that the reaction products $CH_3BO$ and $CH_2BO^{\bullet}$ were from B insertion into the C—O bond of methanol followed by dehydrogenations and that the reaction product HBO was formed by B insertion into the O—H bond of methanol followed by C—O bond cleavage and that no reaction products were observed from B insertion into the C—H bonds of methanol [17]. Suk Ping So used Gaussian-2 (G2) MO calculations (with structures optimized at the MP2(FU)/6-31G* level of theory) to study the reaction of boron insertions into the C—H, O—H, and C—O bonds of $CH_3OH$ to form $CH_2(BH)OH^{\bullet}$, $CH_3OBH^{\bullet}$, $CH_3BOH^{\bullet}$, respectively as well as to investigate the potential decomposition pathways of these reaction products [25]. It was determined that the three isomers are lower in energy than the reactants ($CH_3OH$ + B) by 22.2 kJ mol$^{-1}$, 27.7 kJ mol$^{-1}$, and 13.5 kJ mol$^{-1}$ for the $CH_3OBH^{\bullet}$, $CH_3BOH^{\bullet}$ and $CH_2(BH)OH^{\bullet}$ structures, respectively. The transition states between the two more stable isomers and their decomposition products identified in the FTIR paper [17], were also found at the G2 level and confirmed by

intrinsic reaction coordinate (IRC) calculations, however the transition states of the insertion reactions themselves could not be found. The relative energies of these three isomers at the G2 level were determined to be $CH_3BOH^{\bullet}$ $\Delta E = 0$ kJ $mol^{-1}$, $CH_3OBH^{\bullet}$ 97 kJ $mol^{-1}$ and $CH_2(BH)OH^{\bullet}$ is 249 kJ $mol^{-1}$. No attempt was made at finding transition states between the three isomers.

Ionic and neutral $CH_3OBH^{+/\bullet}$ and $CH_3BOH^{+/\bullet}$ were generated and characterized in the gas phase by tandem mass spectrometry [26]. $CH_3OBH^{+}$ and $CH_3BOH^{+}$ were generated by EI of trimethylborate ($B(OCH_3)_3$) and methyl boronic acid ($CH_3B(OH)_2$), respectively. The structures of the cations were confirmed with collision induced dissociation (CID) mass spectrometry while the neutrals were studied by neutralization reionization mass spectrometry (NRMS). Theoretical calculations at the G2 level of theory were also performed in this study to determine the relative energies of the possible fragmentation channels of the two isomers. The relative energies of the radical isomers $CH_3BOH^{\bullet}$ and $CH_3OBH^{\bullet}$ are $\Delta E = 0$ kJ $mol^{-1}$ and 97 kJ $mol^{-1}$, respectively and the relative energies of the cation isomers $CH_3BOH^{+}$ and $CH_3OBH^{+}$ are $\Delta E = 0$ kJ $mol^{-1}$ and 144 kJ $mol^{-1}$, respectively. This group [26] did attempt to calculate G2 single point energies for $CH_2(BH)OH^{+/\bullet}$, using geometries optimized at the MP2/6-311+G(3df,2p) level of theory, however, all their attempts at optimization led to the $CH_3BOH^{+/\bullet}$ isomer.

## 2. *Approach and Methods*

### *2.1 What is Mass Spectrometry?*

A mass spectrometer measures the mass to charge (*m/z*) ratios of ions thereby giving the mass of the molecule or analyte. There are many types of mass spectrometers, but they are all composed of the same basis parts, an inlet system, an ionization source, a mass analyzer, a detector (interfaced to a CPU), a vacuum system, and the necessary electronics to control the system operation. Figure 2.1 shows a schematic representation of a mass spectrometer.

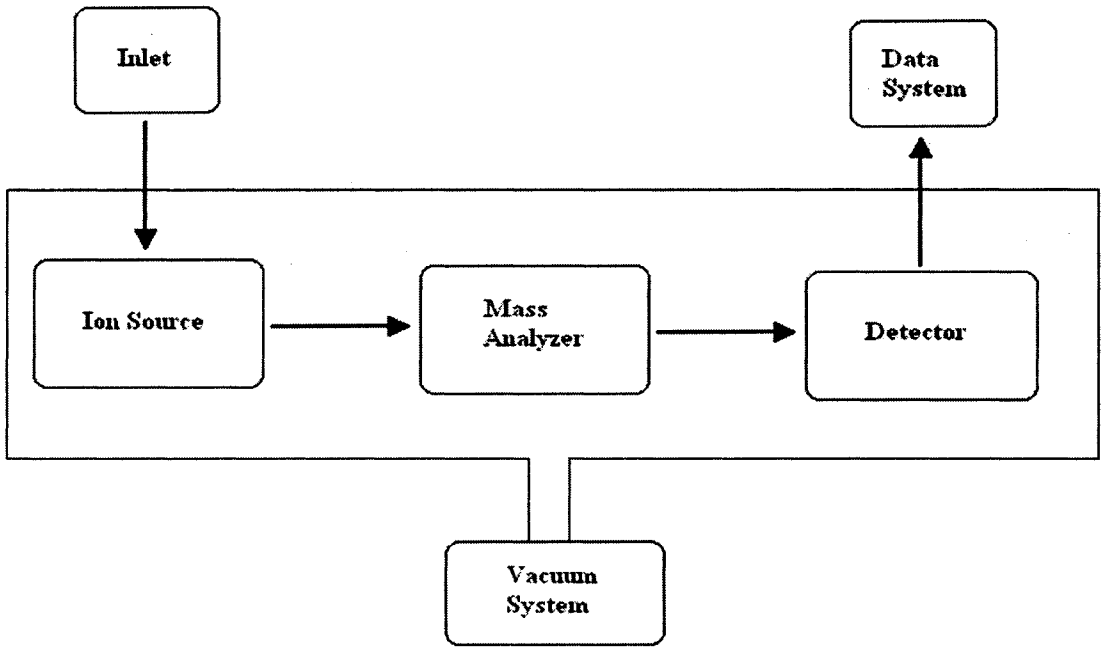


Figure 2.1. Schematic representation of a general mass spectrometer.

The inlet is used to introduce a compound to the ionization source. Sample introduction can be achieved by chromatography (gas or liquid), capillary electrophoresis (CE), and direct infusion or injection. There are several kinds of ionization sources that employ

different methods for ionizing a sample, the most common are electron impact (EI), chemical ionization (CI), electrospray ionization (ESI), and matrix-assisted laser desorption ionization (MALDI). Depending on the method of ionization, positive or negative ions or radical ions are produced. EI is the method of ionization used in this study. It involves the removal of an electron from the vapourized sample by a high-energy beam of electrons producing a radical cation. Figure 2.2 is a schematic representation of an electron impact ionization source. A heated filament composed of either Tungsten or Rhenium produces the high-energy beam of electrons (70 eV) and the gaseous sample is passed through this electron beam resulting in the removal of an electron from the analyte. The ionized sample is then accelerated out of the source through a series of slits, which make a focused beam that is transmitted through to the mass analyzer. An EI mass spectrum usually contains the molecular ion (but not always) as well as several fragment ions due to the excess energy transferred to the molecular ion by the high-energy beam of electrons during the ionization process. The production of the molecular ion and its subsequent fragments are shown in equations 2.1 and 2.2.

$$M(g) + e^{-}(70eV) \rightarrow M^{+\bullet} + 2e^{-} \qquad (2.1)$$

$$M^{+\bullet} \rightarrow M^{+}_{f} + M_{n} \qquad (2.2)$$

EI is considered to be a vertical process since it takes a very short time for an electron to interact with a particular molecule, on the order of $10^{-16}$ s, which doesn't give heavy nuclei the opportunity to have moved perceptibly [27].

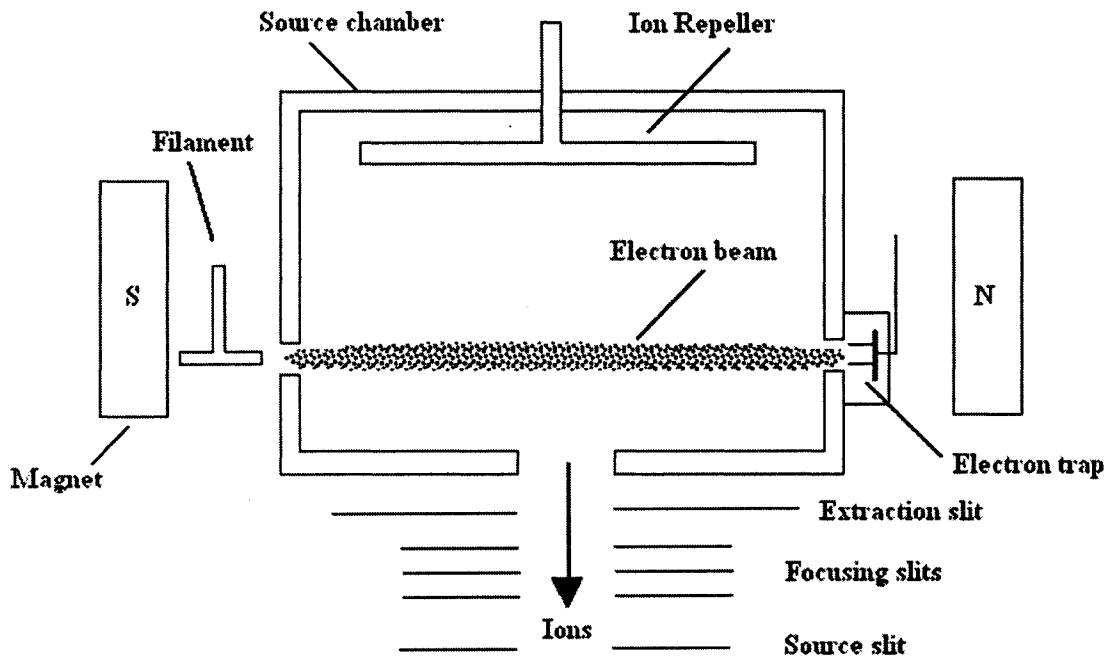


Figure 2.2. Schematic representation of an electron impact ionization source.

There are several types of mass analyzers, all of which use magnetic and/or electric fields to separate ions based on their mass to charge ratios. Some common types of mass analyzers include quadrupoles (q), ion traps, ion cyclotron resonance (ICR) cells, time of flight (TOF) tubes and magnetic sectors. Tandem mass spectrometers have more than one mass analyzer and these types of instruments can be used to gain structural information about the compounds being analyzed. Examples of tandem mass spectrometers include q-TOF, tandem quad, TOF/TOF and double, triple or more focusing sector instruments, etc. A major development leading to the technique of tandem mass spectrometry (MS/MS) occurred when Hipple and Condon first observed and explained the presence of metastable ions [28].

Sector instruments come in several varieties, generally with some combination of magnetic and electric sector. Double focusing instruments have both magnetic and electric sectors. When the magnetic sector (B) is in front of the electric sector (E) the instrument is said to have a reversed geometry (BE). These were the first instruments that were capable of performing MS/MS. In the simplest mode of operation, the accelerating and the electric sector potentials are held constant while the magnetic field (B) is scanned. Ions that have a constant kinetic energy, but different mass-to-charge ratios (*m/z*) are brought into focus at the detector slit (called the 'collector slit') at different magnetic field strengths (*B*). This sequentially ejects ions of increasing *m/z* ratio. Alternatively, *B* can be held constant so that all ions with a particular *m/z* ratio, regardless of kinetic energy can be detected. A double focusing mass spectrometer is ideal for studying gas phase ion energetics and structures. The tandem mass spectrometry experiments described in this thesis were performed on a modified VG ZAB-2F mass spectrometer consisting of a magnetic sector followed by two electrostatic analyzers (BEE geometry) [29]. A schematic diagram of the VG ZAB-2F mass spectrometer is given in Figure 2.3. There are two field free regions (ffr), each of which contains two collision cells with a deflector electrode placed between the collision cells.

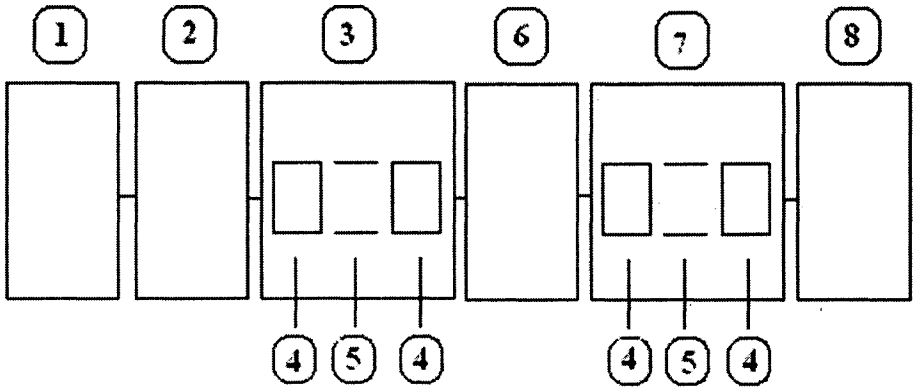


Figure 2.3. Schematic diagram of the modified VG ZAB-2F triple focusing mass spectrometer: (1) ion source, (2) magnet, (3) second field-free region (2 FFR), (4) collision cell, (5) ion beam deflector electrode, (6) electrostatic analyzer (ESA) 1, (7) 3 FFR, (8) ESA 2.

*2.1.1 Charged Particle Motion in an Electric Field*

When a charged particle is moving in the direction of an electric field, it experiences a force. When the electric field is the only significant force acting on the particle, then the particle has an acceleration defined by the following equation; $a = \sum \frac{F}{m} = \frac{q}{m} E$ (2.3), where $E$ is the electric field, $m$ is the mass and $q$ is the fundamental charge ($1.602 \times 10^{-19}$ C) of the particle. The kinetic energy (KE) gained during this process is given by $KE = zV_{acc} = 0.5mv^2$ (2.4), where $V_{acc}$ is the accelerating voltage, $z$ is the number of charges (total charge = $qz$), and $v$ is the ion's velocity. All the charged particles leaving the ion source have essentially the same KE regardless of their mass because they are subjected to a large accelerating voltage (8000 V).

*2.1.2 Electric Sector*

An electric sector consists of two parallel curved metal plates, one at a positive potential and the other at a negative potential of the same magnitude. Like the magnetic sector, the electric sector applies a force perpendicular to the direction of ion motion, and therefore has the form of an arc. Ions in an electric field follow a curved path with radius, $R_e$ that is dependent on the ion's translational kinetic energy. During conventional operation, an electric sector provides no mass separation, rather it separates ions according to their kinetic energy-to-charge ratio. Ions that are accelerated in an electric sector are described in the following equation: $V_{acc} = \frac{E_S R_e}{2}$ (2.5), where $E_S$ is the electric field strength in Volts per meter (V/m) between the plates and $R_e$ is the radius of curvature (flight path).

*2.1.3 Charged Particle Motion in a Magnetic Field*

The motion of a charged particle in a magnetic field is represented in Figure 6. The magnetic force acting on a charged particle is given by; $F_{mag} = qvB = m\frac{v^2}{r}$ (2.6), where $B$ is the magnetic field, r is the radius of curvature and all other parameters are as previously defined. The force is perpendicular to both the magnetic field and the particle's velocity. The magnetic force cannot change the magnitude of the ion's velocity, but it can change the direction of the ion's motion.

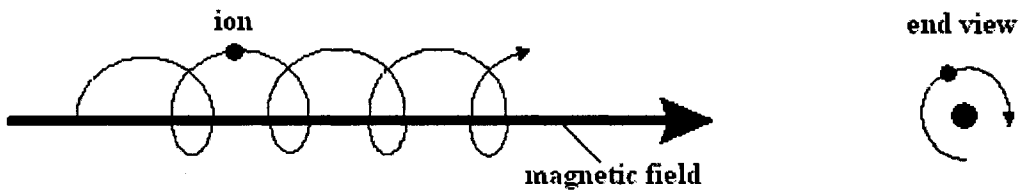


Figure 2.5. The trajectory of a charged particle in the presence of a magnetic field.

*2.1.4 Magnetic Sector*

When a charged particle is subjected to a magnetic field, it is forced to follow a curved trajectory in the plane perpendicular to the magnetic field: $\frac{mv}{z} = Br$ (2.7), where $m$ is the mass of the ion, $v$ is the velocity of the ion, $z$ is its charge, $B$ is the magnetic field strength, and $r$ is the radius of curvature. The magnetic sector analyzer acts as a momentum analyzer, separating ions based on their momentum to charge ratios. When the value for $v$ from equation (2.4) is substituted into equation (2.7) it is apparent that the magnetic sector separates ions based on the $m/z$ ratios; $\frac{m}{z} = \frac{B^2r^2}{2V}$ (2.8). At a given $B$, only ions of one $m/z$ ratio will pass through the central radius of the instrument to reach the detector. $M/z$ ratio is a function of both $B$ and $V_{acc}$, either of which can be varied to change the mass of the ion that follows this trajectory. Scanning $B$ and keeping $V_{acc}$ constant can detect all ions entering the magnetic field.

Detectors include Faraday cups, microchannel plates, photomultipliers and electron multipliers. In an electron multiplier, the sample is bombarded onto a metal plate, which

results in the ejection of electrons. A series of plates are set up so that the ejected electrons will strike the next plate in the series causing even more electrons to be produced and ejected, striking the next plate and so on. In this way the signal produced from the ion can be amplified allowing for better detection. The amplification provided by an electron multiplier under ideal conditions is $2^n$, where n is the number of plates.

*2.2 Mass Spectrometry Experiments*

There are several types of experiments that can be performed on sector mass spectrometers of reverse geometry. Mass-analyzed ion kinetic energy spectrometry [27, 30-32] (MIKES), collision induced dissociation [33-35] (CID), collisionally induced dissociative ionization [36-38] (CIDI), neutralization reionization mass spectrometry [39-42] (NRMS) and kinetic energy release [27] (KER) are some of the important ones.

*2.2.1 MIKES*

There are three types of ions generated in an ion source, stable ions, unstable ions and metastable ions (MIs). Unstable ions dissociate before leaving the ion source while stable ions do not dissociate in the time frame of the experiment and reach the detector intact. MIs fragment after leaving the ion source but before reaching the detector. Their dissociation takes place in the field free region of the mass spectrometer where they are not being acted on by any external forces. MIs make up a small percentage of ions leaving the ion source. Their dissociation takes place on the time frame of a few microseconds, therefore the range of rate constants covered by MI dissociation is ~ $10^3$ – $10^6$ $s^{-1}$, which means that metastable dissociation is a relatively fast process [27]. The

internal energies of metastable ions lie in a relatively narrow range, resulting in only a small number of competing fragmentation reactions being available to the decomposing ion. MIKES spectra of parent ions $m_p^{z_p+}$ (ions of mass $m_p$ and charge state $z_p$) that decay in the 2ffr, according to the following equation,

$$m_p^{z_p+} \rightarrow m_f^{z_f+} + \text{neutral and/or charged particles} \quad (2.9)$$

are monitored as follows; the magnet is set to transmit the desired parent ion while the sector field voltage U of E1 is scanned [43]. If $U_p$ is the voltage required for transmission of a stable parent ion, then the fragment ions, $m_f^{z_f+}$ will be transmitted at an electric sector voltage of $U_f$ according to, $U_f = \frac{m_f z_p}{m_p z_f} U_p$ (2.10). In a similar manner, MIKES spectra are acquired in the 3ffr. In this case both the magnet and the electric sector voltage of E1 are set to transmit stable parent ions and the sector voltage of E2 is scanned.

*2.2.2 CID*

As the name suggests, in collision induced dissociation [33-35] (CID), the mass selected precursor ion dissociates after a collision with a target gas molecule. The target gas does not participate in the reaction in the traditional sense. The collision between the target gas and the ion results in a conversion of translational energy into the internal energy of the precursor. Since the ion has an increased internal energy there are more dissociative pathways available to the ion than in a MIKES experiment. Selected precursor ions that

are stable and therefore have a lifetime that is longer than the experimental time will undergo dissociation in CID.

CID takes place in a collision cell within the field free region (ffr) between the magnetic sector (B) and the electrostatic sector (E) (see Figure 2.3). A neutral target gas is fed into the collision cell. Single collision conditions occur when there is roughly a ten percent decrease in precursor ion signal intensity [44, 45]. Xenon, helium, argon, nitrogen, and oxygen are all examples of commonly used target gases in CID.

CID can also incorporate a charge reversal [46] process. The basic experiment stays the same, but the polarity is reversed on the detector in order to detect the anions that were generated ($M^+ + 2e^- \rightarrow M^-$) from the collision process. A CID charge reversal can be applied to anions or cations generated in the ion source, i.e. +CID− or −CID+.

*2.2.3 CIDI*

In collisionally induced dissociative ionization [36-38] (CIDI), a deflector electrode is used to expel all ions from the ffr (see Figure 2.3). The neutrals pass through the deflector region and are then collided with an appropriate target gas in the collision cell to induce ionization and fragmentation. This type of experiment is used to study the neutral species made during the dissociation of metastable ions. CIDI is the process of ionizing metastably generated neutrals. The first part of the CIDI experiment is basically the same as a MIKES experiment. A selected precursor is allowed to fragment metastably then a voltage is applied to a deflector in the field free region to deflect all

ions away. At this point only the neutrals, unaffected by the deflector, are passing through the ffr to the next collision cell. A collision gas is then used to ionize and fragment all the neutrals that were formed from the MI processes. This experiment allows one to determine the neutral species and their structures being generated from the MI processes. It is a complementary experiment to CID, which gives structural information about ions.

*2.2.4 NRMS*

Neutralization reionization mass spectrometry [39-42] (NRMS) involves an electron transfer between the ions and a target gas (e.g. Xe, He or $O_2$, etc.). The neutralization takes place in the first of two collision cells, while the reionization takes place in the second collision cell (see Figure 2.3). Between the two collision cells a voltage is applied to a deflector electrode to ensure that only neutral molecules can pass, as any ions would be deflected away. Reionization involves another collision with an appropriate target gas to collisionally excite the neutrals back into ions. This type of experiment is conducted to study the stability of the neutral species with the same structure as the corresponding ions that they were made from. A charge reversal $^{+}$NRMS$^{-}$ experiment can also conducted. The experiment stays the same as in the traditional NRMS experiment, but the polarity of the detector is reversed to detect the anionic counterpart of the neutral being studied.

*2.2.5 KER MS*

During metastable ion dissociation, excess internal energy in the ionic and neutral products can be partitioned partially into translational energy. This extra translational

energy results in peak broadening. Two common peak shapes observed MIKES spectrum are Gaussian and dished shaped. The peaks get wider as the KER increases, going from narrow Gaussian, to wide Gaussian, eventually leading to peaks that dish shaped. The dish shaped top is due to the detector slit being of finite length. Any ions that are deflected in the vertical direction (as opposed to horizontal deflection) may fail to reach the detector. The KER for a typical metastable process, $AB^+ \rightarrow A^+ + B$, can be calculated according to the following equation [27]

$$T_{0.5}(meV) = \frac{m_{AB^+}(w_{0.5,A+}^2 - w_{0.5,AB^+}^2)}{16V_{acc}(m_{A^+}m_B)}, \qquad (2.11)$$

where $m_{AB^+}$, $m_{A^+}$, $m_B$ are the masses of the parent ion, fragment ion and neutral lost, $V_{acc}$ is the accelerating voltage (8000 V) and $w_{0.5,A^+}$ and $w_{0.5,AB^+}$ are the peak widths at half height of the fragment ion and parent ion (main beam). This equation needs to be modified slightly when considering a doubly charged parent ion. A doubly charged ion feels twice the field strength as a singly charged ion so the peak widths of the doubly charged ions must be multiplied by a factor of two. In the case of the doubly charged parent ion, there are two possible fragmentation pathways as illustrated in equations 2.12 and 2.13.

$$m_1^{++} \rightarrow m_2^+ + m_3^+ \qquad (2.12)$$

$$m_1^{++} \rightarrow m_2^{++} + m_3 \qquad (2.13)$$

The parent can break apart into two singly charged daughter ions (2.12), or it can lose a neutral and produce a doubly charged daughter (2.13). The equation to calculate the KER of a doubly charged ion losing a neutral and producing a doubly charged daughter ion is as follows,

$$T_{0.5} = \frac{m_1^2((2w_{0.5,2}^2) - (2w_{0.5,1}^2))}{16V_{acc}(m_2 m_3)}. \quad (2.14)$$

When the doubly charged precursor produces two singly charged daughter ions (need to calculate separately for each daughter), the equation becomes,

$$T_{0.5} = \frac{m_1^2(w_{0.5,2}^2 - (2w_{0.5,1}^2))}{16V_{acc}(m_2 m_3)}. \quad (2.15)$$

However, in the case of dish shaped peaks, the distance between the horns ($w_h$) is used instead of the peak width at half height, $w_{0.5}$ [32]. Equation 2.15 then becomes

$$T_h = \frac{m_1^2(w_{h,2}^2 - (2w_{0.5,1}^2))}{16V_{acc}(m_2 m_3)}. \quad (2.16)$$

$T_h$ provides a good approximation to the minimum kinetic energy release ($T_{min}$), $T_h \approx T_{min}$.

When the peak shape is Gaussian, the average kinetic energy released $\langle T \rangle$ can be approximated by $\langle T \rangle = T_{0.5} * 2.16$. (2.17)

This relationship only holds true when the peak has an exact Gaussian profile, which isn't always the case [32, 47]. An empirical procedure suggested by Holmes can be used to determine if the peak shape is purely Gaussian [48].

*2.3 Experimental Procedures*

Tandem mass spectrometry experiments were carried out on a modified VG ZAB mass spectrometer (Figure 2.3) consisting of a magnetic sector followed by two electrostatic analysers (BEE geometry) [29]. Mass analyzed ion-kinetic energy spectra (MIKES) and collision-induced dissociation mass spectra were obtained in the second and third field-free regions of the instrument by the normal procedures [49]. Helium or oxygen target gases were employed in CID experiments with a collision cell pressure sufficient to reduce the precursor ion flux by 10 to 20 %. Neutralization-reionization mass spectra [50] employed $O_2$ in both the neutralization and reionization collision cells and a deflector voltage of +500 V. Charge reversal mass spectra [46] also employed $O_2$ target gas.

Dications were generated by charge stripping MS in the 2 ffr using $O_2$ as a target gas. The dications were then transmitted to the 3ffr where a MIKES MS was obtained and the KER was measured for all observed metastable decompositions.

*2.4 Unimolecular Reactions and RRKM theory*

The statistical theory of unimolecular reactions is known as RRKM theory and is named for the four scientists that developed it: Rice, Ramsperger, Kassel and Marcus. There are both classical and quantum mechanical versions of this theory. It is an extension of RRK theory and Lindeman and Hinshelwood theory. Lindemann proposed that reactant molecules in a thermal system are energized by collisions and that the mechanism for the reaction can be expressed as

$$A + M \xrightarrow{k_1} A^* + M \text{ , (2.18)}$$

$$A^* + M \xrightarrow{k_{-1}} A + M \text{ , (2.19)}$$

$$A^* \xrightarrow{k_2} Pdts \text{ , (2.20)}$$

where A* represents the molecule with a sufficient amount of energy to react [51]. The overall rate of product formation is given by

$$k_{uni}[A] = k_2[A^*] = \frac{k_1 k_2 [A][M]}{k_{-1}[M] + k_2}. \tag{2.21}$$

$k_{uni}$ changes from second order in A and M at low pressures where $k_{-1}[M] << k_2$ to first order in [A] at high pressures where the rate constant is simply [51]

$$k_\infty = \frac{k_1 k_2}{k_{-1}}. \tag{2.22}$$

RRK theory operates on the basis that a molecule can be viewed as an assembly of $s$ identical harmonic oscillators that freely exchange energy. There is one oscillator known as the critical oscillator ($\nu$), which is associated with the reaction coordinate that leads to reaction once the appropriate amount of energy ($E$) has been attained in this configuration. The energized molecule contains a total of $n$ quanta so that its energy is $E = nh\nu$ (2.13), $h$ is Planck's constant. The total number of ways to distribute the $n$ quanta among the $s$ oscillators is given by:

$$W(E) = \frac{(n+s-1)!}{n!(s-1)!}, \tag{2.23}$$

and the total number of ways that a particular distribution leads to a reaction (the number of quanta in the critical oscillator that ranges from $m$ to $n$) is given by:

$$G(E) = \frac{(n+s)!}{n!s!}, \tag{2.24}$$

with a maximum of *n-m* quanta in the remaining *s-1* oscillators being given by:

$$\frac{(n-m+s-1)!}{(n-m)!(s-1)!}. \tag{2.25}$$

The probability that the critical oscillator has energy equal to or above the critical energy ($E \geq E_0$) for reaction is the ratio of *W(E)* (related to the sum and density of states) to *G(E)* (sum of states) given by:

$$probability = \frac{(n-m+s-1)!n!}{(n-m)!(n+s-1)!}, \tag{2.26}$$

where $n$ is the total number of vibrational quanta and $m$ is the number of quanta in the critical oscillator for dissociation to occur ($m = E_0/h\nu$). This is the quantum mechanical expression since the vibrations are treated as discrete energy levels. This probability multiplied by the frequency of passing through the transition state, $\nu$, converts equation 2.26 into a rate constant. When the number of quanta, $n$ is much greater than the number of oscillators, $s$, the rate constant is given by:

$$k(E) \approx \nu(\frac{n-m}{n})^{s-1} = \nu(\frac{E-E_0}{E})^{s-1}. \tag{2.27}$$

The RRK rate constant depends on the number of degrees of vibrational freedom in the molecule as well as the energy in excess of the critical energy (or activation energy), $E_0$. The rate constant increases with increasing energy and decreases as the number of oscillators, $s$ increases. The larger the number of $s$ the more ways there are of distributing the energy, thereby decreasing the chance of the energy being in the critical oscillator. In the high pressure limit both the classical and quantum RRK expressions for $k_{uni}$ become the Arrhenius equation,

$$k_\infty = \nu e^{(-E_0/k_BT)}. \tag{2.28}$$

RRKM theory was developed using the RRK model and extending it to include vibrational and rotational energies as well as zero point energies [52]. However, in the simplest version, the RRKM rate equation only takes into consideration vibrations and ignores the rotations. As opposed to RRK theory where all harmonic oscillators are treated identically, RRKM theory treats each oscillator independently. The RRKM rate constant for a molecule at energy $E$ and with activation energy $E_0$, is given by:

$$k(E) = \frac{\sigma N^{*}(E - E_0)}{h\rho(E)}, \tag{2.29}$$

where $E_0$ is defined as dissociation $E$ at 0K, $\sigma$ is the reaction degeneracy, $N^{\ddagger}(E\text{-}E_0)$ is the transition state sum of states from 0 to $E\text{-}E_0$, $h$ is Planck's constant, and $\rho(E)$ is the parent ion density of states at energy $E$. The reaction degeneracy, $\sigma$ is added to the equation to account for errors in $N^{\ddagger}(E\text{-}E_0)$ and $\rho(E)$, which are calculated ignoring reactant and transition state symmetries. The minimum rate for a unimolecular reaction is at $E=E_0$ and is given by

$$k_{\min} = \sigma \frac{1}{h\rho(E_0)}. \tag{2.30}$$

Figure 2.6 shows a potential energy surface (PES) for a reaction with a saddle point due to reverse activation energy.

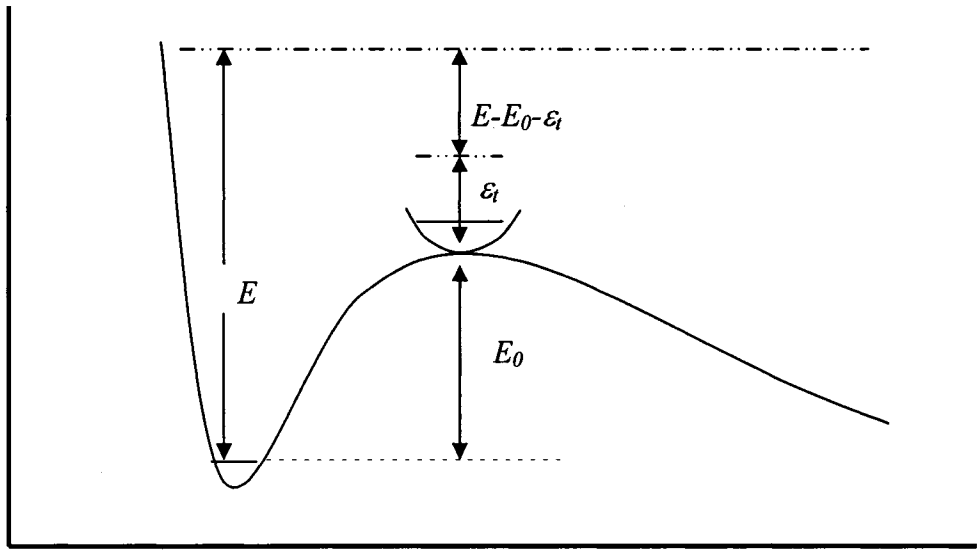


Figure 2.6. Reaction coordinate for dissociation with a real barrier. $E$ and $E_0$ are the total ion energy and the activation energy, $\varepsilon_t$ is the translational in the reaction coordinate. $E$-$E_0$-$\varepsilon_t$ is the energy remaining for statistical distribution.

The activation entropy, $\Delta S^{\ddagger}$ can be determined from the vibrational frequencies of the transition state and reacting ion as defined by the following equation,

$$\Delta S^{\ddagger} = k_B \ln \frac{Q^{\ddagger}}{Q} + \frac{U^{\ddagger} - U}{T} = k_B \ln \frac{\Pi q_i^{\ddagger}}{\Pi q_i} + \frac{U^{\ddagger} - U}{T}, \qquad (2.31)$$

where $Q$ is the total partition function $q1q2q3\ldots$,

$$q_i = \frac{1}{1 - \exp(-h\nu_i / k_B T)} \qquad (2.3.2)$$

and $U$ is the average internal energy. The average internal energies ($U$ and $U^{\ddagger}$) can be calculated using the vibrational partition functions.

When the transition state is more ordered than the reacting ion, the transition state is 'tight' and $\Delta S^{\ddagger}$ is negative. When $\Delta S^{\ddagger}$ is positive, the transition state is less ordered than

the reacting ion and said to be 'loose'. Loose transition states are associated with simple bond cleavages and tight transition states are associated with rearrangement processes.

$E_0$ and $\Delta S^{\ddagger}$ have complementary effects on the rate constant as a function of energy, *k(E)*. When the log of *k(E)* is plotted as a function of *E*, $E_0$ is responsible for the magnitude of *k(E)*, while $\Delta S^{\ddagger}$ is responsible for the slope of the line. For a reaction with a tight transition state ($\Delta S^{\ddagger} < 0$), the *k(E)* curve increases gradually with increasing energy, while for reactions with loose transition states ($\Delta S^{\ddagger} > 0$), the *k(E)* curves increase more rapidly with increasing energy.

## *2.5 Computational chemistry*

### *2.5.1 The Schrödinger Equation*

The Schrödinger equation is a differential equation used in the *ab initio* prediction of molecular structure and energy. There are time-dependent and time-independent forms of the Schrödinger equation. The time-independent Schrödinger equation for one dimension is given by

$$\frac{-\hbar^2}{2m}\frac{\partial^2\Psi(x)}{\partial x^2} + U(x)\Psi(x) = E\Psi(x), \qquad (2.33)$$

where $U(x)$ is the potential energy, $\Psi(x)$ is the wavefunction, $E$ is the system energy, $m$ is the mass of the particle, $x$ is its position and $h$ bar is the reduced Plank's constant ($h/2\pi$). The time-independent Schrödinger is easily converted to three dimensions and often used with spherical polar coordinates. The Schrödinger equation is often written in shorthand notation, $\hat{H}\Psi = E\Psi$ (2.34). The Hamiltonian operator, $\hat{H}$ is the sum of the kinetic and potential energy operators. The equation has solutions $\Psi_i$ that are wavefunctions of the operator $\hat{H}$ and eigenvalues $E_i$ that are allowed quantized total energies of the system.

All molecular orbital calculations are approximate solutions of the Schrödinger partial differential equation. Each level of theory used to approximate solutions to the Schrödinger equation consists of two main components, a method of treating electron correlation and a basis set used to describe the molecular orbitals.

### 2.5.2 *Basis functions*

Molecular orbitals are usually expanded in terms of a set of atomic orbitals, which is known as the linear combination of atomic orbital approximation. The molecular orbitals $\psi_i$, are restricted to being linear combinations of a set of N known one-electron basis functions $\phi_1$ (x,y,z), $\phi_2$(x,y,z), ..., $\phi_N$ (x,y,z):

$$\psi_i = \sum_{u=1}^{N} c_{ui}\phi_u \,, \qquad (2.35)$$

where $c_{ui}$ are unknown coefficients that are determined so as to minimize the total electronic energy calculated from $\Psi$. The one-electron basis functions constitute a basis set. The atomic orbitals were initially represented by Slater type orbitals (STOs). Later Gaussian type orbitals (GTOs) were used to approximate the STOs. Today there are many basis sets composed of GTOs, the smallest of which are referred to as minimal basis sets. Minimal basis sets contain the minimum number of basis functions needed to represent all of the electrons on each atom. A common addition to the minimal basis sets is the addition of polarization functions, for example (2df,p) indicates that the heavy atoms containing p valence orbitals had 2 d and 1 f type functions added while the light atoms had a p function added. The addition of polarization gives added flexibility within the basis set. Diffuse functions can also be added to minimal basis sets. The addition of diffuse functions to the heavy atoms is denoted by +, while ++ indicates that diffuse functions have also been added to the light atoms.

Since it is the valence electrons that mainly take part in the bonding, it is common to represent valence orbitals by more than one basis function. Each basis function is in turn composed of a fixed linear combination of primitive Gaussian functions. The notation for

a split-valence double-zeta basis sets is typically *X-YZg*, where *X* represents the number of primitive Gaussians making up each of the core atomic orbitals and the *Y* and *Z* specifies that the valence orbitals are composed of two basis functions each, the first one containing a linear combination of *Y* primitive Gaussians, and the second one a linear combination of *Z* primitive Gaussians. There are also triple-zeta basis sets, for example the basis set 6-311G indicates that the core orbitals are represented by 6 Gaussian functions and that the valence orbitals are each made up of three basis functions, composed of a linear combination of 3, 1, and 1 Gaussian functions, respectively.

### *2.5.3 Electron correlation*

Electron correlation refers to the interaction of the electrons in a quantum system. Several different levels of electron correlation were used in this study, Hartree-Fock [53] (HF), Møller-Plesset [53-55] (MP), coupled cluster [54, 56] (CC), quadratic configuration interaction [54, 57] (QCI) and density functional theory [58] (DFT).

#### *2.5.3.1 Hartree Fock (self-consistent field theory)*

Hartree-Fock (HF) theory is also called self-consistent field theory because the HF-orbitals are solved iteratively until the change in total electronic energy falls below a predefined threshold. The Fock operator depends on the orbitals used to construct it; the eigenfunctions of the Fock operator are in turn new orbitals that can be used to construct a new Fock operator. In this way a set of self-consistent one-electron orbitals are calculated and the HF wavefunction is the Slater determinant made from these orbitals. HF theory is used to determine the ground state wavefunction and energy of a quantum

system by giving an approximate solution to the electronic (time-independent) Schrödinger equation. Electron correlation is completely ignored meaning that electrons move independently of each other and that each electron sees the average charge distribution of all the other electrons and not the instantaneous electron-electron repulsions. The error introduced in the wavefunction because of electron correlation is called the total correlation energy. The correlation energy is defined as the difference between the true energy and the best possible HF energy obtained with a complete basis (Hartree-Fock limit), $E_{corr} = \varepsilon_{exact} + E_{HF}^{\infty}$ (2.36). HF theory will always yield energies that are higher than the true energy of the system.

*2.5.3.2 Møller-Plesset perturbation theory*

Møller-Plesset perturbation theory (MP) offers an improvement over HF methods by including electron correlation effects using perturbation theory, generally to the second (MP2), third (MP3) or fourth order (MP4). First a generalized electronic Hamiltonian, $\hat{H}_\lambda$ is introduced; $\hat{H}_\lambda = \hat{H}_0 + \lambda\hat{V}$ (2.37), where $\hat{H}_0$ is a Fock operator and $\lambda\hat{V}$ is the perturbation. The perturbation is defined as $\lambda\hat{V} = \lambda(\hat{H} - \hat{H}_0)$ (2.38), where $\hat{H}$ is the correct Hamiltonian and $\lambda$ is a dimensionless parameter. When $\lambda = 1$, $\hat{H}_\lambda = \hat{H}$ and when $\lambda = 0$, $\hat{H}_\lambda = \hat{H}_0$. When the perturbation is small, the wavefunction and energy can both be written as a power series in $\lambda$; $\Psi = \lim_{n\to\infty}\sum_{i}^{n} \lambda^i \Psi^{(i)}$ (2.39) and $E = \lim_{n\to\infty}\sum_{i}^{n} \lambda^i E^{(i)}$ (2.40). Substituting equations (2.38) and (2.39) into the time-independent Schrödinger equation gives; $(\hat{H}_0 + \lambda\hat{V})(\sum_{i}^{n} \lambda^i \Psi^{(i)}) = (\sum_{i}^{n} \lambda^i E^{(i)})(\sum_{i}^{n} \lambda^i \Psi^{(i)})$ (2.41). The first order (n=1)

solution gives the HF wavefunction and energy, so it is necessary to go beyond first order. Møller-Plesset calculations to the second (MP2), third (MP3), and fourth order (MP4) are typical levels used in calculations.

*2.5.3.3 Configuration interaction*

Configuration interaction (CI) uses a variational wavefunction that is analogous to HF theory. A trial wavefunction is written as a linear combination of determinants with the expansion coefficients calculated to minimize the E. The molecular orbitals used for building excited Slater determinants are taken from a HF calculation and held fixed. S, D, and T indicate determinants that are singly, doubly, and triply excited relative to the HF configuration, $\Psi_{CI} = a_0\Phi_{HF} + \sum_S a_S\Phi_S + \sum_D a_D\Phi_D + \sum_T a_T\Phi_T + \ldots = \sum_{i=0} a_i\Phi_i$ (2.42). The CI energy needs a quadratic modification to be size consistent. Quadratic configuration interaction (QCI) is a modified version of CI that adds a quadratic term to the energy calculation to give size consistency. QCISD and QCISD(T) give similar results to CCSD and CCSD(T), respectively.

*2.5.3.4 Coupled Cluster*

The wavefunction of coupled cluster (CC) theory is written as an exponential ansatz; $|\Psi\rangle = e^{\hat{T}}|\Phi_0\rangle$ (2.43), where $|\Phi_0\rangle$ is a Slater determinant constructed from HF MOs, $\hat{T}$ is the excitation (cluster) operator that produces a linear combination of excited Slater determinants when acting on $|\Phi_0\rangle$. The cluster operator can be written as, $\hat{T} = \hat{T}_1 + \hat{T}_2 + \hat{T}_3 + \ldots$ (2.44), where $\hat{T}_1$ is the operator for all single excitations, $\hat{T}_2$ is the

operator for all double excitations and so on. $\hat{T}_1$ and $\hat{T}_2$ convert the reference function, $|\Phi_0\rangle$ into a linear combination of the singly- and doubly-excited Slater determinants, respectively. The exponential operator, $e^{\hat{T}}$ can be expanded into a Taylor series; $e^{\hat{T}} = 1 + \hat{T} + \frac{\hat{T}^2}{2!} + \frac{\hat{T}^3}{3!} + \ldots$ (2.45). The expansion of $\hat{T}$ into individual excitation operators is generally stopped at the second (CCSD) or third level (CCSD(T)) of excitation.

*2.5.3.5 Density Functional Theory (DFT)*

In density functional theory (DFT), the electrons and their wavefunctions are calculated using electron density rather than MOs. DFT methods use functionals to treat electron correlation and electron exchange. Density functional theory is based on the notion that the density is uniquely determined given a potential, and vice versa. In other words, all properties are a functional of the density, because the density determines the potential, which determines the Hamiltonian, which determines the energy ($E[\rho]$) and the wave function ($\Psi[\rho]$), from which all physical properties can be determined [59]. Some common DFT methods are B-LYP, B3-LYP, and B3-PW91. B-LYP uses Becke's electron exchange functional [60] and an electron correlation functional developed by Lee, Yang, and Par [61]. B3-LYP and B3-PW91 both use the exchange functional developed by Becke [62] that is a hybrid between HF and DFT. B3-LYP is between HF and MP2 in terms of speed and computational resource usage, however, its electron correlation treatment is as good as that of MP2.

*2.5.3.6 G3 Composite method*

G3 [63] theory is the third in a series of methods known as Gaussian-n theories proposed for the calculation of energies of molecules containing the elements H-Cl. The Gaussian-n theories are composite techniques that involve performing a series of single point calculations on a molecular structure initially optimized at the HF/6-31G(d) level of theory. The zero point energy (ZPE) at this level is used scaled by a factor of 0.8929. This equilibrium geometry is then refined at the MP2(full)/6-31G(d) level where the full denotes that both core and valence electrons for the calculation of correlation energy. A series of higher level single point calculations are then performed to account for corrections for diffuse functions, polarization functions, correlation effects beyond the fourth order perturbation theory and finally a correction for larger basis set effects as defined in equations 2.46 through 2.49, respectively .

$$\Delta E(+) = E[MP4/6-31+G(d)] - E[MP4/6-31G(d)] \qquad (2.46)$$

$$\Delta E(2df,p) = E[MP4/6-31G(2df,p)] - E[MP4/6-31G(d) \qquad (2.47)$$

$$\Delta E(QCI) = E[QCISD(T)/6-31G(d)] - E[MP4/6-31G(d)] \qquad (2.48)$$

$$\begin{aligned}\Delta E(G3l\arg e) &= E[MP2(full)/G3l\arg e] \\ &- E[MP2/6-31G(2df,p)] - E[MP2/6-31+G(d)] + E[MP2/6-31G(d)]\end{aligned} \qquad (2.49)$$

The MP4/6-31G(d) energy and the four corrections in equations 2.46 to 2.49 are added together along with a spin orbit correction (for atomic species only),

$$\begin{aligned}E(combined) &= E[MP4/6-31G(d)] + \Delta E(+) + \Delta E(2df,p) + \Delta E(QCI) \\ &+ \Delta E(G3l\arg e) + \Delta E(SO).\end{aligned} \qquad (2.50)$$

The higher level correction (HLC) is then added to *E(combined)* to account for the remaining deficiencies in the energy calculations,

$$E_e(G3) = E(combined) + E(HLC). \qquad (2.51)$$

The HLC is defined as $-An_\beta\text{-}B(n_\alpha\text{-}n_\beta)$ for molecules and $-Cn_\beta\text{-}D(n_\alpha\text{-}n_\beta)$ for atoms, where $n_\alpha$ and $n_\beta$ are the number of $\alpha$ and $\beta$ valence electrons and A, B, C, and D are constants chosen from the G2/97 test set [64, 65] to give the lowest standard deviation from experiment. Finally the ZPE is added to give the total energy at 0K,

$$E_0(G3) = E_e(G3) + E(ZPE). \qquad (2.52)$$

The final total energy ($E_0$(G3)) is effectively at the QCISD(T,FULL)/G3large level of theory.

## *2.6 Computational Procedures*

Standard *ab initio* molecular orbital calculations [53] were carried out using the GAUSSIAN 98 [66] suite of programs. Geometries were optimized (and vibrational frequencies calculated) with several electron correlation treatments (HF, ROHF, B3-PW91, B3-LYP, MP2, ROMP2, CCSD, QCISD, CCSD(T) and QCISD(T)) using a variety of basis sets. Single point energies on selected optimized geometries were obtained at the G3 level of theory [28] using a small modification. Instead of calculating optimized geometries using MP2(FU)/6-31G(d) and ZPEs using HF/6-31G(d) (scaled by a factor of 0.8929), geometries were optimized at six different levels of theory (both B3-LYP and MP2 using basis sets 6-31+G(d), 6-311+G(d) and 6-311+(2df,p)) and ZPEs corresponding to each of the respective levels of theory. Scaling factors for the zero-point energy (ZPE) values were those recommended by Scott and Radom [67]. If a basis set was not in the previously mentioned paper, the scale factor for the next closest match was used. Heats of formation at 0 K were calculated by the atomization method [68], using the experimental heats of formation of the constituent atoms [63]. The connection

between a transition state structure and its reactants and products was established at the G3//B3-LYP/6-311+G(d) level of theory by the intrinsic reaction coordinate [69, 70] (IRC) calculations as coded in GAUSSIAN 98 [66].

$CH_3BH^{\dagger+}$ and $CH_2BH_2^{\dagger\bullet}$ are calculated to have $C_{3V}$ and $C_{2V}$ symmetry, respectively, at most levels of theory employed in this study. However, it proved impossible to optimize these high symmetry species at CCSD, QCISD(T), CCSD(T) (and QCISD for $CH_2BH_2^{\dagger\bullet}$) using Gaussian 98, the symmetry always lowering, sometimes to $C_1$. At the precision of the geometric parameters quoted in the tables in this thesis $CH_3BH^{\dagger+}$ and $CH_2BH_2^{\dagger\bullet}$ appear to be $C_{3V}$ and $C_{2V}$ but the lower symmetry designation has been retained according to the output of the calculations. Fang and Peyerimhoff quote a $C_{2V}$ symmetry for $CH_2BH_2^{\dagger\bullet}$ at the QCISD level of theory using Gaussian 94 [11]. For the purposes of investigating the observability of these species in the gas phase, the exact nature of their symmetry is irrelevant as there are no energy consequences from the above symmetry changes.

*Chapter 3. Results and discussion*

*3.1 Selecting an appropriate level of theory for calculating the properties of B-containing ions and radical.*

A strategy for selecting an appropriate level of theory with which to study a set of ions is outlined in the book by Holmes, et al [71]. It involves five basic steps, selecting a prototypic set of ions, followed by an assessment of geometry, zero point energy, relative energy and absolute thermochemistry calculated at different levels of theory. The set of ions selected for the assessment should be chemically equivalent and smaller than the target set of ions.

The geometry assessment involves two steps. First, the ion's structure should be optimized using a wide range of basis sets differing from the previous set by one factor at HF, MP2, B3LYP (see Figures 3.3 and 3.4). In this way, the effect of basis set size can be examined and it can be determined which factors are important for describing the MOs. In the next geometry assessment step, one basis set is chosen and then optimized using several different electron correlation treatments (Figure 3.5). It is assumed that CCSD(T) and QCISD(T) are the best in terms of electron correlation and that 6-311+G(3df,2p) gives the best molecular orbital description. The lowest level of theory that comes close to that obtained using the best electron correlation and the best basis set should be chosen for the target ion study. The geometric assessment is provided in section 3.2 and considers each of the five isomeric species separately.

In the ZPE assessment, which is given in section 3.3, it is important to ensure that the level of theory selected in the geometry assessment has ZPE values that are consistent with the best ZPE values. The ZPE themselves need to be scaled as described in section 2.5.

The relative energies obtained at the different levels of theory should also be compared to see which are in best agreement with the higher levels of theory. Finally an assessment of absolute thermochemistry is needed. This assessment involves comparing the best relative energies and heats of formation using one or several composite methods. This shows the sensitivity of the heat of formation on the level of theory used in the initial geometry optimization. If possible, a comparison with reliable experimental data should also be made at this point. An assessment of relative energy and absolute thermochemistry is provided in section 3.4.

### *3.2 Determination of an appropriate level of theory at which to optimize the geometries of $CH_4B$ ions and radicals*

Optimized values for selected geometric parameters for the cation, anion and radical isomers of $CH_4B$ are listed in Tables 3.1-3.6 according to structure definitions provided in Fig 3.1.

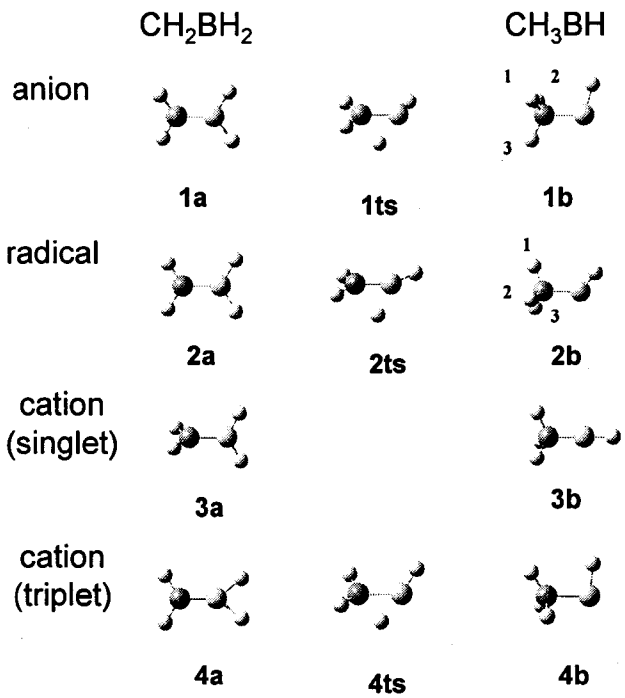


Figure. 3.1. Structures of the $CH_2BH_2$ and $CH_3BH$ cation, anion and radical isomers and their transition states.

Figures 3.2 and 3.3 show the effect of basis set size at the HF level and higher levels of correlation treatments, respectively. Figure 3.4 shows the effect of electron correlation using the 6-31+G(d) basis set. Only one representative isomer has been selected for each figure, while those for the other structures have not been included. Each isomer is discussed separately in their respective sections.

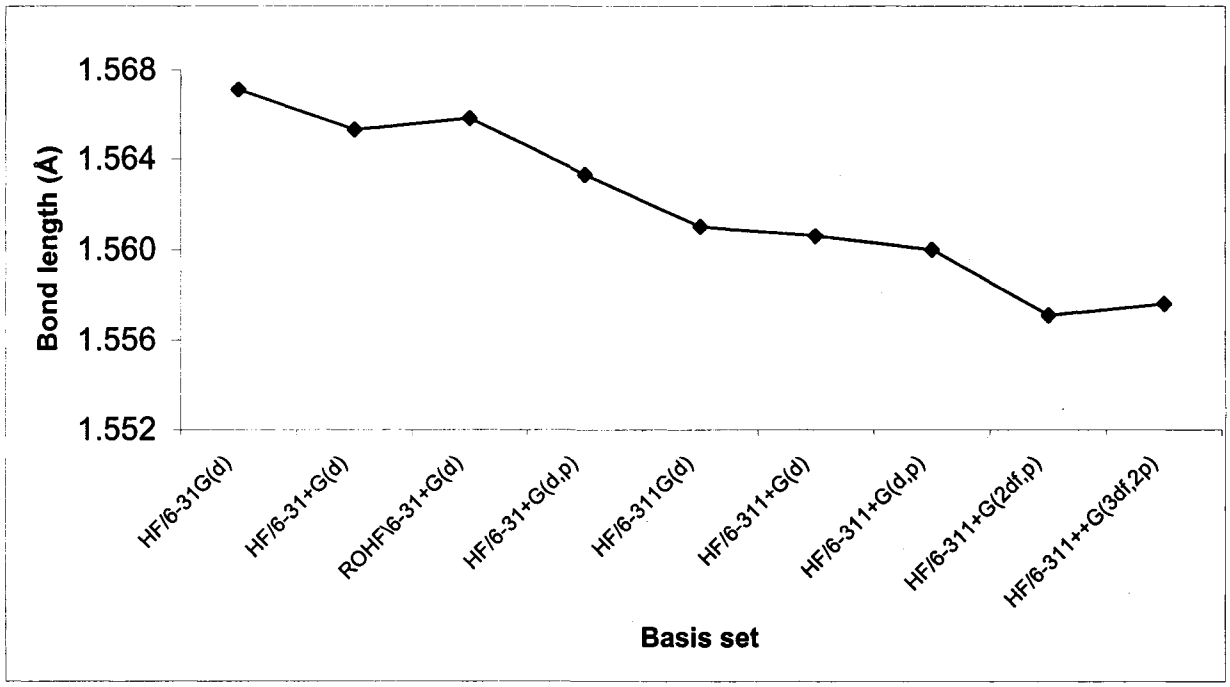


Figure 3.2. The effect of basis set size using electron correlation at the HF level on the C—B bond length of the $CH_3BH^{\bullet}$ isomer.

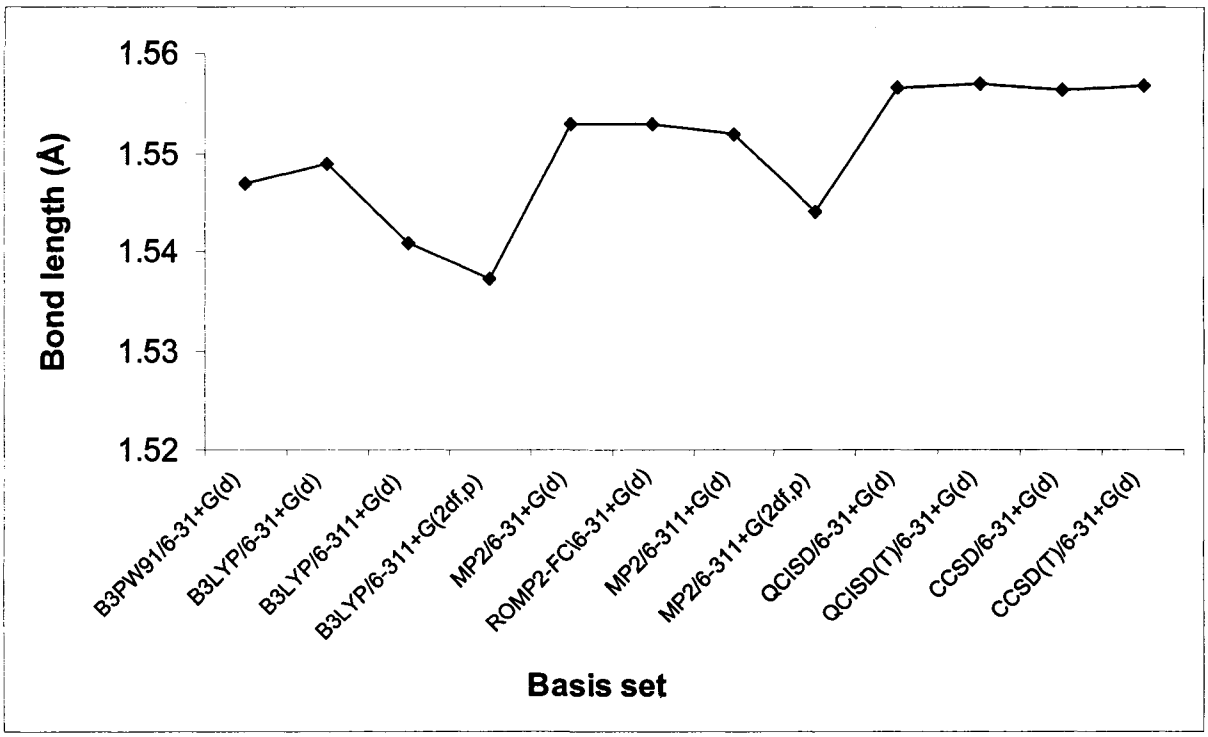


Figure 3.3. The effect of basis set size using higher levels for the treatment of electron correlation on the C—B bond length of the $CH_3BH^{\bullet}$ isomer.

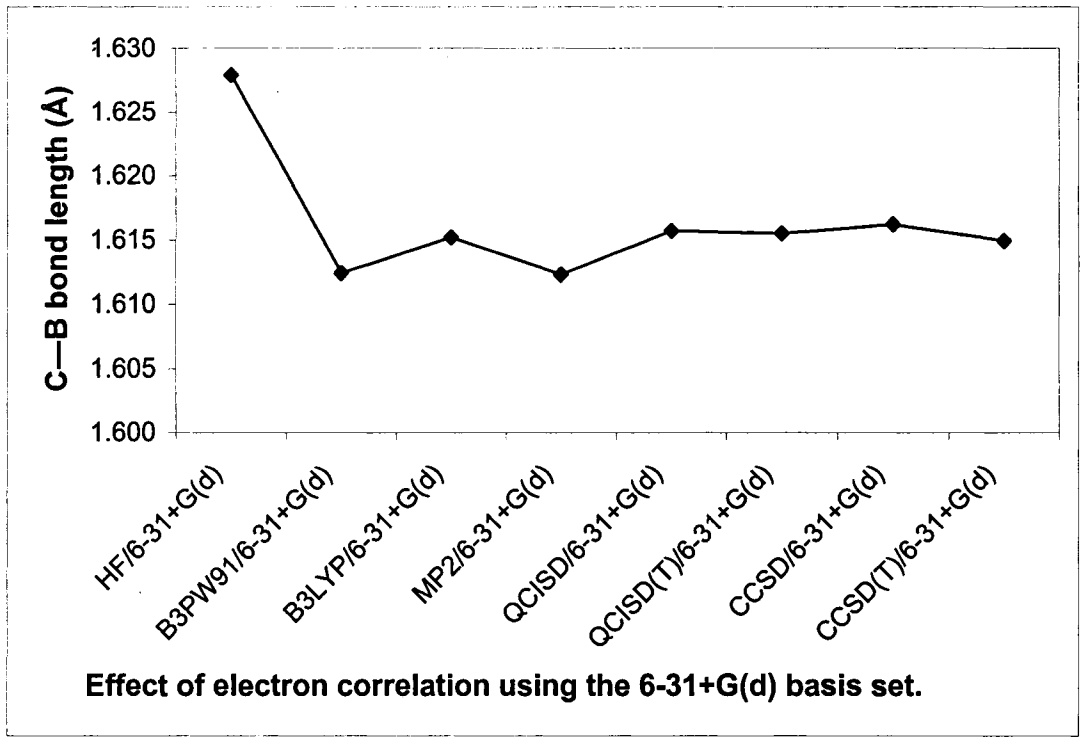


Figure 3.4. Effect of electron correlation treatment using the 6-31+G(d) basis set on the C—B bond length of the $CH_3BH^-$ isomer.

### 3.2.1. $CH_3BH^-$

Table 3.1 shows that all levels of theory give $C_1$ symmetry since the three carbon hydrogen bonds are not equivalent. The lone pair of electrons is located on boron, so this anion is stabilized by their interaction with the vacant pseudo-$\pi^*$ orbital on the methyl group. At the HF level, addition of diffuse functions to the double-zeta and triple-zeta valence basis sets results in a large change in geometry as is expected for anions. The C—B and B—H bonds are both shortened by 0.04 Å for the double-zeta valence basis set and 0.026 Å and 0.035 Å, respectively, for the triple-zeta valence basis set. There is a small change in geometry with the addition of polarization functions. The B3-LYP, B3-PW91, and MP2 levels of theory all yield similar geometric parameters when using the 6-31+G(d) basis set (Figure 3.4). Interestingly the 6-311+G(d) basis set has the effect of slightly lengthening the C—B and B—H bonds relative to the 6-31+G(d) basis set at the MP2 level of theory, but shortening them when using the B3-LYP level of theory. The addition of polarization (6-311+G(2df,p)) to the basis set at both these levels of theory has the effect of shortening the bond lengths. The QCISD and CCSD levels of theory give very similar results to each other. The geometries are not greatly affected by the addition of the triples excitation with either of these levels of theory. B3-LYP is the best at reproducing both the CCSD(T) and QCISD(T) results.

Table 3.1.
Selected optimized geometric parameters for $CH_3BH^-$.[a]

| Method | Sym | r(CB) | $r(CH_1)$ | $r(CH_2)$ | $r(CH_3)$ | r(BH) | a∠(CBH) | d∠($H_1$CBH) |
|---|---|---|---|---|---|---|---|---|
| Effect of Basis Set | | | | | | | | |
| HF/6-31G(d) | $C_1$ | 1.669 | 1.100 | 1.101 | 1.096 | 1.278 | 99.6 | 51.0 |
| /6-31+G(d) | $C_1$ | 1.628 | 1.100 | 1.100 | 1.085 | 1.236 | 105.3 | 58.0 |
| /6-31+G(d,p) | $C_1$ | 1.626 | 1.100 | 1.100 | 1.085 | 1.236 | 105.5 | 58.0 |
| /6-311G(d) | $C_1$ | 1.649 | 1.100 | 1.100 | 1.092 | 1.272 | 101.2 | 58.3 |
| /6-311+G(d) | $C_1$ | 1.623 | 1.100 | 1.100 | 1.086 | 1.241 | 105.0 | 57.9 |
| /6-311+G(d,p) | $C_1$ | 1.623 | 1.101 | 1.101 | 1.086 | 1.239 | 105.3 | 57.9 |
| /6-311+G(2df,p) | $C_1$ | 1.619 | 1.099 | 1.099 | 1.085 | 1.236 | 105.8 | 57.9 |
| /6-311++G(3df,2p) | $C_1$ | 1.617 | 1.098 | 1.098 | 1.084 | 1.234 | 106.3 | 57.9 |
| B3-LYP/6-31+G(d) | $C_1$ | 1.615 | 1.114 | 1.114 | 1.094 | 1.242 | 105.3 | 51.3 |
| /6-311+G(d) | $C_1$ | 1.606 | 1.112 | 1.112 | 1.093 | 1.241 | 105.0 | 57.6 |
| /6-311+G(2df,p) | $C_1$ | 1.601 | 1.110 | 1.110 | 1.091 | 1.234 | 105.9 | 57.6 |
| MP2/6-31+G(d) | $C_1$ | 1.612 | 1.109 | 1.109 | 1.091 | 1.234 | 105.5 | 55.4 |
| /6-311+G(d) | $C_1$ | 1.613 | 1.107 | 1.108 | 1.091 | 1.239 | 104.7 | 52.0 |
| /6-311+G(2df,p) | $C_1$ | 1.607 | 1.105 | 1.108 | 1.090 | 1.235 | 105.3 | 45.4 |
| Effect of electron correlation [with the 6-31+G(d) basis set] | | | | | | | | |
| HF | $C_1$ | 1.628 | 1.100 | 1.100 | 1.085 | 1.236 | 105.3 | 51.0 |
| B3-PW91 | $C_1$ | 1.612 | 1.112 | 1.113 | 1.095 | 1.246 | 105.3 | 44.4 |
| B3-LYP | $C_1$ | 1.615 | 1.114 | 1.114 | 1.094 | 1.242 | 105.3 | 51.3 |
| MP2 | $C_1$ | 1.612 | 1.109 | 1.109 | 1.091 | 1.234 | 105.5 | 55.4 |
| QCISD | $C_1$ | 1.616 | 1.113 | 1.113 | 1.095 | 1.240 | 105.8 | 57.6 |
| CCSD | $C_1$ | 1.616 | 1.106 | 1.106 | 1.106 | 1.241 | 105.7 | 57.8 |
| QCISD(T) | $C_1$ | 1.616 | 1.115 | 1.115 | 1.096 | 1.241 | 106.0 | 57.7 |
| CCSD(T) | $C_1$ | 1.615 | 1.115 | 1.115 | 1.096 | 1.240 | 106.0 | 57.6 |

[a]Bond lengths in Å, bond angles in degrees.

### 3.2.2. $CH_3BH^{\bullet}$

Similar to the anion, all levels of theory give $C_1$ symmetry for the neutral $CH_3BH^{\bullet}$ species (Table 3.2). This species differs from the anion in that it has a single electron on B rather than a lone pair, so it is stabilized only by the single electron interaction with the pseudo-$\pi^*$ orbital on the methyl group resulting in less antibonding character (and thus shorter) C—B, C—H and B—H bonds. Figure 3.2 shows the change in the C—B bond length with increasing basis set size at the HF level of electron correlation. The C—B bond length seems to converge using the 6-311+G(2df,p) basis set. The addition of diffuse functions to heavy atoms in the double-zeta basis set shortens both the C—B and B—H bonds by only 0.002 Å and 0.001 Å, respectively. When the diffuse functions are added to the triple-zeta basis set there is virtually no change in geometry. The addition of polarization functions results in only minor geometry changes. The QCISD and CCSD results are very similar to each other and are not affected a great deal by the addition of triples excitation. Figure 3.3 shows the change in C—B bond length with increasing basis set at higher levels of electron correlation. From Table 3.2 it is clear that B3-LYP is best at reproducing the CCSD(T) and QCISD(T) results. The exception is the C—B bond, which is best represented by the MP2 level of theory (see Figure 3.3).

The restricted open shell geometries calculated at the HF and MP2 levels of theory are almost identical to the corresponding unrestricted geometries.

Table 3.2.
Selected optimized geometric parameters for $CH_3BH^{\bullet}$.[a]

| Method | Sym | r(CB) | $r(CH_1)$ | $r(CH_2)$ | $r(CH_3)$ | r(BH) | a∠(CBH) | d∠($H_1$CBH) |
|---|---|---|---|---|---|---|---|---|
| Effect of basis set | | | | | | | | |
| HF/6-31G(d) | $C_1$ | 1.567 | 1.091 | 1.084 | 1.091 | 1.191 | 125.4 | 58.0 |
| /6-31+G(d) | $C_1$ | 1.565 | 1.092 | 1.084 | 1.092 | 1.190 | 125.9 | 57.7 |
| /6-31+G(d,p) | $C_1$ | 1.563 | 1.092 | 1.084 | 1.091 | 1.189 | 126.1 | 63.6 |
| /6-311G(d) | $C_1$ | 1.561 | 1.089 | 1.083 | 1.092 | 1.193 | 125.9 | 50.0 |
| /6-311+G(d) | $C_1$ | 1.561 | 1.090 | 1.084 | 1.092 | 1.192 | 126.1 | 49.9 |
| /6-311+G(d,p) | $C_1$ | 1.560 | 1.090 | 1.084 | 1.094 | 1.190 | 126.6 | 46.1 |
| /6-311+G(2df,p) | $C_1$ | 1.557 | 1.089 | 1.083 | 1.093 | 1.189 | 126.6 | 46.1 |
| /6-311++G(3df,2p) | $C_1$ | 1.558 | 1.088 | 1.082 | 1.092 | 1.188 | 126.6 | 45.6 |
| B3-LYP/6-31+G(d) | $C_1$ | 1.549 | 1.102 | 1.095 | 1.106 | 1.197 | 127.5 | 45.4 |
| /6-311+G(d) | $C_1$ | 1.541 | 1.099 | 1.093 | 1.104 | 1.195 | 127.9 | 43.2 |
| /6-311+G(2df,p) | $C_1$ | 1.537 | 1.098 | 1.091 | 1.103 | 1.191 | 128.4 | 41.8 |
| MP2/6-31+G(d) | $C_1$ | 1.553 | 1.098 | 1.092 | 1.102 | 1.194 | 126.8 | 48.2 |
| /6-311+G(d) | $C_1$ | 1.552 | 1.096 | 1.090 | 1.101 | 1.196 | 127.3 | 42.4 |
| /6-311+G(2df,p) | $C_1$ | 1.544 | 1.095 | 1.089 | 1.102 | 1.192 | 127.6 | 39.0 |
| Effect of electron correlation [using the 6-31+G(d) basis set] | | | | | | | | |
| HF | $C_1$ | 1.565 | 1.092 | 1.084 | 1.092 | 1.190 | 125.9 | 57.7 |
| ROHF | $C_1$ | 1.566 | 1.091 | 1.084 | 1.091 | 1.190 | 125.6 | 57.8 |
| B3-PW91 | $C_1$ | 1.547 | 1.101 | 1.095 | 1.106 | 1.199 | 127.5 | 42.3 |
| B3-LYP | $C_1$ | 1.549 | 1.102 | 1.095 | 1.106 | 1.197 | 127.5 | 45.4 |
| MP2 | $C_1$ | 1.553 | 1.098 | 1.092 | 1.102 | 1.194 | 126.8 | 48.2 |
| ROMP2 | $C_1$ | 1.553 | 1.099 | 1.092 | 1.101 | 1.194 | 126.8 | 49.3 |
| QCISD | $C_1$ | 1.557 | 1.103 | 1.096 | 1.104 | 1.200 | 126.8 | 52.6 |
| CCSD | $C_1$ | 1.556 | 1.103 | 1.095 | 1.104 | 1.199 | 126.9 | 53.5 |
| QCISD(T) | $C_1$ | 1.557 | 1.104 | 1.097 | 1.106 | 1.201 | 126.8 | 51.1 |
| CCSD(T)) | $C_1$ | 1.557 | 1.104 | 1.097 | 1.106 | 1.201 | 126.9 | 50.8 |

[a]Bond lengths in Å, bond angles in degrees.

### 3.2.3. $CH_3BH^+$

Unlike the $CH_3BH$ anion and neutral, the cation has equivalent carbon-hydrogen bonds and all levels of theory give $C_{3V}$ symmetry, with the exception of QCISD(T), CCSD, and CCSD(T) which all yield $C_1$ symmetry. As there are no electrons in the $p_z$ orbital of B to interact with the pseudo-$\pi^*$ orbital of the methyl group, this ion can be stabilized by a favorable two electron interaction between the methyl pseudo-$\pi$ orbital and the vacant p(B) orbital. Thus the C—B, C—H and B—H bonds of the cation are shorter than those of the neutral. The cation is not affected by the addition of diffuse functions to either heavy or light atoms. There is a small change in geometry when going from double-zeta to triple-zeta valence basis set and with the addition of polarization functions. As mentioned in the computational procedures (section 2.5), this species failed to optimize to $C_{3V}$ symmetry at QCISD(T), CCSD, CCSD(T) levels of theory. It is interesting to note that the QCISD level of theory does give $C_{3v}$ symmetry and has almost identical geometric parameters as the CCSD level of theory with $C_1$ symmetry. The QCISD and CCSD geometries are very similar to one another and again there is virtually no change in geometry with the addition of the triples correction. The B3-LYP geometry best represents the CCSD(T) and QCISD(T) results, with the exception of the C—B bond, where MP2 is closest to the CCSD(T) and QCISD(T) lengths.

Table 3.3.
Selected optimized geometric parameters for $CH_3BH^+$.[a]

| Method | Sym | r(CB) | r($CH_C$) | a∠(BCH) | r(BH) | a∠(CBH) | d∠($H_CBCH_C$) |
|---|---|---|---|---|---|---|---|
| Effect of basis set | | | | | | | |
| HF/6-31G(d) | $C_{3v}$ | 1.485 | 1.092 | 110.3 | 1.166 | 180.0 | 120.0 |
| /6-31+G(d) | $C_{3v}$ | 1.485 | 1.092 | 110.3 | 1.166 | 180.0 | 120.0 |
| /6-31+G(d,p) | $C_{3v}$ | 1.483 | 1.092 | 110.1 | 1.166 | 180.0 | 120.0 |
| /6-311G(d) | $C_{3v}$ | 1.480 | 1.091 | 110.2 | 1.168 | 180.0 | 120.0 |
| /6-311+G(d) | $C_{3v}$ | 1.480 | 1.091 | 110.2 | 1.168 | 180.0 | 120.0 |
| /6-311+G(d,p) | $C_{3v}$ | 1.479 | 1.093 | 109.9 | 1.167 | 180.0 | 120.0 |
| /6-311+G(2df,p) | $C_{3v}$ | 1.477 | 1.092 | 109.8 | 1.166 | 180.0 | 120.0 |
| /6-311++G(3df,2p) | $C_{3v}$ | 1.477 | 1.091 | 109.8 | 1.165 | 180.0 | 120.0 |
| B3-LYP/6-31+G(d) | $C_{3v}$ | 1.463 | 1.106 | 110.8 | 1.176 | 180.0 | 120.0 |
| /6-311+G(d) | $C_{3v}$ | 1.456 | 1.104 | 110.9 | 1.173 | 180.0 | 120.0 |
| /6-311+G(2df,p) | $C_{3v}$ | 1.452 | 1.103 | 110.5 | 1.171 | 180.0 | 120.0 |
| MP2/6-31+G(d) | $C_{3v}$ | 1.467 | 1.102 | 110.4 | 1.175 | 180.0 | 120.0 |
| /6-311+G(d) | $C_{3v}$ | 1.465 | 1.101 | 110.4 | 1.175 | 180.0 | 120.0 |
| /6-311+G(2df,p) | $C_{3v}$ | 1.460 | 1.101 | 110.0 | 1.173 | 180.0 | 120.0 |
| Effect of electron correlation [with the 6-31+G(d) basis set] | | | | | | | |
| HF | $C_{3v}$ | 1.485 | 1.092 | 110.3 | 1.166 | 180.0 | 120.0 |
| B3-PW91 | $C_{3v}$ | 1.462 | 1.106 | 110.8 | 1.178 | 180.0 | 120.0 |
| B3-LYP | $C_{3v}$ | 1.463 | 1.107 | 110.8 | 1.176 | 180.0 | 120.0 |
| MP2 | $C_{3v}$ | 1.467 | 1.102 | 110.4 | 1.175 | 180.0 | 120.0 |
| QCISD | $C_{3v}$ | 1.472 | 1.105 | 110.4 | 1.179 | 180.0 | 120.0 |
| CCSD | $C_1$[b] | 1.472 | 1.105 | 110.4 | 1.179 | 180.0 | 120.0 |
| QCISD(T) | $C_1$[b] | 1.472 | 1.107 | 110.4 | 1.180 | 180.0 | 120.0 |
| CCSD(T) | $C_1$[b] | 1.472 | 1.107 | 110.4 | 1.180 | 180.0 | 120.0 |

[a] Bond lengths in Å, bond angles in degrees.
[b] See section 2.5

### 3.2.4. $CH_2BH_2^-$

The $CH_2BH_2^-$ anion has $C_{2V}$ symmetry at all levels of theory (Table 3.4). This anion structure is particularly stable due to the lone pair of electrons on C, which overlap with the empty $2p_z$ orbital of B. This two electron p(C) — p(B) interaction results in a pseudo $\pi$ bond. The C—B bond of the $CH_2BH_2^-$ anion has some double bond character with a length of 1.47 Å, roughly between the lengths of C—C single and double bonds. As expected the $CH_2BH_2^-$ anion exhibits a significant change in geometry with the addition of diffuse functions. For the double-zeta valence basis set, the C—B bond is lengthened by 0.02 Å and the C—H and B—H bonds are shortened by 0.003 Å and 0.005 Å, respectively. When diffuse functions are added to the triple-zeta basis set, the C—B bond is lengthened by 0.013 Å and the C—H and B—H bonds are shortened by 0.002 Å and 0.005 Å, respectively. The addition of polarization to the basis set has a smaller effect than the addition of diffuse functions, the bond lengths are shortened but to a much smaller extent. With the triple-zeta basis set, all bonds are generally shortened upon addition of polarization, to a maximum of 0.006 Å (in the case of the C—B bond in going from MP2/6-311+G(d) to MP2/6-311+G(2df,p)). The CCSD and QCISD theories give similar geometric parameters. The addition of the triples correction lengthens the bonds, the most significant of which is the C—B bond, which is 0.004 Å longer. Overall, MP2 theory best approximates the CCSD(T) and QCISD(T) results.

Table 3.4.
Selected optimized geometric parameters for $CH_2BH_2^-$.[a]

| Method | Sym | r(CB) | r(CH) | r(BH) | a∠(CBH) | a∠(BCH) | d∠(HCBH) |
|---|---|---|---|---|---|---|---|
| Effect of basis set | | | | | | | |
| HF/6-31G(d) | $C_{2v}$ | 1.444 | 1.089 | 1.229 | 124.1 | 122.9 | 180.0 |
| /6-31+G(d) | $C_{2v}$ | 1.462 | 1.086 | 1.224 | 123.6 | 122.4 | 180.0 |
| /6-31+G(d,p) | $C_{2v}$ | 1.462 | 1.086 | 1.224 | 123.6 | 122.4 | 180.0 |
| /6-311G(d) | $C_{2v}$ | 1.444 | 1.089 | 1.231 | 123.8 | 122.8 | 180.0 |
| /6-311+G(d) | $C_{2v}$ | 1.457 | 1.086 | 1.226 | 123.7 | 122.6 | 180.0 |
| /6-311+G(d,p) | $C_{2v}$ | 1.457 | 1.086 | 1.224 | 123.5 | 122.5 | 180.0 |
| /6-311+G(2df,p) | $C_{2v}$ | 1.453 | 1.085 | 1.223 | 123.5 | 122.5 | 180.0 |
| /6-311++G(3df,2p) | $C_{2v}$ | 1.454 | 1.084 | 1.222 | 123.5 | 122.5 | 180.0 |
| B3-LYP/6-31+G(d) | $C_{2v}$ | 1.466 | 1.098 | 1.227 | 123.8 | 122.2 | 180.0 |
| /6-311+G(d) | $C_{2v}$ | 1.457 | 1.096 | 1.224 | 123.8 | 122.3 | 180.0 |
| /6-311+G(2df,p) | $C_{2v}$ | 1.454 | 1.093 | 1.221 | 123.8 | 122.2 | 180.0 |
| MP2/6-31+G(d) | $C_{2v}$ | 1.469 | 1.096 | 1.224 | 123.6 | 122.1 | 180.0 |
| /6-311+G(d) | $C_{2v}$ | 1.465 | 1.096 | 1.225 | 123.5 | 122.0 | 180.0 |
| /6-311+G(2df,p) | $C_{2v}$ | 1.459 | 1.094 | 1.221 | 123.5 | 122.0 | 180.0 |
| Effect of electron correlation [with the 6-31+G(d) basis set] | | | | | | | |
| HF | $C_{2v}$ | 1.462 | 1.086 | 1.224 | 123.6 | 122.4 | 180.0 |
| B3-PW91 | $C_{2v}$ | 1.465 | 1.098 | 1.229 | 123.8 | 122.2 | 180.0 |
| B3-LYP | $C_{2v}$ | 1.466 | 1.098 | 1.227 | 123.8 | 122.2 | 180.0 |
| MP2 | $C_{2v}$ | 1.469 | 1.096 | 1.224 | 123.6 | 122.1 | 180.0 |
| QCISD | $C_{2v}$ | 1.471 | 1.099 | 1.229 | 123.7 | 122.3 | 180.0 |
| CCSD | $C_{2v}$ | 1.470 | 1.099 | 1.229 | 123.7 | 122.2 | 180.0 |
| QCISD(T) | $C_{2v}$ | 1.474 | 1.101 | 1.230 | 123.7 | 122.1 | 180.0 |
| CCSD(T) | $C_{2v}$ | 1.474 | 1.101 | 1.230 | 123.7 | 122.1 | 180.0 |

[a]Bond lengths in Å, bond angles in degrees.

### *3.2.5. $CH_2BH_2^-$*

As can be seen in Table 3.5, all HF and MP2 geometries have $C_{2V}$ symmetry. The B3-LYP and B3-PW91calculations using the 6-31+G(d) basis set also gives $C_{2V}$ symmetry, but the other DFT calculations with the larger basis sets give $C_2$ symmetry. The restricted MP2 (ROMP2) calculation and all other higher levels of theory (QCISD, QCISD(T), CCSD, and CCSD(T)) formally give either $C_2$ or $C_1$ symmetry, but to the precision quoted in Table 3.5 the structures are $C_{2V}$ (see procedures section 2.5). The radical is stabilized in the same manner as the anion, but with a one-electron p(C) – p(B) overlap. The B—C bond of the radical is thus slightly longer than that of the anion at 1.54 Å. There is a small change in geometry with the addition of diffuse functions to the double-zeta and triple-zeta basis set, with the C—B bond being shortened by 0.002 Å and 0.001 Å, respectively, while all the other bond lengths are unaffected. As with the other $CH_4B$ species the addition of polarization functions has a minor effect. The most notable is a shortening of the C—B bond at the B3-LYP and MP2 levels of theory. The CCSD and QCISD results are very similar to each other and change only very slightly with the addition of the triples correction. Both density functional methods provide good approximations to the CCSD(T) and QCISD(T) results.

Table 3.5. Selected optimized geometric parameters for $CH_2BH_2^{\bullet}$.[a]

| Method | Sym | r(CB) | r(CH) | r(BH) | a∠(BCH) | a∠(CBH) | d∠(HCBH) |
|---|---|---|---|---|---|---|---|
| Effect of basis set | | | | | | | |
| HF/6-31G(d) | $C_{2V}$ | 1.536 | 1.078 | 1.192 | 123.0 | 120.5 | 180.0 |
| /6-31+G(d) | $C_{2V}$ | 1.538 | 1.078 | 1.192 | 122.9 | 120.5 | 180.0 |
| /6-31+G(d,p) | $C_{2V}$ | 1.538 | 1.079 | 1.192 | 122.9 | 120.4 | 180.0 |
| /6-311G(d) | $C_{2V}$ | 1.534 | 1.078 | 1.194 | 122.9 | 120.4 | 180.0 |
| /6-311+G(d) | $C_{2V}$ | 1.535 | 1.078 | 1.194 | 123.0 | 120.5 | 180.0 |
| /6-311+G(d,p) | $C_{2V}$ | 1.535 | 1.079 | 1.192 | 122.9 | 120.4 | 180.0 |
| /6-311+G(2df,p) | $C_{2V}$ | 1.532 | 1.078 | 1.191 | 122.9 | 120.4 | 180.0 |
| /6-311++G(3df,2p) | $C_{2V}$ | 1.532 | 1.077 | 1.190 | 122.9 | 120.5 | 180.0 |
| B3-LYP/6-31+G(d) | $C_{2V}$ | 1.536 | 1.091 | 1.197 | 123.2 | 120.3 | 180.0 |
| /6-311+G(d) | $C_2$[b] | 1.529 | 1.088 | 1.195 | 123.2 | 120.3 | 174.7 |
| /6-311+G(2df,p) | $C_2$[b] | 1.523 | 1.087 | 1.192 | 123.2 | 120.3 | 166.6 |
| MP2/6-31+G(d) | $C_{2V}$ | 1.535 | 1.087 | 1.195 | 123.0 | 120.3 | 180.0 |
| /6-311+G(d) | $C_{2V}$ | 1.535 | 1.086 | 1.197 | 123.0 | 120.2 | 180.0 |
| /6-311+G(2df,p) | $C_{2V}$ | 1.529 | 1.084 | 1.192 | 122.9 | 120.2 | 180.0 |
| Effect of electron correlation [with the 6-31+G(d) basis set] | | | | | | | |
| HF | $C_{2V}$ | 1.536 | 1.078 | 1.192 | 123.0 | 120.5 | 180.0 |
| ROHF | $C_{2V}$ | 1.537 | 1.077 | 1.192 | 123.0 | 120.4 | 180.0 |
| B3-PW91 | $C_{2V}$ | 1.534 | 1.091 | 1.199 | 123.2 | 120.2 | 180.0 |
| B3-LYP | $C_{2V}$ | 1.536 | 1.091 | 1.197 | 123.2 | 120.3 | 180.0 |
| MP2 | $C_{2V}$ | 1.535 | 1.087 | 1.195 | 123.0 | 120.3 | 180.0 |
| ROMP2 | $C_1$[b] | 1.535 | 1.087 | 1.195 | 123.0 | 120.3 | 180.0 |
| QCISD/6-31+G(d) | $C_2$[b] | 1.538 | 1.091 | 1.200 | 123.0 | 120.3 | 180.0 |
| CCSD/6-31+G(d) | $C_2$[b] | 1.538 | 1.091 | 1.200 | 123.0 | 120.3 | 180.0 |
| QCISD(T)/6-31+G(d) | $C_1$[b] | 1.539 | 1.093 | 1.201 | 123.0 | 120.3 | 180.0 |
| CCSD(T)/6-31+G(d) | $C_1$[b] | 1.539 | 1.093 | 1.201 | 123.0 | 120.3 | 180.0 |

[a] Bond lengths in Å, bond angles in degrees.
[b] See section 2.5

### 3.2.6. $CH_2BH_2^+$

This species only exists at the HF level of theory. At all other levels of theory the structure optimized to $CH_3BH^+$ when symmetry constraints were lifted. At higher levels of theory, when $CH_2BH_2^+$ is forced to have $C_{2V}$ symmetry, the structure is a transition state corresponding to the out-of-plane umbrella motion of the $CH_2$ and $BH_2$ groups. The HF geometric parameters for $CH_2BH_2^+$ are summarized in Table 3.6. Since there are no electrons on C to form a p(C) – p(B) overlap, the hydrogen atoms on C and B lie perpendicular to each other, permitting at least some interaction between vacant p-orbitals and the electrons in the C—H and B—H bonds. The geometry of the cation is completely unaffected by the addition of diffuse functions and changes only slightly with the inclusion of polarization functions.

Table 3.6. Selected optimized geometric parameters for $CH_2BH_2^+$.[a]

| Method | Sym | r(CB) | r(CH) | r(BH) | a∠(BCH) | a∠(CBH) | d∠(HCBH) |
|---|---|---|---|---|---|---|---|
| HF/6-31G(d) | $C_{2V}$ | 1.543 | 1.083 | 1.184 | 122.6 | 116.9 | 90.0 |
| /6-31+G(d) | $C_{2V}$ | 1.543 | 1.083 | 1.184 | 122.6 | 116.9 | 90.0 |
| /6-31+G(d,p) | $C_{2V}$ | 1.542 | 1.084 | 1.184 | 122.5 | 116.9 | 90.0 |
| /6-311G(d) | $C_{2V}$ | 1.539 | 1.083 | 1.186 | 122.6 | 116.9 | 90.0 |
| /6-311+G(d) | $C_{2V}$ | 1.539 | 1.083 | 1.186 | 122.6 | 116.9 | 90.0 |
| /6-311+G(d,p) | $C_{2V}$ | 1.538 | 1.086 | 1.184 | 122.5 | 116.8 | 90.0 |
| /6-311+G(2df,p) | $C_{2V}$ | 1.535 | 1.094 | 1.184 | 122.6 | 116.8 | 90.0 |
| /6-311++G(3df,2p) | $C_{2V}$ | 1.535 | 1.083 | 1.183 | 122.6 | 116.9 | 90.0 |

[a]Bond lengths in Å, bond angles in degrees.

*3.2.7 Comparing the geometries of the radicals, cations and anions.*

The geometric parameters in this section are all from the QCISD(T)6-31/+g(d) level of theory, except for $CH_2BH_2^+$ where HF/6-311++G(3df, 2p) is used since it was the largest calculation that converged. In the $CH_3BH$ anion, there is a two electron interaction with the pseudo-π* orbital on the methyl group. In the radical there is one electron involved in this interaction, and in the cation there are no electrons on B to interact with the pseudo-π* orbital on the methyl group but rather a favorable two electron interaction between the methyl pseudo-π and p(B). The C—B and B—H bonds increase from cation to radical to anion as more electron density is added to the π* orbital. The C—B and B—H bond lengths of the $CH_3BH$ anion are 0.059 Å and 0.04 Å longer than those of the radical, while the C—B and B—H bond lengths of the $CH_3BH$ cation are 0.085 Å and 0.021Å shorter than those of the radical.

The opposite trend is seen in the $CH_2BH_2$ species, where the bonding interaction is between p(C) and p(B) and adding electron density leads to shorter bond lengths. The radical and anion have one and two electrons, respectively, located in the 2p orbital of carbon. Since B also has an empty p orbital, these electrons are able to form a favourable pseudo π-bond. The C—B bond length of the anion is 0.065 Å shorter than the radical, while the C—H and B—H bonds are 0.008 Å and 0.029 Å longer than those of the radical (since electron density is being pulled away from those bonds). The cation has no lone electrons on C, so this species has empty 2p orbitals on both C and B. At the highest level of theory where $CH_2BH_2^+$ exists, the C—B, C—H, and B—H bonds of the cation are 0.004 Å, 0.01 Å, and 0.018 Å shorter than those in the radical.

*3.3 Selecting an appropriate level of theory for determining ZPEs*

Figure 3.5 shows ZPEs for the $CH_3BH^{\bullet}$ radical (similar figures for the other five isomers have not been included) as a function of level of theory. It is apparent the MP2 correlation treatment with the larger basis sets (6-311+G(d) and 6-311+G(2df,p) are the lowest levels of theory that are most consistent with the QCISD(T)/CCSD(T) levels of theory.

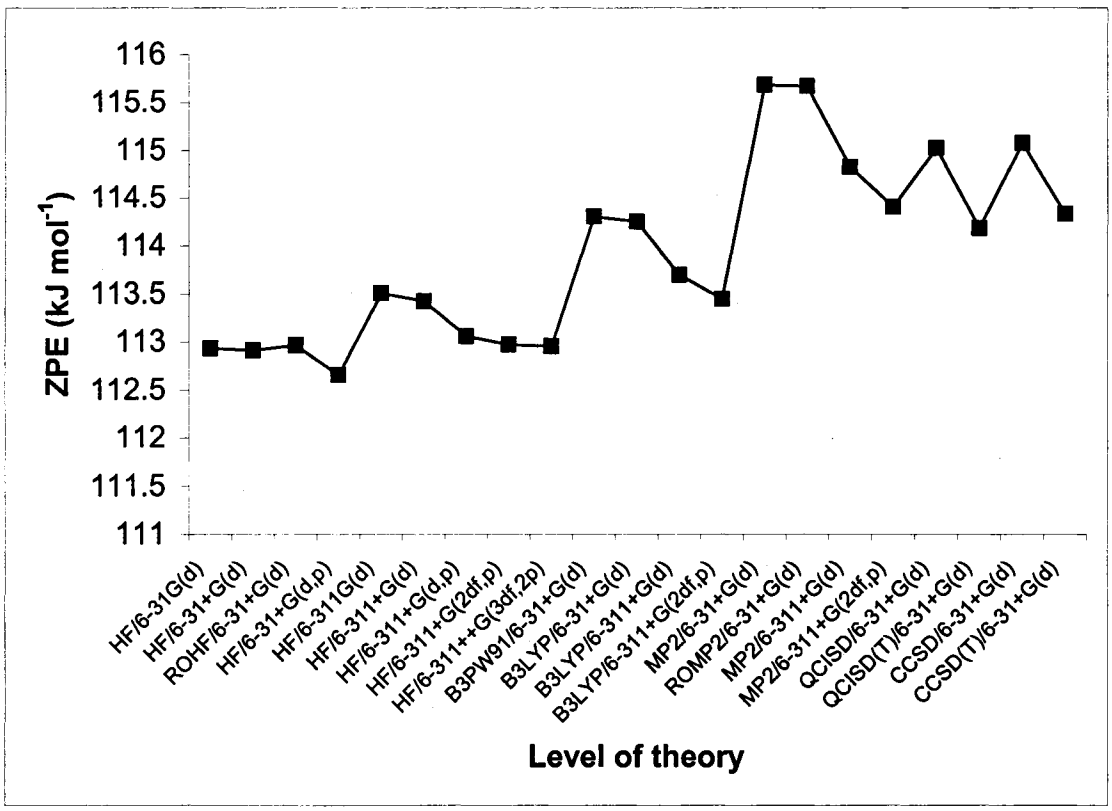


Figure 3.5 ZPE (kJ $mol^{-1}$) of the $CH_3BH^{\bullet}$ as a function of level of theory.

*3.4 Determination of an appropriate level of theory for obtaining reliable energies.*

*3.4.1 Relative energies of the isomers*

A summary of the 0 K total energies calculated at different levels of theory is given in Table 3.7. Table 3.8 lists the relative energy of each isomer calculated at each level of theory. In each case the relative energy is calculated as $E_0$ [$CH_3BH$] – $E_0$ [$CH_2BH_2$]. $CH_2BH_2^-$ and $CH_2BH_2^{\bullet}$ are more stable than the corresponding $CH_3BH$ species. The anion is more stable by about 220 kJ $mol^{-1}$ while the radical is more stable by roughly 40 kJ $mol^{-1}$. Conversely, $CH_2BH_2^+$ is about 125 kJ $mol^{-1}$ less stable than $CH_3BH^+$, where it exists at the HF level of theory.

Of the levels of theory investigated, the B3-LYP and B3-PW91 calculations are the best at reproducing the relative energies obtained at the CCSD(T) and QCISD(T) levels of theory. The QCISD(T) and CCSD(T) results are themselves similar to the composite G3 results (performed on different optimized geometries). All of the G3 results are within 3 kJ $mol^{-1}$ of each other, regardless of theory and basis set used for geometry optimization.

Table 3.7.
Total energies[a] for the $CH_4B$ isomers at the levels of theory explored in this study.

| Method | $CH_3BH^-$ | $CH_2BH_2^-$ | $CH_3BH^+$ | $CH_2BH_2^+$ | $CH_3BH^\bullet$ | $CH_2BH_2^\bullet$ |
|---|---|---|---|---|---|---|
| HF/6-31G(d) | -169802 | -170051 | -169393 | -169271 | -170026 | -170085 |
| /6-31+G(d) | -169903 | -170114 | -169393 | -169272 | -170032 | -170091 |
| /6-31+G(d,p) | -169919 | -170130 | -169412 | -169289 | -170049 | -170105 |
| /6-311G(d) | -169892 | -170118 | -169418 | -169295 | -170058 | -170114 |
| /6-311+G(d) | -169933 | -170141 | -169420 | -169296 | -170059 | -170115 |
| /6-311+G(d,p) | -169949 | -170159 | -169440 | -169314 | -170076 | -170131 |
| /6-311+G(2df,p) | -169957 | -170168 | -169448 | -169322 | -170084 | -170140 |
| /6-311++G(3df,2p) | -169964 | -170172 | -169453 | -169327 | -170089 | -170145 |
| ROHF/6-31+G(d) | | | | | -170029 | -170083 |
| B3PW91/6-31+G(d) | -171172 | -171398 | -170503 | | -171189 | -171230 |
| B3LYP/6-31+G(d) | -171262 | -171488 | -170586 | | -171267 | -171316 |
| /6-311+G(d) | -171296 | -171521 | -170615 | | -171298 | -171344 |
| /6-311+G(2df,p) | -171319 | -171547 | -170639 | | -171321 | -171366 |
| MP2/6-31+G(d) | -170470 | -170707 | -169874 | | -170521 | -170559 |
| /6-311+G(d) | -170537 | -170770 | -169926 | | -170578 | -170611 |
| /6-311+G(2df,p) | -170705 | -170944 | -170067 | | -170730 | -170763 |
| ROMP2/6-31+G(d) | | | | | -170521 | -170560 |
| QCISD/6-31+G(d) | -170560 | -170779 | -169947 | | -170599 | -170644 |
| QCISD(T)/6-31+G(d) | -170581 | -170803 | -169962 | | -170614 | -170658 |
| CCSD/6-31+G(d) | -170558 | -170777 | -169946 | | -170598 | -170643 |
| CCSD(T)/6-31+G(d) | -170580 | -170802 | -169961 | | -170613 | -170657 |
| G3//B3LYP/6-31+G(d) | -171168 | -171389 | -170478 | | -171157 | -171199 |
| G3// /6-311+G(d) | -171168 | -171390 | -170479 | | -171158 | -171200 |
| G3// /6-311+G(2df,p) | -171170 | -171389 | -170480 | | -171158 | -171199 |
| G3// MP2/6-31+G(d) | -171167 | -171387 | -170478 | | -171156 | -171197 |
| G3// /6-311+G(d) | -171168 | -171390 | -170479 | | -171157 | -171198 |
| G3// /6-311+G(2df,p) | -171168 | -171389 | -170480 | | -171157 | -171198 |

[a] Values are in kJ $mol^{-1}$ at 0 K.

Table 3.8.
Relative energies, $E_0$ [$CH_3BH$] – $E_0$ [$CH_2BH_2$] as a function of level of theory.[a]

| Method | Radical[b] | Cation | Anion |
|---|---|---|---|
| HF/6-31G(d) | 59 | -121 | 249 |
| /6-31+G(d) | 59 | -121 | 212 |
| /6-31+G(d,p) | 56 | -124 | 211 |
| /6-311G(d) | 56 | -123 | 226 |
| /6-311+G(d) | 56 | -124 | 208 |
| /6-311+G(d,p) | 55 | -126 | 209 |
| /6-311+G(2df,p) | 56 | -126 | 211 |
| /6-311++G(3df,2p) | 56 | -127 | 209 |
| ROHF/6-31G(d) | 53 | | |
| B3PW91/6-31+G(d) | 41 | | 226 |
| B3LYP/6-31+G(d) | 48 | | 226 |
| /6-311+G(d) | 46 | | 225 |
| /6-311+G(2df,p) | 45 | | 228 |
| MP2/6-31+G(d) | 38 | | 236 |
| /6-311+G(d) | 33 | | 232 |
| /6-311+G(2df,p) | 33 | | 239 |
| ROMP2/6-31+G(d) | 39 | | |
| QCISD/6-31+G(d) | 45 | | 220 |
| QCISD(T)/6-31+G(d) | 44 | | 222 |
| CCSD/6-31+G(d) | 45 | | 219 |
| CCSD(T)/6-31+G(d) | 44 | | 222 |
| G3//B3LYP/6-31+G(d) | 42 | | 221 |
| G3// /6-311+G(d) | 42 | | 222 |
| G3// /6-311+G(2df,p) | 41 | | 219 |
| G3//MP2/6-31+G(d) | 41 | | 220 |
| G3// /6-311+G(d) | 41 | | 222 |
| G3// /6-311+G(2df,p) | 41 | | 221 |

[a] Values are in kJ $mol^{-1}$ at 0 K.

*3.4.2. Ionization energies and electron affinities*

Table 3.9 has a summary of ionization energies (IE) and electron affinities (EA) calculated at each level of theory. In all cases it appears necessary to use the composite G3 approach to achieve convergence of the values. Of the direct levels of theory, the B3-LYP results are closest to the G3 composite results. The ionization energy is roughly 8.5

eV for the $CH_2BH_2^{\bullet}$ radical (at the HF level of theory only) and 7.0 eV for the $CH_3BH^{\bullet}$ radical (G3 result). $CH_3BH^{\bullet}$ has a small positive electron affinity that is only evident at the G3 level of theory. $CH_2BH_2^{\bullet}$ has a positive EA of approximately 2 eV since this anion structure is particularly stable due to the favourable two electron p(C) – p(B) overlap. For $CH_3BH^{-}$, the lone pair of electrons is located on boron so any interaction is with a pseudo-$\pi^*$ orbital on the methyl group has only a small stabilizing effect.

*3.4.3 Selecting an appropriate level of theory for determining absolute thermochemistry*

Heats of formation at 0 K (Table 3.10) were calculated by the atomization method [68], using the experimental heats of formation of the constituent atoms [72]. All of the G3 heats of formation converge to within 3 kJ $mol^{-1}$ of each other, regardless of the initial level of theory used to optimize geometries and ZPEs. Therefore it seems necessary to use the G3 composite method to obtain reliable heats of formation and that MP2 or B3-LYP are adequate for optimizing structures.

*3.5 Computational assessment summary*

From the previous discussion it appears that B3-LYP is the best overall choice (in terms of results and computational time) for optimizing geometries. Since this study involves anions, radicals, and cations, it is important to include polarization and diffuse functions on heavy atoms. For these reasons, B3-LYP/6-311+G(d) is the level of theory selected from the above assessment for the rest of this study. In terms of obtaining reliable relative energies, ionization energies, electron affinities and heats of formation, it has been determined that it is necessary to go to the G3 composite method.

Table 3.9.
Ionization energies and electron affinities for $CH_4B$ isomers.[a]

| Method | IE $CH_2BH_2^{\bullet}$ | IE $CH_3BH^{\bullet}$ | EA $CH_2BH_2^{\bullet}$ | EA $CH_3BH^{\bullet}$ |
|---|---|---|---|---|
| HF/6-31G(d) | 8.43 | 6.56 | -0.35 | -2.32 |
| /6-31+G(d) | 8.49 | 6.63 | 0.24 | -1.34 |
| /6-31+G(d,p) | 8.46 | 6.60 | 0.25 | -1.35 |
| /6-311G(d) | 8.48 | 6.63 | 0.04 | -1.72 |
| /6-311+G(d) | 8.48 | 6.62 | 0.27 | -1.31 |
| /6-311+G(d,p) | 8.47 | 6.60 | 0.29 | -1.32 |
| /6-311+G(2df,p) | 8.49 | 6.60 | 0.29 | -1.32 |
| /6-311++G(3df,2p) | 8.48 | 6.59 | 0.29 | -1.30 |
| B3PW91/6-31+G(d) | | 7.11 | 1.74 | -0.18 |
| B3LYP/6-31+G(d) | | 7.06 | 1.78 | -0.06 |
| /6-311+G(d) | | 7.08 | 1.84 | -0.02 |
| /6-311+G(2df,p) | | 7.06 | 1.88 | -0.02 |
| MP2/6-31+G(d) | | 6.71 | 1.53 | -0.53 |
| /6-311+G(d) | | 6.76 | 1.64 | -0.42 |
| /6-311+G(2df,p) | | 6.87 | 1.87 | -0.26 |
| QCISD/6-31+G(d) | | 6.76 | 1.40 | -0.41 |
| QCISD(T)/6-31+G(d) | | 6.76 | 1.51 | -0.34 |
| CCSD/6-31+G(d) | | 6.76 | 1.38 | -0.41 |
| CCSD(T)/6-31+G(d) | | 6.76 | 1.51 | -0.34 |
| G3//B3LYP/6-31+G(d) | | 7.04 | 1.97 | 0.11 |
| G3// /6-311+G(d) | | 7.04 | 1.97 | 0.10 |
| G3// /6-311+G(2df,p) | | 7.03 | 1.97 | 0.12 |
| G3//MP2/6-31+G(d) | | 7.03 | 1.97 | 0.12 |
| G3// /6-311+G(d) | | 7.03 | 1.99 | 0.12 |
| G3// /6-311+G(2df,p) | | 7.02 | 1.98 | 0.11 |

[a] Values in eV at 0 K.

Table 3.10 Calculated heats of formation at the G3 level of theory for the $CH_4B$ isomers.[a]

| **Level of theory** | $\Delta H^0_f{}^{at}CH_3BH^{\bullet}$ | $\Delta H^0_f{}^{at}CH_3BH^{+}$ | $\Delta H^0_f{}^{at}CH_3BH^{-}$ | $\Delta H^0_f{}^{at}CH_2BH_2^{\bullet}$ | $\Delta H^0_f{}^{at}CH_2BH_2^{-}$ |
|---|---|---|---|---|---|
| **G3//B3LYP/6-31+g(d)** | 141 | 820 | 130 | 98 | -91 |
| **G3// /6-311 +g(d)** | 140 | 819 | 130 | 98 | -92 |
| **G3// /6-311+g(2df,p)** | 140 | 818 | 128 | 99 | -91 |
| **G3//MP2/6-31+g(d)** | 142 | 820 | 131 | 101 | -89 |
| **G3// /6-311 +g(d)** | 141 | 819 | 130 | 100 | -92 |
| **G3// /6-311+g(2df,p)** | 140 | 818 | 130 | 100 | -91 |

[a] Values are in kJ mol.$l^{-1}$ at 0 K.

*Chapter 4: Modelling the Potential Energy Surfaces for $CH_4B$ radicals and ions and their experimental charaterization*

*4.1 Modelling the potential energy surfaces for the $CH_4B$ radical and ions*

From the previous discussion it was clear that the G3 composite method was necessary to reliably determine relative energies. All energies quoted below were obtained at the G3//B3-LYP/6-311+G(d) level of theory. High level ab initio molecular orbital calculations were used to explore the structure and stability of the $CH_2BH_2$ and $CH_3BH$ cations, radicals and anions. Contrary to the results from lower level calculations, the $CH_2BH_2^{+}$ ion was not found to reside in a potential well. The relative energy surface of $CH_4B^{+}$ is shown in Fig. 4.1. There is no singlet state $CH_2BH_2^{+}$ cation so only the singlet $CH_3BH^{+}$ ion is shown along with its dissociation products. Hydrogen can be lost from either C or B resulting in $CH_2BH^{+\bullet}$ or $CH_3B^{+\bullet}$, respectively. H loss from C is 72 kJ $mol^{-1}$ lower in energy than H loss from B. Both $CH_2BH_2^{+}$ and $CH_3BH^{+}$ exist as triplet states so the isomerization between the two species has been included in Fig. 3.6. Clearly the formation of ground state $CH_2BH_2^{+}$ would not be possible, but the triplet state may be accessible as it is bound with respect to $CH_2BH^{+\bullet} + H^{\bullet}$ by 50 kJ $mol^{-1}$.

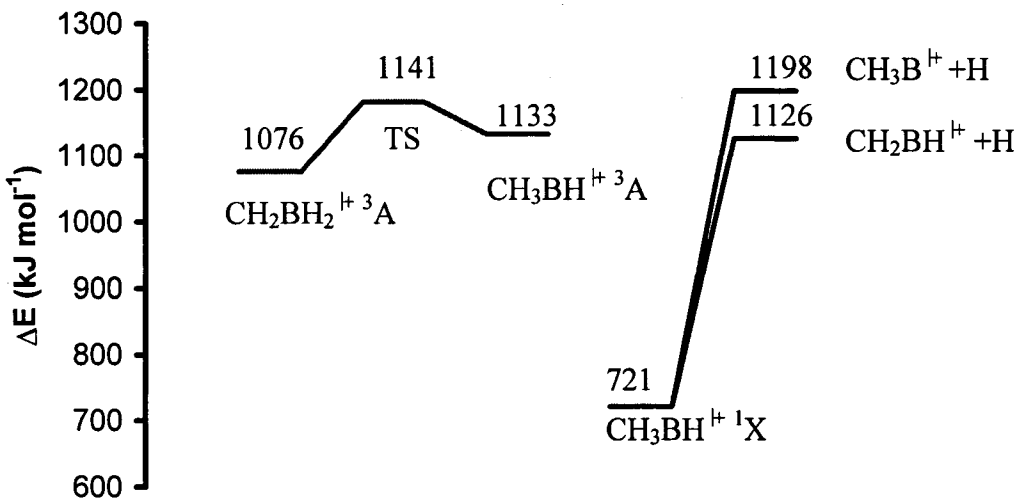


Figure 4.1. Relative energy (G3//B3-LYP/6-311+G(d) surface of $CH_4B^{+\bullet}$, all energies relative to $CH_2BH_2^{+\bullet}$.

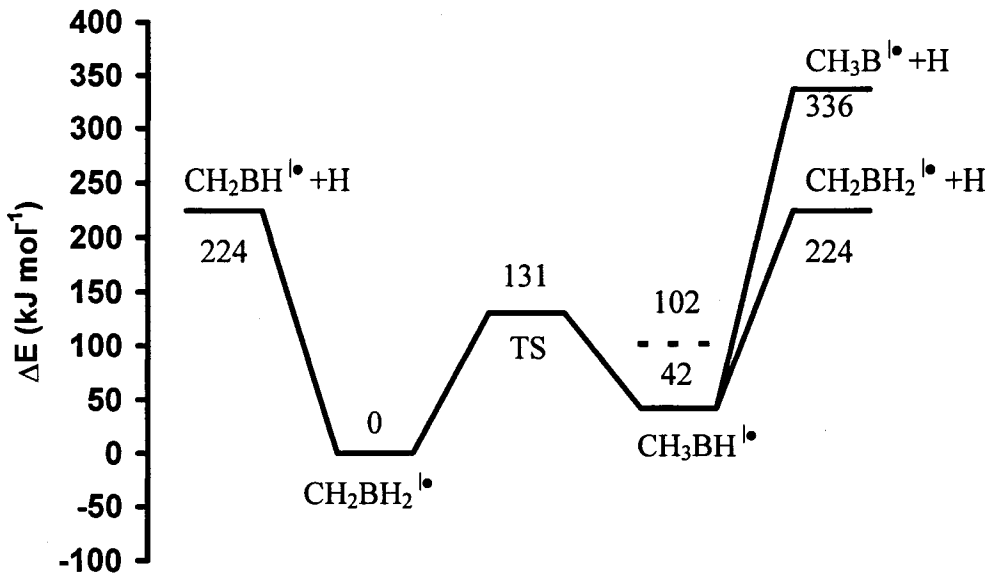


Figure 4.2. Relative energy (G3//B3-LYP/6-311+G(d) surface of $CH_4B^{+\bullet}$, all energies relative to $CH_2BH_2^{+\bullet}$. Relative energies of the vertically neutralized cations are shown as dashed lines.

The relative energy surface of the $CH_4B^{\bullet}$ isomers and their dissociation products is shown in Fig. 4.2. Both isomers are stable with respect to isomerization and dissociation, consistent with literature evidence for their independent formation. We were unable to locate a minimum energy structure for the $CHBH_2$ neutral fragment that would result from H-loss from C in $CH_2BH_2^{\bullet}$. Most attempts converged to $CH_2BH$, indicating that there is likely a trivial barrier between these two isomers. The transition state (TS) and $CH_3BH^{\bullet}$ are 131 and 42 kJ $mol^{-1}$, respectively, higher in energy than $CH_2BH_2^{\bullet}$. $CH_3BH^{\bullet}$ can lose H from either C or B to form $CH_2BH$ or $CH_3B$, the latter channel being 112 kJ $mol^{-1}$ more endothermic than the former.

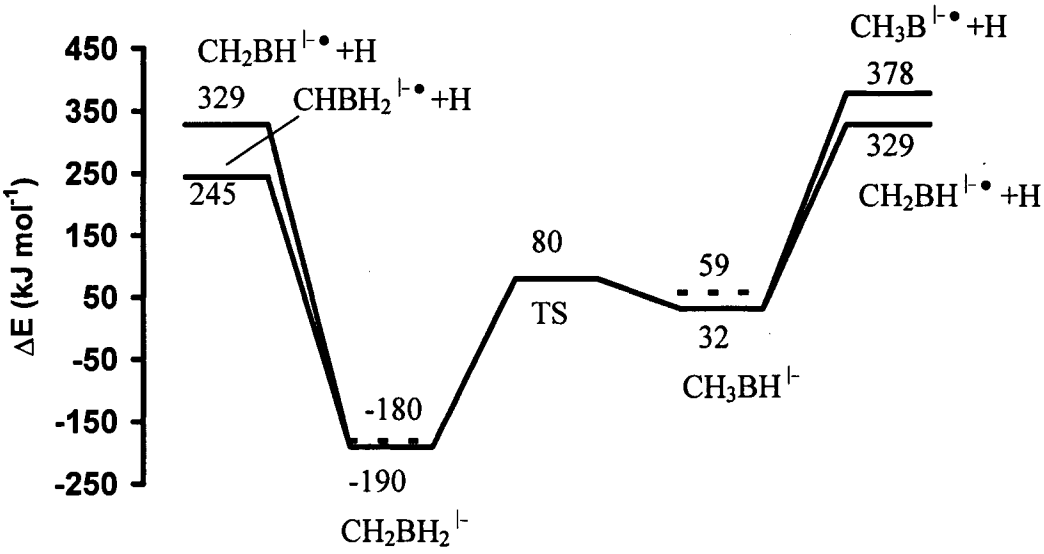


Figure 4.3. Relative energy (G3//B3-LYP/6-311+G(d) surface of $CH_4B^-$, all energies relative to $CH_2BH_2^{\bullet}$. Relative energies of the anions formed by vertical electron attachment from the radicals are shown as dashed lines.

The energetics of the isomerization of $CH_2BH_2^-$ to $CH_3BH^-$ is shown in Fig. 4.3. The TS and $CH_3BH^-$ lie 270 kJ $mol^{-1}$ and 222 kJ $mol^{-1}$ higher in energy than $CH_2BH_2^-$, respectively. Unlike the cation and neutral species, both $CH_2BH_2^-$ and $CH_3BH^-$ can lose H from either C or B. The H-loss products from $CH_2BH_2^-$ are $CHBH_2^{-\bullet}$ and $CH_2BH^{-\bullet}$. H-loss from C yields a product that is more stable by 84 kJ $mol^{-1}$ than the H-loss product from B. The H-loss products from $CH_3BH^-$ are $CH_2BH^{-\bullet}$ and $CH_3B^{-\bullet}$. Here H-loss from B is 49 kJ $mol^{-1}$ more endothermic than from C. Both isomers are stable with respect to dissociation, though it may be difficult to generate $CH_3BH^-$ in a pure form due to the moderate barrier (50 kJ $mol^{-1}$) to isomerization to the significantly more stable $CH_2BH_2^-$.

*4.2. Experimental characterization of $CH_4B$ ions and radicals.*

Several compounds were considered as possible precursors to *m/z* 27 corresponding to molecular formula $CH_4B^+$. Since *m/z* 27 also corresponds to $C_2H_3^+$, compounds that have significant hydrocarbon moieties can pose a problem. Trimethylboroxine, 2-methylpropyl boronic acid, methoxy diethyl borane, and tris(dimethylamino)borane were all investigated by mass spectrometry. Methoxy diethyl borane was not used since this compound yielded a peak at *m/z* 27 with no evidence of B (*m/z* 11 not observed in its CID mass spectrum, figure not shown). The 2-methylpropyl boronic acid was not used for this study since it did not give a peak at *m/z* 27 with sufficient intensity to be useful. Tris(dimethylamino)borane has a substantial signal at *m/z* 27 in its mass spectrum, but upon further investigation it became evident that this peak was the result of a mixture of ions (this compound is discussed further in Chapter 5). The full mass spectrum of

trimethylboroxine shows a relatively small peak at *m/z* 27 (Figure 4.4). Since trimethylboroxine contains C, H, B, and O, the peak at *m/z* 27 can either be $C_2H_3^+$, $CH_4B^+$, $^{11}BO^+$ or $^{10}BOH^+$. The MIKE mass spectrum of *m/z* 27, shown in Figure 4.5 contains peaks at *m/z* 26 and *m/z* 25 corresponding to losses of H and $H_2$. The CID (He) mass spectrum (Fig. 4.6) exhibits peaks at *m/z* 26 through to 23 and 15 to 11. The peaks from *m/z* 26 to 23 indicate that the ion has four hydrogen atoms and thus cannot be $C_2H_3^+$, $^{11}BO^+$ or $^{10}BOH^+$. There is no peak corresponding to $^{10}B$ at *m/z* 10 thereby also excluding $^{10}BOH^+$. When $O_2$ was used as the target gas instead of He (Figure 4.7), a doubly-charged ion with *m/z* 13.5 corresponding to $CH_4B^{2+}$ was observed. Thus the CID mass spectrum in Fig. 4.6 can be assigned to $CH_4B^+$. Given that $CH_2BH_2^+$ is not an equilibrium species on the $CH_4B^+$ potential energy surface, this mass spectrum must be for $CH_3BH^+$.

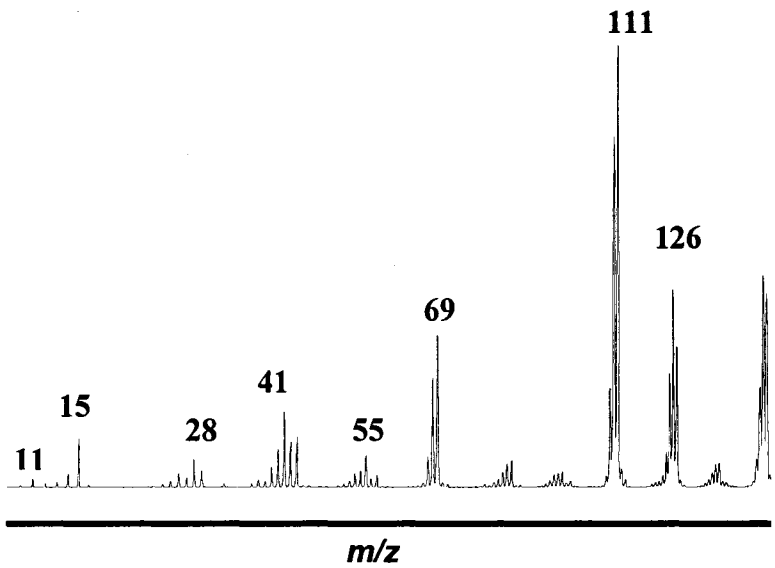


Figure 4.4. Full mass spectrum of trimethylboroxine.

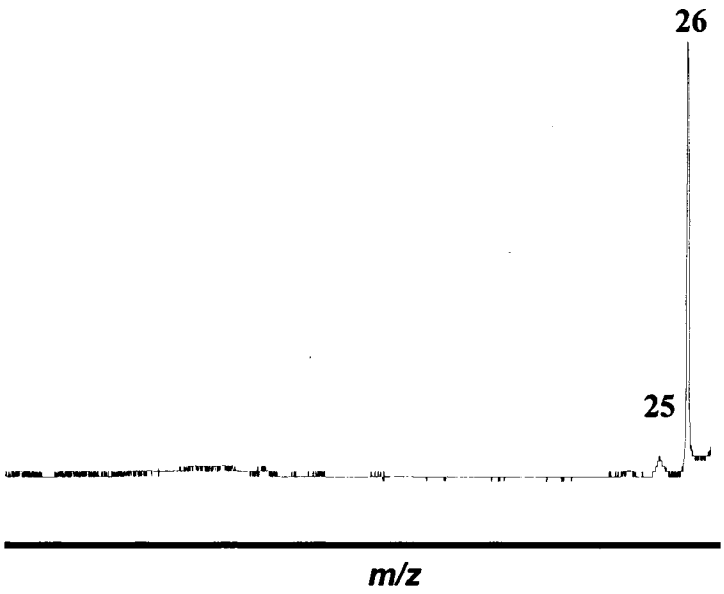


Figure 4.5. MIKE mass spectrum of *m/z* 27 from trimethylboroxine.

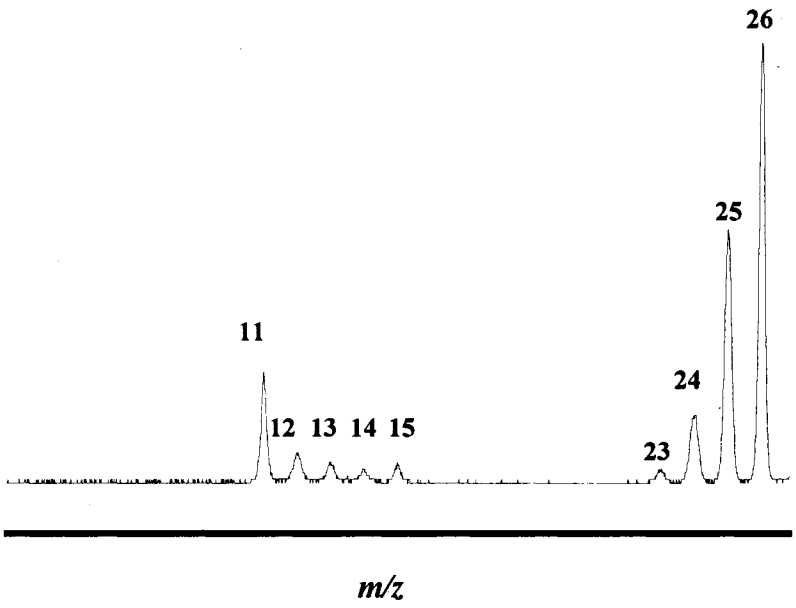


Figure 4.6. CID (He, 20 % beam reduction) mass spectrum of *m/z* 27 from trimethylboroxine.

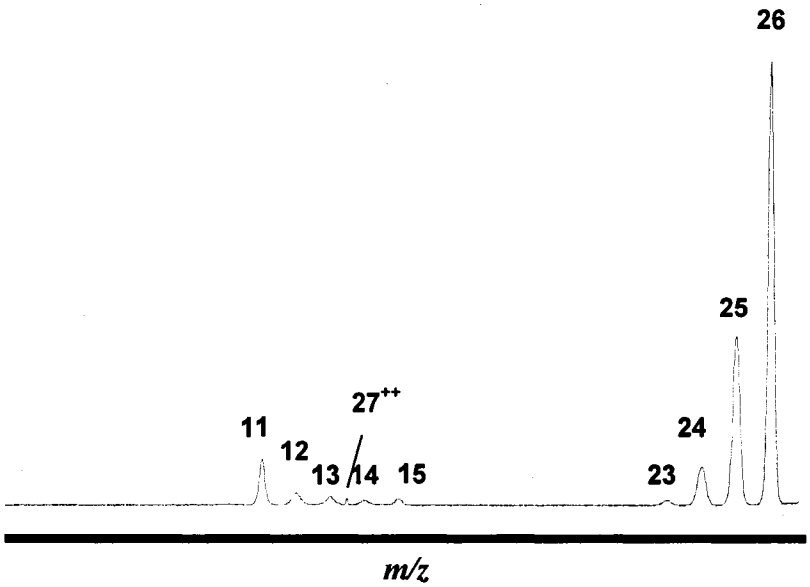


Figure 4.7. CID ($O_2$, 20% beam reduction) mass spectrum of *m/z* 27 from trimethylboroxine.

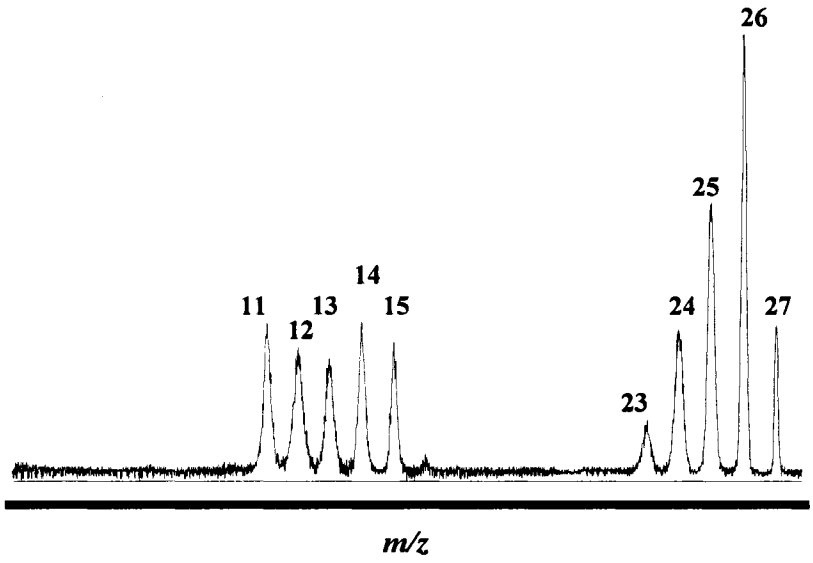


Figure 4.8. NRMS ($O_2/O_2$, 20% beam reduction) mass spectrum of *m/z* 27 from trimethylboroxine.

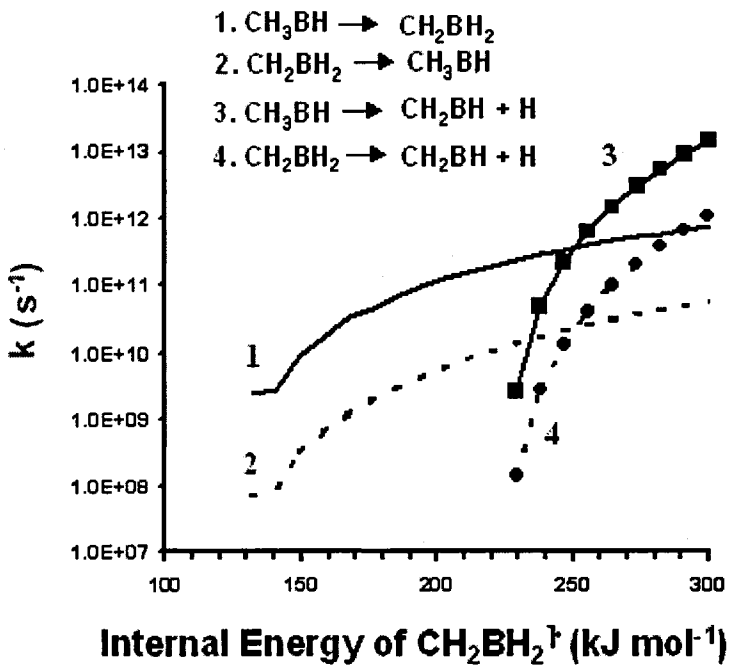


Figure 4.9. RRKM *k(E)* vs. *E* curves for the interconversion of $CH_2BH_2^{+\bullet}$ and $CH_3BH^{+\bullet}$ and their lowest energy dissociation processes.

The NRMS mass spectrum, Fig. 4.8, of this *m/z* 27 ion contains a recovery signal (*m/z* 27) which means that a stable $CH_4B^{+\bullet}$ radical was produced upon neutralization of $CH_3BH^{+\bullet}$. Vertical neutralization of this ion forms $CH_3BH^{+\bullet}$ 60 kJ $mol^{-1}$ higher than the adiabatic structure (Fig. 4.2). At this internal energy $CH_3BH^{+\bullet}$ is stable both to dissociation and isomerization to $CH_2BH_2^{+\bullet}$, though the latter process is only endothermic by ~ 30 kJ $mol^{-1}$. RRKM calculations of the microcanonical rate constants, *k(E)*, were carried out to investigate the possible interconversion of the two radicals (Fig. 4.9) [51, 73]. The rate constant for the isomerization of $CH_3BH^{+\bullet}$ to $CH_2BH_2^{+\bullet}$ is greater than $10^9$ $s^{-1}$ just 1 kJ $mol^{-1}$ above the transition state (due to the low density of states of

these small species) and is greater than that for dissociation up to 25 kJ $mol^{-1}$ above threshold. So it is apparent that any $CH_3BH^{\rceil\bullet}$ made in the neutralization step of the NRMS experiment will undergo a fast equilibration with $CH_2BH_2^{\rceil\bullet}$ prior to dissociation or re-ionization, with the majority of the neutral residing in the $CH_2BH_2^{\rceil\bullet}$ potential energy well (microcanonical equilibrium constant $K = \rho(CH_2BH_2^{\rceil\bullet})/\rho(CH_3BH^{\rceil\bullet}) \sim 100$, where $\rho$ refers to the density-of-states of the ion). While both radicals were found to be equilibrium structures stable with respect to isomerization and dissociation, RRKM calculations predict that it would be difficult to make pure $CH_3BH^{\rceil\bullet}$ by neutralizing the cation.

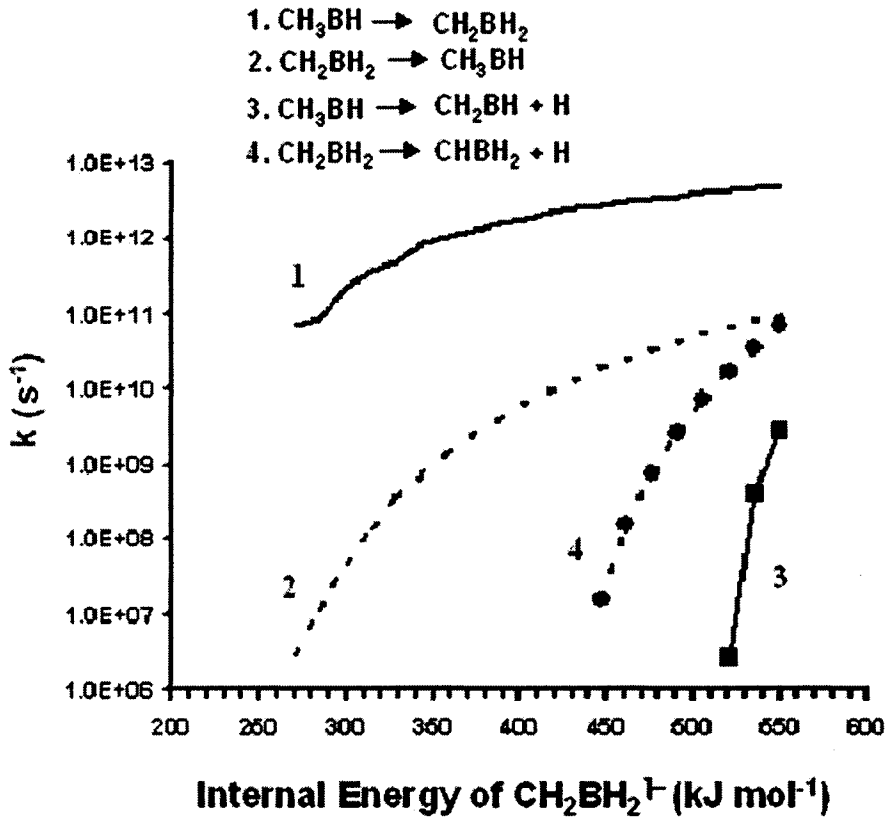


Figure 4.10. RRKM *k(E)* vs. *E* curves for the interconversion of $CH_2BH_2^{\rceil-}$ and $CH_3BH^{\rceil-}$ and their lowest energy dissociation processes.

When the polarity of the electrostatic analyzer was flipped to transmit negatively charged product ions from the above NRMS experiment, no ions were observed. Addition of an electron to $CH_3BH^{\bullet}$ is exothermic by 10 kJ $mol^{-1}$ but the vertical addition is *endothermic* by 17 kJ $mol^{-1}$ (Fig. 4.9 and 4.10). So the anion is unlikely to be generated by charge transfer to the radical. Similarly, a single step double charge-transfer to $CH_3BH^{+}$ did not result in the observation of $CH_3BH^{-}$. The RRKM prediction of the relative rate constants involved in the isomerization of $CH_3BH^{-}$ and $CH_2BH_2^{-}$ (Fig. 4.10) indicates that the former ion undergoes fast interconversion to the latter ion. Thus it would be difficult to experimentally generate the $CH_3BH^{-}$ ion independently unless they could be made cold, i.e., at a very low internal energy with narrow distribution. It should be possible to form $CH_2BH_2^{-}$ by charge transfer from the radical (vertical electron attachment gives an ion with only 10 kJ $mol^{-1}$ of internal energy) but not from the cation for obvious reasons. Unfortunately we were unable to find a suitable precursor ion that would yield neutral $CH_2BH_2^{\bullet}$ in a dissociative process to explore this possibility. Vertical electron attachment to $CH_3BH^{\bullet}$ is endothermic which means the $CH_3BH^{-}$ anion is unlikely to be made from the cation or radical. In addition, the anion lies in a shallow well of only 48 kJ $mol^{-1}$ and RRKM calculations predict it will undergo fast isomerize to $CH_2BH_2^{-}$ below the dissociation limit.

*Chapter 5: Experimental characterization and modeling the Potential Energy Surfaces for the $B(N(CH_3)_2)_3$ radical cation, dication and their metastable decomposition products*

*5.1 Introduction*

Dications can exhibit unusual structures and chemical bonding. They can be generated using techniques like charge-stripping (CS) mass spectrometry, electron impact (EI) ionization, photoionization, electrospray ionization (ESI), and double charge transfer (DCT). CS was first introduced by Benyon's group about three decades ago [74] and it still remains a leading method for the formation and characterization of unusual dications in the gas phase [75, 76]. Mass spectrometry and theoretical calculations can be used to study the formation, structures, stability and reactivity of dications. Many dications formed by CS are metastable and can undergo charge separation ('Coulomb explosion') or neutral loss dissociations. KER and MIKES are two techniques that can be used to study singly, doubly or multiply charge ions in the gas phase.

Lammertsma *et al*, published and extensive review of organic dications, including heterodications, carbodications (ranging from C1 – C12) which included a variety of substituents [77]. The only dication including B in this review was for $BNH_4^{2+}$ (isoelectronic with ethylene), which is discussed further below. Dications of benzene ($C_6H_6^{2+}$) [78-82] and other aromatics [43, 79], as well as smaller hydrocarbon dications like methane ($CH_4^{2+}$) [83-85], ethylene ($C_2H_4^{2+}$) [86, 87], ethane ($C_2H_5^{2+}$) [88, 89], $C_3H_5^{2+}$ [90], diacetylene $C_4H_3^{2+}$ [91], etc. have received considerable attention in the literature.

The potential energy surfaces of the mono- and dications of aminoborane ($NH_2BH_2$) and ammoniaborene ($NH_3BH$) were investigated by *ab initio* calculations at the MP4/6-311G(d,p)//6-31G(d) level of theory [92]. $NH_3BH^{\bullet+}$ ($C_S$) ($2^{\bullet+}$) is more stable than $NH_2BH_2^{\bullet+}$ ($C_{2V}$) by 10.5 kJ $mol^{-1}$ and a transition state barrier of 135.6 kJ $mol^{-1}$ separates the two isomers. Likewise, for the dications, $NH_3BH^{2+}$ ($C_{3V}$) is more stable than $NH_2BH_2^{2+}$ ($C_{2V}$) by 253.5 kJ $mol^{-1}$ and a transition state barrier of 326.8 kJ $mol^{-1}$ separates the two isomers. $BNH_4^{\bullet+}$ / $BNH_4^{2+}$ ions are isoelectronic with $C_2H_4^{\bullet+}$ / $C_2H_4^{2+}$ ions, however, the more stable $C_2H_4^{2+}$ structure is $CH_2CH_2^{2+}$ and $CH_3CH^{2+}$ does not exist at all [86]. Similarly for the cations, as mentioned previously, $CH_3CH^{\bullet+}$ has been shown not to occupy a minimum on the ionized ethene potential energy surface [7].

The ammoniaborene dication ($NH_3BH^{2+}$) was the only isomer of $BNH_4^{2+}$ to be generated experimentally. It was made by charge stripping mass spectrometry of mass selected $BNH_4^{\bullet+}$, which was itself generated by 80 eV electron impact ionization of aminoborane. According to the *ab initio* calculations, $NH_2BH_2^{2+}$ cannot be generated from $NH_2BH_2^{\bullet+}$ since its vertical ionization energy is located above the threshold for dissociation / isomerization [92]. The same is not true for $NH_3BH^{2+}$, which can be generated by vertical electron removal from $NH_3BH^{\bullet+}$ since this generates a dication species below the transition state energies for further reactions of $NH_3BH^{2+}$.

*5.2 Procedures*

Experimental procedures were as outlined in Chapter 2. Computational procedures involved geometry optimization at the B3-LYP/6-311+G(d) level of theory for the cation and dication of $(B(N(CH_3)_2)_3$ as well as for the metastable dissociation products from each. Single point calculations were performed at the B3-LYP/6-311+G(3df,2p)//B3/LYP/6-311+G(d) level and all energies quoted in this chapter are at this level of theory. Unfortunately, due to the size of the molecules under investigation, calculations using the G3 composite method were unattainable.

*5.3 The $B(N(CH_3)_2)_3$ radical cation*

A prominent molecular ion peak, $1^{+\bullet}$ (*m/z* 143) is observed in the regular EI mass spectrum of tris(dimethyl)amino borane (figure not shown). This molecular ion has three MI processes in its MIKES mass spectrum (Figure 5.1). They are summarized in equations 5.1 to 5.3 and the structures are defined in Figure 5.2.

$$1^{+\bullet} \rightarrow (CH_3)NB(N(CH_3)_2)_2^{+} (2^+) + CH_3 \qquad (5.1)$$

$$1^{+\bullet} \rightarrow B(N(CH_3)_2)_2^{+} (3^+) + N(CH_3)_2 \qquad (5.2a)$$

$$\rightarrow 3^+ + CH_3NHCH_2 \qquad (5.2b)$$

$$\rightarrow 3^+ + CH_3CHNH_2 \qquad (5.2c)$$

$$1^{+\bullet} \rightarrow CH_3CHB(NCH_3)(N(CH_3)_2)^{+} (6a^+) + CH_3NH_2 \qquad (5.3a)$$

$$1^{+\bullet} \rightarrow CH_3CH_2B(NCH_2)(N(CH_3)_2)^{+} (6b^+) + CH_3NH_2 \qquad (5.3b)$$

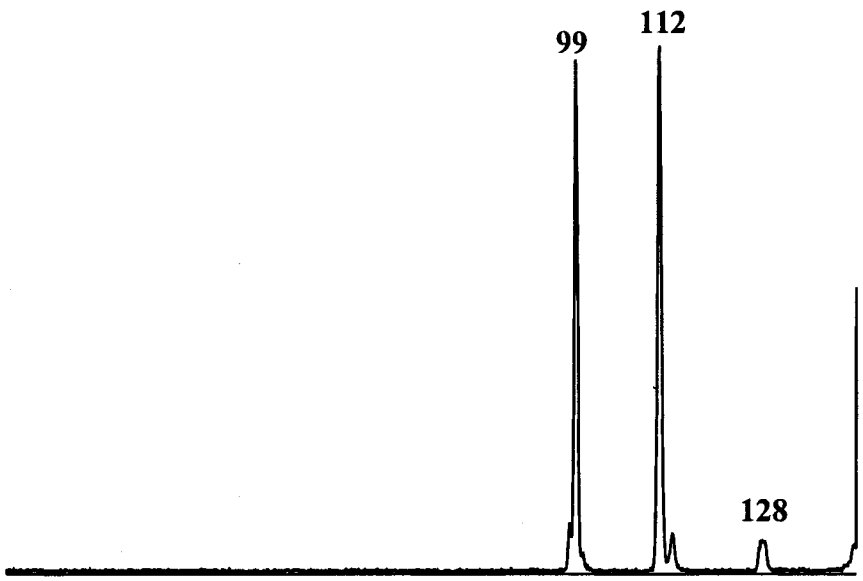


Figure 5.1. MIKEs MS in the 2 ffr of *m/z* 143 ($1^{+\bullet}$).

The loss of methyl ($CH_3^{\bullet}$) (M-15), methylamine ($CH_3NH_2$) (M-31) and dimethyl amino or some isomer of ($N(CH_3)_2^{\bullet}$) (M-44), yield MI product peaks at *m/z* $128^+$, $112^+$, and $99^+$, respectively (Figure 5.1). Interestingly, *m/z* 128 and 112 are not generated in significant amounts from the ion source (these peaks in the full mass spectrum are less than 2 % of the base peak intensity, figure not shown).

Three isomeric forms of $NC_2H_6^{\bullet}$ neutral loss are considered, $N(CH_3)_2^{\bullet}$, $CH_3CHNH_2^{\bullet}$, and $CH_3NHCH_2^{\bullet}$ (Equation 2a-2c). The loss of $N(CH_3)_2^{\bullet}$ results from a simple bond cleavage, while loss of $CH_3CHNH_2^{\bullet}$ or $CH_3NHCH_2^{\bullet}$ would require a rearrangement prior to bond rupture. The CID mass spectrum of ion source generated *m/z* 44 (Fig 5.3a) is indicative of the $CH_3NHCH_2^+$ ion structure, which interconverts on the microsecond

timescale with $CH_3CHNH_2^{+}$ to give the prominent *m/z* 18 peak [71]. The $(CH_3)_2N^{+}$ ion is some 282 kJ/mol less stable than $CH_3NHCH_2^{+}$ and is unlikely to be made in the ion source where sufficient energy exists to isomerize it to the more stable isomer. The CIDI mass spectrum of the neutral $C_2H_6N^{\bullet}$ radical made upon metastable decomposition of *m/z* 143 (Fig 5.3b) is completely different, notably in the absence of *m/z* 18. Thus, collisional reionization of the $C_2H_6N^{\bullet}$ radical does not make the more stable $CH_3NHCH_2^{+}$ or $CH_3CHNH_2^{+}$ ions. We can only conclude that Fig 5.3b corresponds to the $(CH_3)_2N^{+}$ cation, which has never before been generated in the gas-phase as a distinct species [71].

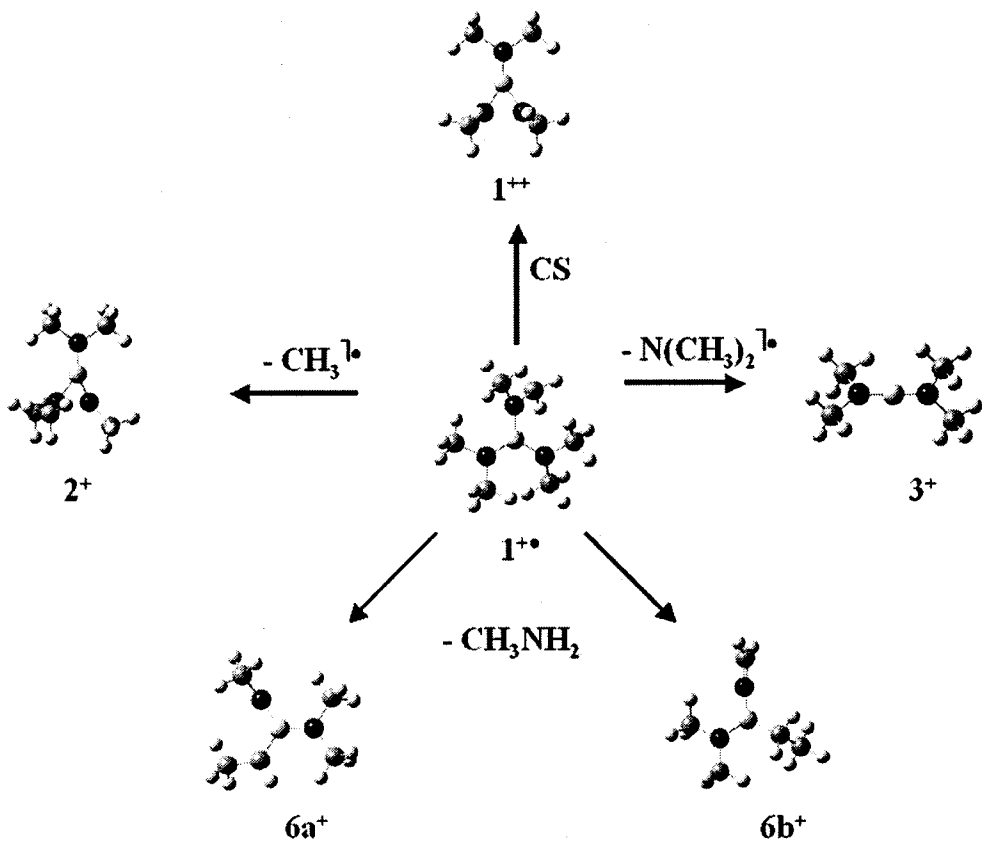


Figure 5.2. Structures for the reaction pathways of $B(N(CH_3)_2)_3^{+}$ ($1^{+\bullet}$) and its charge striping and metastable reaction products; $B(N(CH_3)_2)_3^{++}$ ($1^{++}$), $2^{+}$, $3^{+}$, $6a^{+}$, and $6b^{+}$.

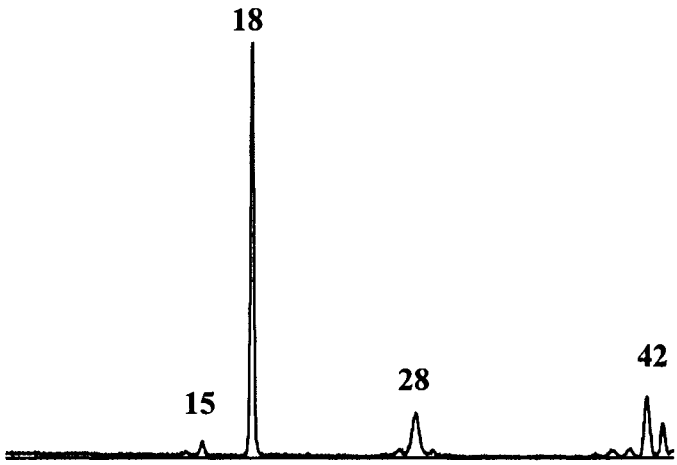


Figure 5.3a. CID ($O_2$, 10% beam reduction, 3 ffr) of *m/z* 44 from tris(dimethylamino)borane

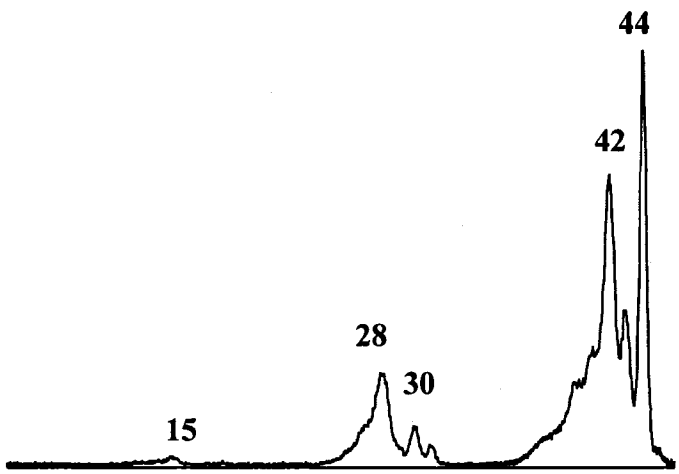


Figure 5.3b. CIDI (deflector electrode set to 90 V, $O_2$ used for reionization) of *m/z* 143 from tris(dimethyl)amino borane.

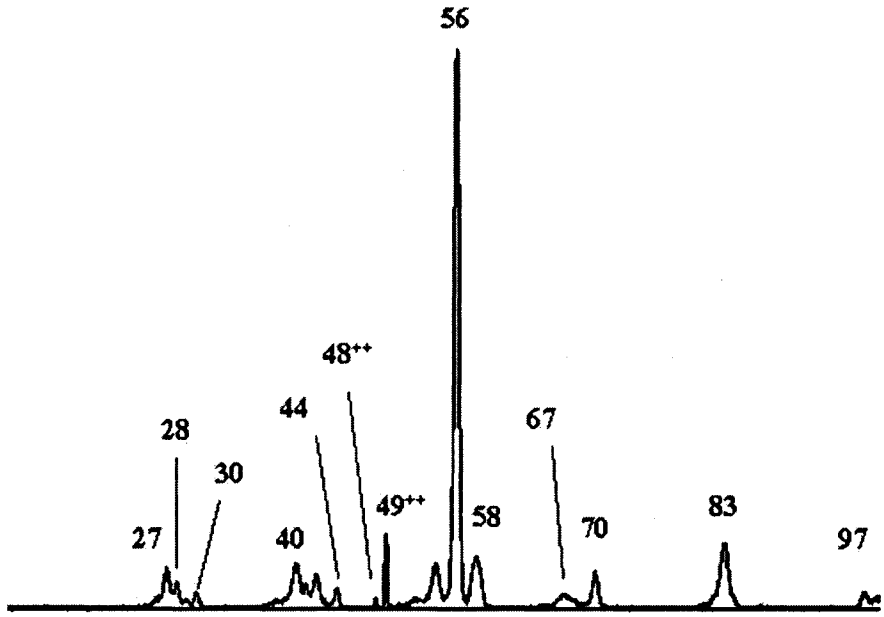


Figure 5.4a. CID ($O_2$, 20 % beam reduction, 3 ffr) MS of ion source generated *m/z* 99 from tris(dimethylamino) borane.

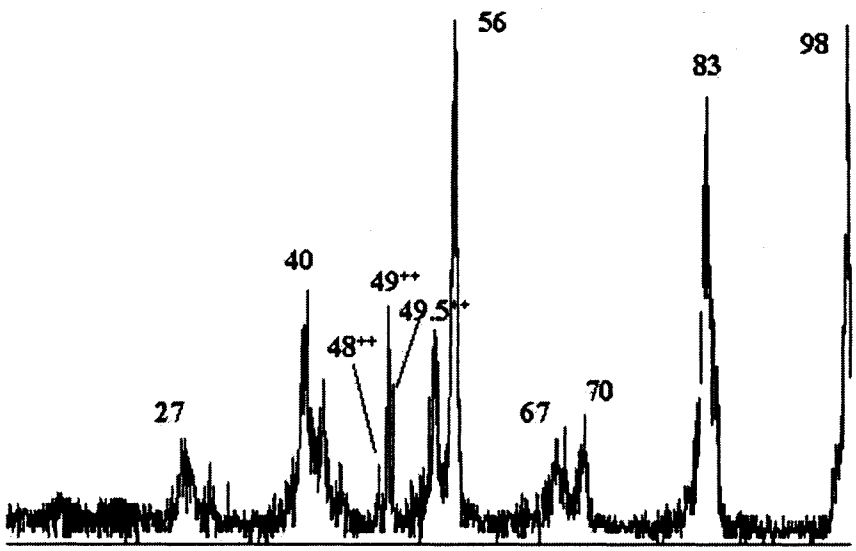


Figure 5.4b. CID ($O_2$, 20 % beam reduction, 3 ffr) MS of metastably generated *m/z* 99 from $1^{+\bullet}$.

Figure 5.4a and b show the CID ($O_2$, 20 % beam reduction, 3 ffr) MS of source generated and metastably generated *m/z* 99. The main MI process of *m/z* 99 is the loss of 43 yielding a product ion at *m/z* 56. Taking this fact into account, both these spectra are very similar. The main differences are the appearance of a doubly charged peak at *m/z* 49.5++ and the disappearance of *m/z* 58.

The loss of methylamine producing a product ion peak at *m/z* 112 requires a rearrangement prior to bond rupture. Two structures resulting from the rearragement and dissociation have been proposed according to equations 5.3a and 5.3b with structure definitions provided in Figure 5.2.

*5.3.1 Potential Energy Surface modeling for $B(N(CH_3)_2)_3$ cation ($1^{+\bullet}$) and its metastable decomposition products*

The relative energy surface of $1^{+\bullet}$ is shown in Fig. 5.5. Only one isomer is considered for product $2^+$, resulting from the loss of $CH_3^\bullet$ since it is assumed that the three dimethylamino branches are equivalent. Three isomers were originally considered for the loss of $NC_2H_6^\bullet$. From the above discussion, the isomer in question was determined to be $N(CH_3)_2\rceil^\bullet$, implying that a simple bond cleavage takes place resulting in $3^+$ and $N(CH_3)_2\rceil^\bullet$. The simple bond cleavage is 5 kJ $mol^{-1}$ and 38 kJ $mol^{-1}$ higher in energy than $CH_3CHNH_2\rceil^\bullet$ and $CH_3NHCH_2\rceil^\bullet$ for the rearrangement paths, respectively. The loss of methylamine resulting in structure $6a^+$ is 191 kJ $mol^{-1}$ less stable than that resulting in $6b^+$.

The dissociation products, $2^+$ from the loss of $CH_3^\bullet$ and $6a^+$ from loss of $CH_3NH_2$ are 73 kJ $mol^{-1}$ and 129 kJ $mol^{-1}$ higher in energy than $3^+$ from loss of $N(CH_3)_2^\bullet$, respectively, while $6b^+$ from loss of $CH_3NH_2$ is 62 kJ $mol^{-1}$ more stable than $3^+$ from loss of $N(CH_3)_2^\bullet$. Since the formation of 6a+ is considerably more endothermic than the formation of 3+, it should not be able to compete with the latter channel on the microsecond timescale. Thus methylamine loss should be accompanied by formation of 6b+ with an appropriate barrier.

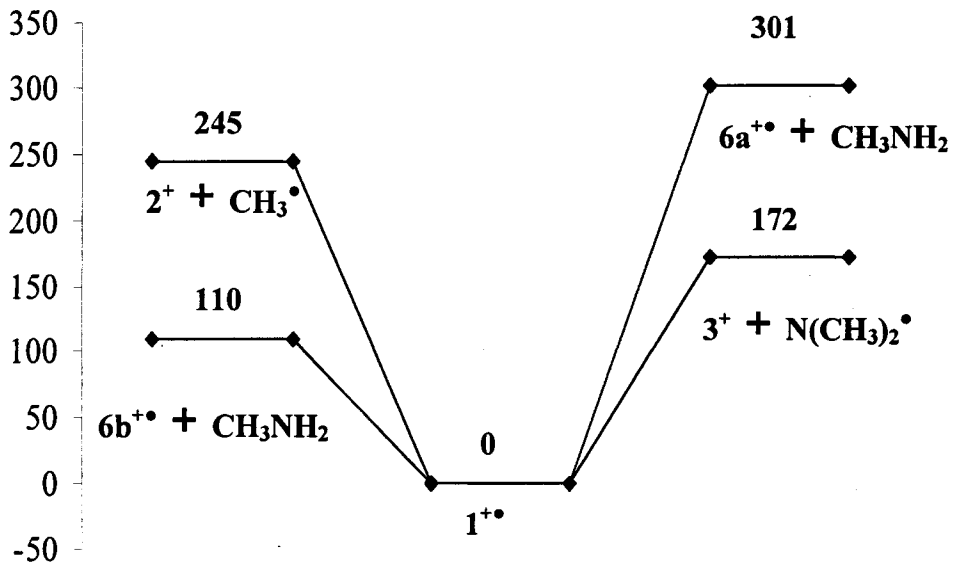


Figure 5.5. Relative energy (B3-LYP/6-311+G(3df,2p)//B3-LYP/6-311+G(d)) surface of $1^{+\bullet}$, all energies relative to $1^{+\bullet}$ in kJ $mol^{-1}$.

*5.4 The $B(N(CH_3)_2)_3$ dication*

Charge stripping (CS) MS is a two step process. Monocations are generated in the ion source by EI, the cation of interest is mass selected by the magnetic field (B) and dications are generated through ionization of the monocations ($M^+$) (lifetime > $10^{-5}$s) by a collision with a target gas (G) [77] in this case $O_2$ is used in the collision cell of the 2ffr. The charge stripping MS (CID ($O_2$), 10% beam reduction) of *m/z* 143 is shown in Figure 5.6. The collision with the target gas produces the dication according to Equation 5.4.

$$M^+ + G \rightarrow M^{++} + G + e^- \qquad \text{(Eqn. 5.4)}$$

Since the charge stripping process takes place in an isolated system, the E required to drive the reaction is supplied by the translational E of $M^+$ (8keV) [77]. The dication is transmitted to the 3ffr, where its MIKES mass spectrum is acquired. The MIKES mass spectrum of the dication ($1^{++}$) has four competing metastable channels (Figure 5.7), two that involve the elimination of a neutral (structures defined in Figure 5.8) and two that involve charge separation (structures defined in Figure 5.9). $H_2$ elimination is the dominant channel. It is interesting to note that there have been few reports of doubly charged systems where neutral loss successfully competes with charge separation [43]. Charge separation reactions may take place via tunneling, curve crossing, thermal activation or other mechanisms resulting in two ionic fragments that are accelerated to several eV in their mutual electric fields [43, 90].

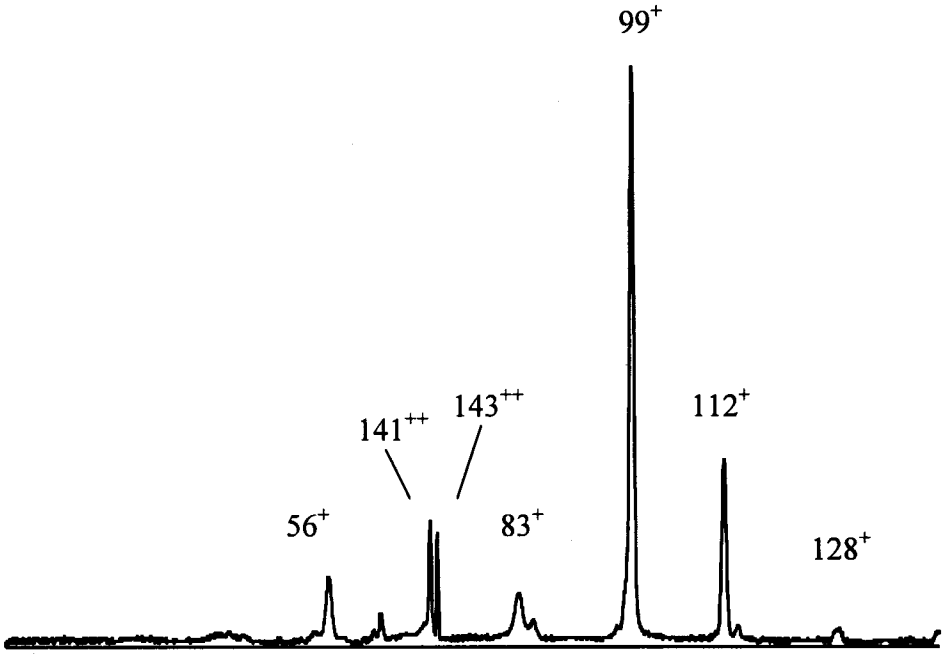


Figure 5.6. Charge striping MS (CID ($O_2$), 10% beam reduction, 2ffr) of *m/z* 143 ($1^{+\bullet}$).

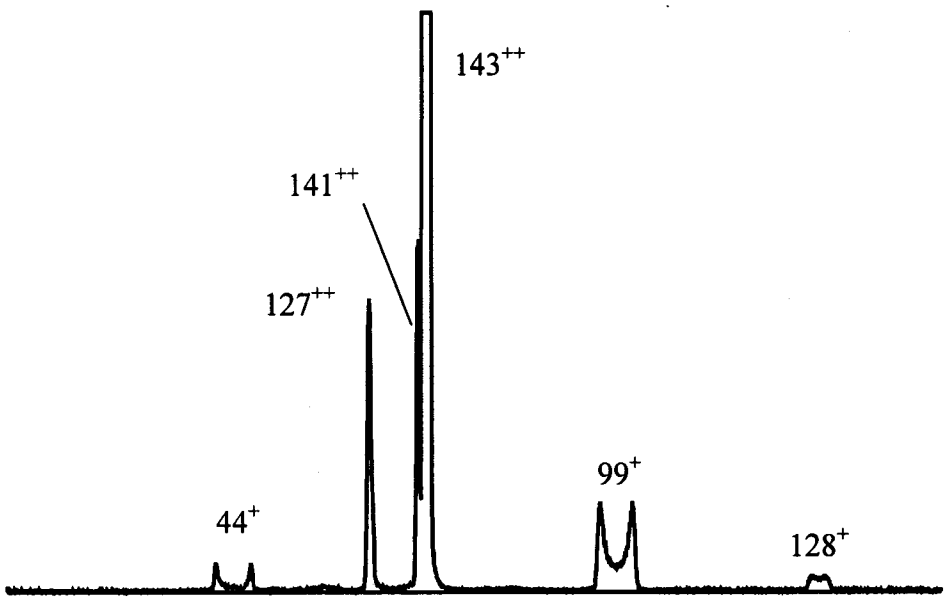


Figure 5.7. MIKES MS of *m/z* 71.5 ($143^{++}$) from tris(dimethyl)amino borane.

*5.4.1 Neutral loss channels*

The two neutrals lost from $1^{++}$ are $H_2$ and $CH_4$; these reactions are shown in equations 5.5 and 5.6 and structure definitions are given in Figure 5.8.

$1^{++} \rightarrow 4a^{++} + H_2$ (5.5a)

$\rightarrow 4b^{++} + H_2$ (5.5b)

$1^{++} \rightarrow 5a^{++} + CH_4$ (5.6a)

$\rightarrow 5b^{++} + CH_4$ (5.6b)

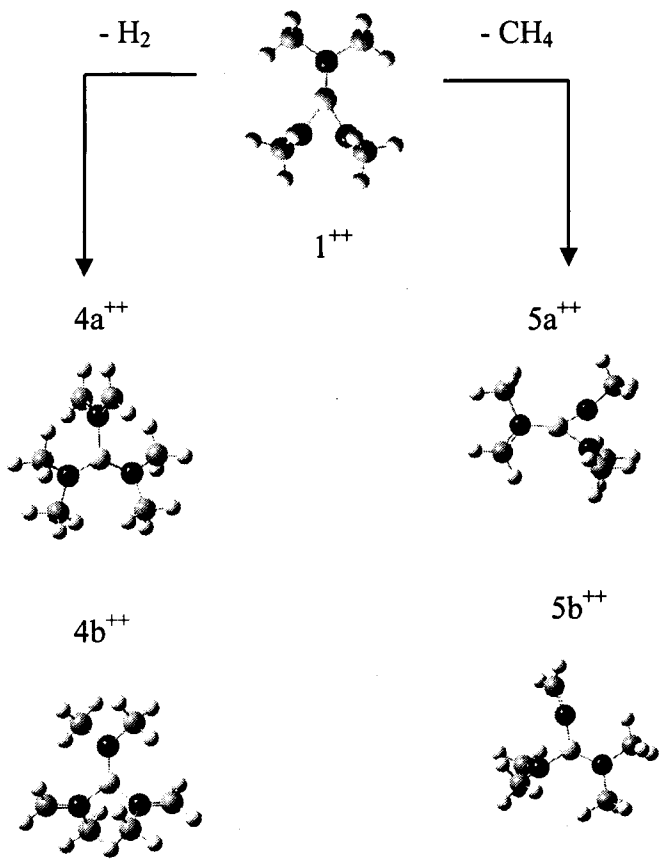


Figure 5.8. Structure of $B(N(CH_3)_2)_3^{]++}$ ($1^{++}$) and its neutral loss reaction products; $4a^{++}$, $4b^{++}$, $5a^{++}$, and $5b^{++}$.

Both neutral loss channels produced peaks that were Gaussian in shape. For the loss of $H_2$, $T_{0.5} = 368 \pm 18$ meV and for the loss of $CH_4$, $T_{0.5} = 150 \pm 12$ meV. Both $T_{0.5}$ values are significant and indicate that the dissociation products are generated with excess energy, some of which has been partitioned into their translational degrees of freedom. This is expected since both reactions involve the rearrangement of $1^{++}$ by H-atom transfer, and so a significant reverse energy barrier should be present in the reaction.

### *5.4.2 Charge separation channels*

There are two separate charge separation channels in the MIKES MS of $1^{++}$ shown in Figure 5.7. These reactions are given in equations 5.7 and 5.8 and their structure definitions are provided in Figure 5.9.

$$1^{++} \rightarrow 2^{+} + CH_3^{+} \qquad (5.7)$$

$$1^{++} \rightarrow 3^{+} + N(CH_3)_2^{+} \ / \ CH_3NHCH_2^{+} \qquad (5.8a)$$

Daughter ion peaks at *m/z* 99 and 44 are from the same channel due to the complimentary nature of the kinetic energy release calculated for the two peaks (see below) and again this can either be a bond cleavage reaction or involve a rearrangement process leading to the lower energy $CH_3NHCH_2^{+}$ ion.

The second channel is loss of methyl cation, $CH_3^{+}$ from $143^{++}$ producing $2^{+}$, although in this case, the methyl cation is not observed in the MS (Figure 5.7) due to mass discrimination. The corresponding neutral loss channels (loss of $CH_3^{\bullet}$ and $N(CH_3)_2^{\bullet}$) are also observed in the MIKES MS of the cation $1^{+\bullet}$ (Figure 5.2).

Both charge separation channels produced peak shapes that were dish shaped (due to z axial discrimination in the instrument); therefore the distance between the horns was used to calculate the *minimum* KER ($T_h \approx T_{min}$) for these reactions as defined in section 2.2.5. These charge separation channels should give large KER values because of the repulsive nature of the potential energy curve governing the dissociation reaction. For the charge separation channel producing ions at *m/z* $99^+$ and $44^+$, $T_h$ could be calculated separately for each daughter ion. $T_{h\,(99+)} = 2365 \pm 156$ meV and $T_{h\,(44+)} = 2065 \pm 279$ meV. Only one daughter ion was observed for the charge separation involving loss of a methyl cation from $1^{++}$. In this case the minimum KER was calculated to be, $T_{h\,(128+)} = 1942 \pm 332$ meV.

*5.2.3 Potential Energy Surfaces modeling for $B(N(CH_3)_2)_3$ dication ($1^{++}$) and its metastable decomposition products*

The relative energy surface of $1^{++}$ is shown in Fig. 5.10. Two isomers are considered for both neutral loss pathways. For the loss of $H_2$, structure $4a^{++}$ would result from the loss of H's on adjacent methyl groups on the same N, while structure $4b^{++}$ comes from the loss of H's from methyl groups on two different N's. The loss of both H's from methyl groups on the same N is 281 kJ $mol^{-1}$ higher in energy than when they are lost from methyl groups on two different N's.

Likewise, two isomers are considered for loss of $CH_4$. Structure $5a^{++}$ is the result of H loss from a methyl group on one N and the methyl group lost from a different N, while

$5b^{++}$ is the result of H loss from one methyl group and the remaining methyl group being lost from the same N. Here structure $5a^{++}$ is more stable than $5b^{++}$ by 63 kJ $mol^{-1}$.

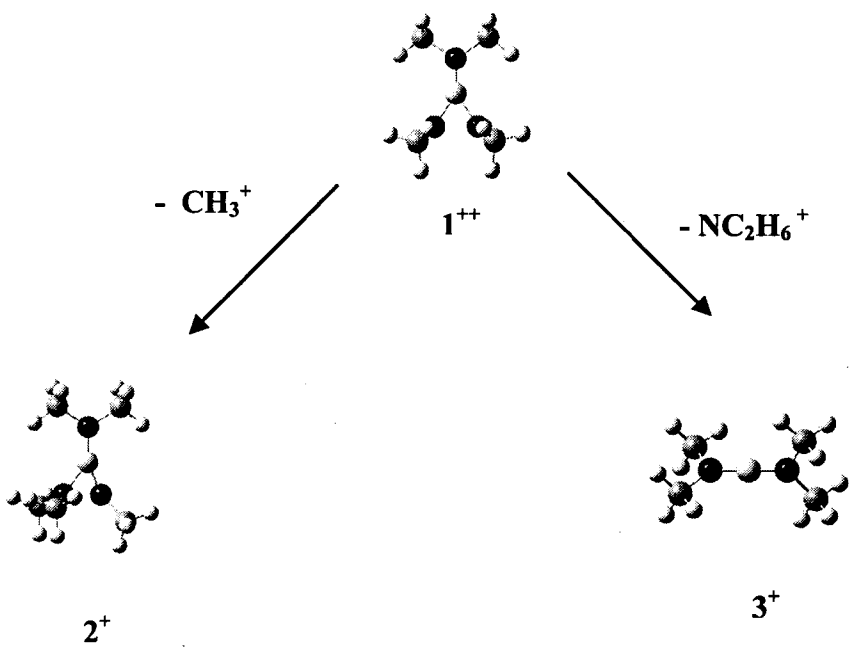


Figure 5.9. Structure of $B(N(CH_3)_2)_3^{|++}$ ($1^{++}$) and its charge separation reaction products; $(CH_3)NB(N(CH_3)_2)_2^{]+}$ ($2^+$), $B(N(CH_3)_2)_2^{]+}$ ($3^+$).

The charge separation reactions are similar to the neutral loss pathways of the cation, $1^{+\bullet}$ the difference being that two cations are formed rather than one cation and one neutral. Again, two isomers are considered in the case of loss of $NC_2H_6^+$. One involves a simple bond cleavage resulting in $3a^+$ and $N(CH_3)_2^+$ and the other involves a rearrangement prior to bond cleavage resulting in $3b^+$ and $CH_3NHCH_2^+$ or $CH_3CHNH_2^+$. The simple bond cleavage is 289 kJ $mol^{-1}$ and 338 kJ $mol^{-1}$ higher in energy than for the rearrangement paths involving $CH_3NHCH_2^+$ and $CH_3CHNH_2^+$, respectively. The dissociation product,

$2^+$ from the loss of $CH_3^+$ is 174 kJ $mol^{-1}$, 463 kJ $mol^{-1}$ and 512 kJ $mol^{-1}$ higher in energy $3^+$ from loss of $NC_2H_6^+$, $CH_3NHCH_2^+$ and $CH_3CHNH_2^+$, respectively.

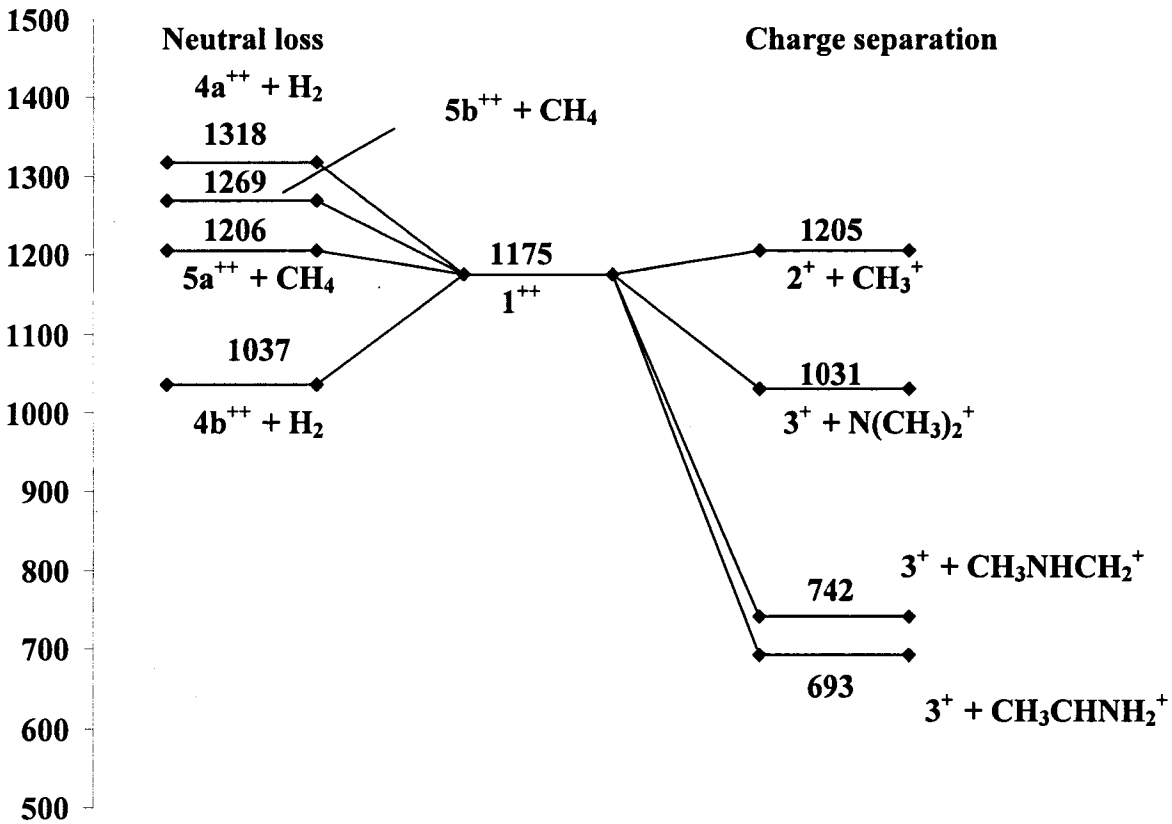


Figure 5.10. Relative energy (B3-LYP/6-311+G(3df,2p)//B3-LYP/6-311+G(d)) surface of $1^{++}$, all energies relative to $1^{+\bullet}$ in kJ $mol^{-1}$.

$143^{++}$ has a highly symmetric geometry in which the N atoms are nearly planar, indicating that the two positive charges are delocalized over all three atoms. From Figure 5.8 it is possible to assign a structure to the neutral loss product ions. Ions 4a and b are due to loss of $H_2$, with the two H atoms originating from carbon atoms on the same N atom ($4a^{++}$) or different N atoms ($4b^{++}$). The structure of $4a^{++}$ exhibits a planar $CH_2$-N-$CH_2$ ligand indicative of an allyl like structure in which the lone electron can be delocalized across the ligand (the charge remains on N). The second positive charge is symmetry divided between the other two ligands. The formation of $4a^{++}$ requires a 1,3-$H_2$ elimination that is normally forbidden on orbital symmetry arguments. Formation of $4b^{++}$ involves a 1,5-$H_2$ elimination, which is normally favoured over a 1,3-$H_2$ elimination. $4b^{++}$ is essentially two $CH_3NCH_2^+$ ligands on the B atom. The N-$CH_2$ bonds are shorter than the N-$CH_3$ bonds, indicating significant double-bond character, as one would expect as the charge is localized on N in this ligand. While the barrier for the 1,5-$H_2$ elimination may be lower than that for 1,3-$H_2$ elimination, the entropy of activation of the former process will be much less favourable due to the constraint of many internal degrees of freedom. This being said, it is doubtful that the formation of $4a^{++}$ would be accompanied by a kinetic energy release as large as the measured value of 366 meV. If it were formed over a sufficiently high barrier to have this $T_{0.5}$ value, it would not compete with the other observed dissociation channels.

The formation of $127^{++}$ is accompanied by a modest KER of 136 meV. Thus the barrier to the formation of this ion is not as large as that for $H_2$ loss noted above. While both structures $5a^{++}$ and $5b^{++}$ are energetically feasible, given both reactions require a

rearrangement, the lowest energy product ion should be generated, namely $5a^{++}$, with a barrier that is near, or slightly higher than that for $H_2$ loss (see Figure 5.10).

The three charge separation reactions can be described by repulsive potential curves that intersect those of the two small molecule loss reactions. Their large KER is due to the partitioning of most of the excess internal energy into translational degrees of freedom on the repulsive surface (see Figure 5.11).

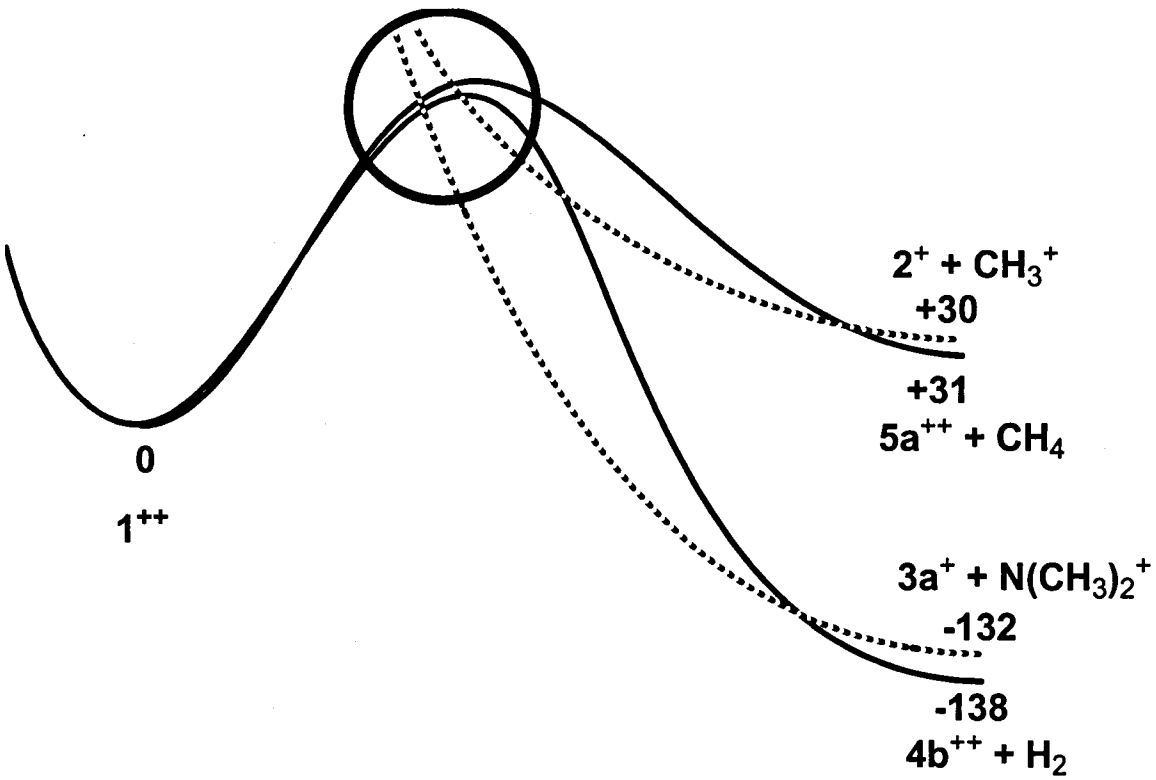


Figure 5.11: Schematic potential energy diagram indicating the interaction of the four competing dissociation channels for $1^{++}$. The circled area indicates the place the repulsive charge separation curves likely cross, allowing all four reactions to compete on the microsecond timescale.

*Chapter 6 Conclusions*

*Ab initio* calculations using several of levels of computational theory were used to study the structure, thermochemistry, isomerization and dissociation of the $CH_2BH_2$ and $CH_3BH$ radicals, cations and anions. The results of these *ab initio* calculations were used as a computational assessment that was applied to the other molecules in this study.

The formation of the $CH_4B$ radicals, cations, and anions was also explored by tandem mass spectrometry and RRKM kinetic theory. Calculations predict that $CH_2BH_2^{+\bullet}$ is not an equilibrium structure on the potential energy surface. The $CH_3BH^{+}$ was characterized by its collision-induced dissociation mass spectrum and neutralization–reionization (NR) mass spectrometry was used to generate the $CH_3BH^{\bullet}$ radical. While both $CH_2BH_2^{\bullet}$ and $CH_3BH^{\bullet}$ are stable with respect to isomerization and dissociation, a relatively low barrier to the 1,2-hydrogen shift means that pure $CH_3BH^{\bullet}$ can only be made cold, and so the above NR experiment likely produces a mixture of neutrals, of which only $CH_3BH^{\bullet}$ can be reionized. Contrary to the results from lower level calculations, the $CH_2BH_2^{+}$ ion was not found to reside in a potential well. While both radicals were found to be equilibrium structures stable with respect to isomerization and dissociation, RRKM calculations predict that it would be difficult to make pure $CH_3BH^{\bullet}$ by neutralizing the cation. Vertical electron attachment to $CH_3BH^{\bullet}$ is endothermic which means the $CH_3BH$ anion is unlikely to be made from the cation or radical. In addition, the anion lies in a shallow well of only 48 kJ $mol^{-1}$ and RRKM calculations predict it will undergo fast isomerization to $CH_2BH_2^{-}$ below the dissociation limit.

The $B(N(CH_3)_2)_3$ radical cation and dication structures and dissociation products have been investigated by high level *ab initio* calculations as determined by the initial computational assessment and experimentally characterized by tandem mass spectrometry. The $B(N(CH_3)_2)_3$ dication was generated by charge stripping mass spectrometry and the KER was measured for its metastable dissociation products. There were four observed dissociation channels, two involving neutral losses and two involving charge separations. The neutral loss channels successfully compete with the charge separations, the dominant process actually being neutral loss of $H_2$. The KER for the four metastable dissociations were determined to be $T_{0.5\ (141^{++})} = 368 \pm 18$ meV, $T_{0.5\ (127^{++})} = 144 \pm 12$ meV, $T_{h\ (99^{+})} = 2365 \pm 156$ meV, $T_{h(44^{+})} = 2046 \pm 279$ meV, and $T_{h\ (128^{+})} = 1942 \pm 332$ meV.

### *6.1 Claims to Original Research*

The results from the theoretical and experimental study of the system of $CH_4B$ radicals, cations and anions have been accepted for publication (Dec. 2006) in the Journal of Molecular Structure: THEOCHEM, 2007, in press.

$B(N(CH_2)_2)_3^{+\bullet\ /\ ++}$ were successfully generated in the gas phase and the metastable decomposition products were investigated experimentally and theoretically for both. During the experimental characterization of $B(N(CH_2)_2)_3^{+\bullet}$ a new CID MS was observed for $N(CH_3)_2^{+}$. There are few published reports of metastable dissociation of dications where neutral losses successfully compete with charge separations. Likewise, there are few experimental studies of boron containing molecules and ions.

1. P.M. Mayer and T. Baer, J. Phys. Chem. 100 (1996) 14949.
2. Z.-w. Qu, Z.-s. Li, Y.-h. Ding, and C.-c. Sun, J. Phys. Chem. A. 104 (2000) 11952.
3. A. Papakondylis, E. Miliordos, and A. Mavridis, J. Phys. Chem. A. 108 (2004) 4335.
4. J.D. Dill, P.v.R. Schleyer, and J.A. Pople, J. Am. Chem. Soc. 97 (1975) 3402.
5. *Boron Nitiride*. 2006, Wikipedia.
6. *Metallocene Catalyst Breakthrough*. 2004, cheresources.
7. W.J.v.d. Hart, Int. J. Mass. Spectrom. Ion Processes. 151 (1995) 27.
8. P. Hassanzadeh, Y. Hannachi, and L. Andrews, J. Phys. Chem. 97 (1993) 6418.
9. Y. Hannachi, P. Hassanzadeh, and L. Andrews, J. Phys. Chem. A. 98 (1994) 6950.
10. P. Hassanzadeh and L. Andrews, J. Am. Chem. Soc. 114 (1992) 9239.
11. W.-H. Fang and S.D. Peyerimhoff, Molecular Physics. 93 (1998) 329.
12. G.H. Jeong, R. Boucher, and K.J. Klabunde, J. Am. Chem. Soc. 112 (1990) 3332.
13. M.K. Murphy and J.L. Beauchamp, J. Am. Chem. Soc. 98 (1976) 1433.
14. J.A. Pople, Y. Apeloig, and P.v.R. Schleyer, Chem. Phys. Letts. 85 (1982) 489.
15. C. Poon and P.M. Mayer, Canadian J. Chem. 80 (2002) 25.
16. D.V. Lanzisera and L. Andrews, J. Phys. Chem. A. 101 (1997) 824.
17. D.V. Lanzisera and L. Andrews, J. Phys. Chem. A. 101 (1997) 1482.
18. J.M.L. Martin, P.R. Taylor, P. Hassanzadeh, and L. Andrews, J. Am. Chem. Soc. 115 (1993) 2510.
19. C.A. Thompson and L. Andrews, J. Am. Chem. Soc. 117 (1995) 10125.
20. C.A. Thompson, L. Andrews, J.M.L. Martin, and J. El-Yazal, J. Phys. Chem. 99 (1995) 13839.
21. T.R. Burkholder, L. Andrews, and R.J. Bartlett, J. Phys. Chem. 97 (1993) 3500.
22. T.R. Burkholder and L. Andrews, J. Phys. Chem. 96 (1992) 10195.
23. P. Hassanzadeh and L. Andrews, J. Phys. Chem. 97 (1993) 4910.
24. S.P. So, J. Phys. Chem. A. 107 (2003) 1819.
25. S.P. So, J. Phys. Chem. A. 106 (2002) 3181.
26. R. Srinivas, S. Vivekananda, S.J. Blanksby, D. Schroder, M.A. Trikoupis, J.K. Terlouw, and H. Schwarz, Int. J. Mass. Spectrom. Ion Processes. 202 (2000) 315.
27. R.G. Cooks, J.H. Benyon, R.M. Caprioli, and G.R. Lester, *Metastable Ions*. 1973, Amsterdam: Elsevier Scientific Publishing Company. 296.
28. J.A. Hipple and E.U. Condon, Phys. Rev. 68 (1945) 54.
29. J.L. Holmes and P.M. Mayer, J. Phys. Chem. 99 (1995) 1366.
30. J.L. Holmes and F. Benoit, *MTP International Review of Science*, ed. A. Maccoll. Vol. 5. 1972, London: Butterworths. 259.
31. P.J. Derrick and K.F. Donchi, in *Comprehensive Chemical Kinetics*. 1983, Elsevier: Amsterdam. p. 53.
32. J.L. Holmes and J.K. Terlouw, Org. Mass Spectrom. 15 (1980) 383.
33. K.R. Jennings, Int. J. Mass. Spectrom. Ion Phys. 1 (1968) 227.
34. W.K. Haddon and F.W. McLafferty, J. Am. Chem. Soc. 90 (1968) 4745.
35. F.W. McLafferty, P.F.B. III, F.C. Kornfeld, S.-C. Tsai, and I. Howe, J. Am. Chem. Soc. 95 (1973) 2120.

36. P.C. Burgers, J.L. Holmes, A.A. Mommers, and J.K. Terlouw, Org. Mass Spectrom. 19 (1984) 442.
37. C. Lifshitz, P. Gotchiguian, and R. Roller, Chem. Phys. Letts. 95 (1983) 106.
38. P.C. Burgers, J.L. Holmes, A.A. Mommers, and J.K. Terlouw, Chem. Phys. Letts. 102 (1983) 1.
39. J.L. Holmes, Mass Spectrom. Rev. 8 (1989) 513.
40. F.W. McLafferty, Science. 247 (1990) 925.
41. C.A. Schally, G. Hornung, D. Schroder, and H. Schwarz, Chem. Soc. Rev. 27 (1998) 91.
42. F. Turecek, Org. Mass Spectrom. 27 (1992) 1087.
43. S. Feil, O. Echt, K. Gluch, V.G. Hasan, S. Matt-Leubner, T. Tepnual, V. Grill, A. Bacher, P. Scheier, and T.D. Mark, Chem. Phys. Letts. 411 (2005) 366.
44. P.J. Todd and F.W. McLafferty, Int. J. Mass. Spectrom. Ion Phys. 38 (1981) 371.
45. J.L. Holmes, Org. Mass Spectrom. 20(3) (1985) 169.
46. M.M. Bursey, J.R. Hass, D.J. Harvan, and C.E. Parker, J. Am. Chem. Soc. 101 (1979) 5485.
47. J.L. Holmes and J.K. Terlouw, Org. Mass Spectrom. 15(8) (1980) 383.
48. J.L. Holmes, Adv. in Mass Spectrom. 6 (1974) 865.
49. K.L. Busch, G.L. Glish, and S.A. McLuckey, *Mass Spectrometry/Mass Spectrometry*. 1988, New York: VCH Publishers.
50. J.K. Terlouw, W.M. Kieskamp, J.L. Holmes, A.A. Mommers, and P.C. Burgers, Int. J. Mass. Spectrom. Ion Processes. 64 (1985) 245.
51. T. Baer and W.L. Hase, *Unimolecular Reaction Dynamics: Theory and Experiments*. 1996, New York: Oxford University Press. 438.
52. J.I. Steinfeld, J.S. Francisco, and W.L. Hase, *Chemical Kinetics and Dynamics*. Second Edition ed. 1999, New Jersey: Prentice Hall.
53. W.J. Hehre, L. Radom, P.v.R. Schleyer, and J.A. Pople, *Ab Initio Molecular Orbital Theory*. 1986, New York: Wiley.
54. F. Jensen, *Introduction to Computational Chemistry*. 1999, Chichester: John Wiley and Sons. 429.
55. C. Moller and M.S. Plesset, Phys. Rev. 46 (1934) 618.
56. J. Cizek, J. Chem. Phys. 45 (1966) 4256.
57. J.A. Pople, M. Head-Gordon, and K. Raghavachari, J. Chem. Phys. 87(10) (5968) 5968.
58. W. Koch and M.C. Holthausen, *A Chemist's Guide to Density Functional Theory*. 2000, New York: Wiley-VCH.
59. B. Ensing, *Density Functional Theory*. 2003.
60. A.D. Becke, Phys. Rev. A. 38 (1988) 3098.
61. C. Lee, W. Yang, and R.G. Par, Phys. Rev. B. 37 (1988) 785.
62. A.D. Becke, J. Chem. Phys. 98 (1993) 5648.
63. L.A. Curtiss, K. Raghavachari, P.C. Redfern, V. Rassolov, and J.A. Pople, J. Chem. Phys. 109 (1998) 7764.
64. L.A. Curtiss, K. Raghavachari, P.C. Redfern, and J.A. Pople, J. Chem. Phys. 106 (1997) 1063.
65. L.A. Curtiss, P.C. Redfern, K. Raghavachari, and J.A. Pople, J. Chem. Phys. 109 (1998) 42.

66. M.J. Frisch, G.W. Trucks, H.B. Schlegel, G.E. Scuseria, M.A. Robb, J.R. Cheeseman, V.G. Zakrzewski, J.A.M. Jr., R.E. Stratmann, J.C. Burant, S. Dapprich, J.M. Millam, A.D. Daniels, K.N. Kudin, M.C. Strain, O. Farkas, J. Tomasi, V. Barone, M. Cossi, R. Cammi, B. Mennucci, C. Pomelli, C. Adamo, S. Clifford, J. Ochterski, G.A. Petersson, P.Y. Ayala, Q. Cui, K. Morokuma, D.K. Malick, A.D. Rabuck, K. Raghavachari, J.B. Foresman, J. Cioslowski, J.V. Ortiz, B.B. Stefanov, G. Liu, A. Liashenko, P. Piskorz, I. Komaromi, R. Gomperts, R.L. Martin, D.J. Fox, T. Keith, M.A. AL-Laham, C.Y. Peng, A. Nanayakkara, C. Gonzalez, M. Challacombe, P.M.W. Gill, B. Johnson, W. Chen, M.W. Wong, J.L. Andres, M. Head-Gordon, E.S. Replogle, and J.A. Pople, *GAUSSIAN 98*. 1998, Gaussian Inc.: Pittsburg, PA.
67. A.P. Scott and L. Radom, J. Phys. Chem. 100 (1996) 16502.
68. A. Nicolaides, A. Rauk, M.N. Glukhovtsev, and L. Radom, J. Phys. Chem. 100 (1996) 17460.
69. C. Gonzalez and H.B. Schlegel, J. Chem. Phys. 90 (1989) 2154.
70. C. Gonzalez and H.B. Schlegel, J. Chem. Phys. 94 (1990) 5523.
71. J.L. Holmes, C. Aubry, and P.M. Mayer, *Assigning Structures to Ions in Mass Spectrometry*. 2007, Boca Raton: CRC Press. 446.
72. S.G. Lias, J.E. Bartmess, J.F. Liebman, J.L. Holmes, R.D. Levin, and W.G. Mallard, J. Phys. Chem. Ref. Data Suppl. 1 (1988) 17.
73. T. Baer and P.M. Mayer, J. Am. Soc. Mass Spectrom. 8 (1997) 103.
74. R.G. Cooks, J.H. Benyon, and J.F. Litton, Org. Mass Spectrom. 10 (1975) 503 (and references therein).
75. K. Vékey, Mass Spectrom. Rev. 14 (1995) 195.
76. D. Schröder and H. Schwarz, J. Phys. Chem. A. 103 (1999) 7385.
77. K. Lammertsma, P.v.R. Schleyer, and H. Schwarz, Angew. Chem. Int. Ed. Engl. 28 (1989) 1321.
78. M. Rosi, C.W.B. Jr., and E.L.O. Bakes, The Astrophysical Journal. 609(2) (2004) 1192.
79. M.A. Mabud, M.J. Dekrey, R.G. Cooks, and T. Ast, Int. J. Mass. Spectrom. Ion Processes. 69 (1986) 277.
80. T.W. Bentley and C.A. Wellington, Org. Mass Spectrom. 16 (1981) 533.
81. W. Higgins and K.R. Jennings, Trans. Faraday Soc. 62 (1966) 97.
82. T. Ast, J.H. Beynon, and R.G. Cooks, Org. Mass Spectrom. 14 (1972) 307.
83. M. Rabrenovic, A.G. Brenton, and J.H. Beynon, Int. J. Mass. Spectrom. Ion Phys. 52 (1983) 175.
84. J.A. Pople, B. Tidor, and P.R. Schleyer, Chem. Phys. Letts. 88 (1982) 533.
85. J.L. Holmes, F.D. Lossing, J.K. Terlouw, and P.C. Lossing, J. Am. Chem. Soc. 104 (1982) 2931.
86. K. Lammertsma, M. Barzaghi, G.A. Olah, and J.A. Pople, J. Am. Chem. Soc. 105 (1983) 5252.
87. M.D. Wong, B.F. Yates, R.H. Nobes, and L. Radom, J. Am. Chem. Soc. 109 (1987) 3181.
88. S.D. Peyerimhoff and R.J. Buenker, J. Chem. Phys. 49 (1968) 312.
89. G.A. Olah and M. Simonetta, J. Am. Chem. Soc. 104 (1982) 330.

90. K. Gluch, J. Fedor, S. Matt-Leubner, O. Echt, A. Stamatovic, M. Probst, P. Scheier, and T.D. Mark, J. Chem. Phys. 118(7) (2003) 3090.
91. D. Schroder, J. Loos, H. Schwarz, R. Thissen, J. Roithova, and Z. Herman, Int. J. Mass. Spectrom. 230 (2003) 113.
92. T. Drewello, W. Koch, C.B. Lebrilla, D. Stahl, and H. Schwarz, J. Am. Chem. Soc. 109 (1987) 2922.